CHARACTERIZATION OF OLEFIN POLYMERIZATION REACTIONS USING DISSOLUTION DYNAMIC NUCLEAR POLARIZATION

A Dissertation

by

CHIA-HSIU CHEN

Submitted to the Office of Graduate and Professional Studies of
Texas A&M University
in partial fulfillment of the requirements for the degree of

DOCTOR OF PHILOSOPHY

Chair of Committee,	Christian Hilty
Committee Members,	Simon North
	Emile Schweikert
	Steven Wright
Head of Department,	Simon North

December 2018

Major Subject: Chemistry

ABSTRACT

Nuclear magnetic resonance (NMR) spectroscopy is a powerful analytical tool with widespread applications in all areas of synthetic chemistry including polymer chemistry. High-resolution solution-state NMR not only provides accurate qualitative and quantitative information on the chemical structure from small molecules to macromolecules, but it is also capable of determining detailed local structure, i.e., microstructure, which is not accessible by any other techniques. However, the major drawback of NMR is its low sensitivity.

Dissolution Dynamic Nuclear Polarization (D-DNP), a hyperpolarization technique, provides a several thousand-fold enhancement of NMR signals. When combined with stopped-flow techniques, time scales on the order of seconds can be accessed by real-time NMR spectroscopy. We demonstrate that polymer microstructures and reaction kinetics can be determined simultaneously using this method. Examples used for this purpose are metallocene-catalyzed polymerization and ring-opening metathesis polymerization (ROMP). We discuss model equations used for describing the time evolution of hyperpolarized monomer signals and for determining rate constants of initiation, propagation, and deactivation. The results can be used to distinguish mechanisms leading to living polymerization, polymerization subject to deactivation, or to slow initiation. When applying the D-DNP NMR method with a copolymerization reaction, cross-propagation and self-propagation rate constants are calculated using comonomer signals detected simultaneously in ^{13}C spectra. These rate constants further

determine the copolymer composition. Finally, we demonstrate the use of real-time NMR to measure the polarization transfer between hyperpolarized small molecules and polymers in an equilibrium chemical system. The improved signal-to-noise ratio provided by hyperpolarization allows for site specific characterization of intermolecular interactions in a single-scan measurement.

CONTRIBUTORS AND FUNDING SOURCES

Contributors

This work was supported by a dissertation committee consisting of Professors Christian Hilty, Simon North, and Emile Schweikert of the Department of Chemistry and Professor Steven Wright of the Department of Electrical and Computer Engineering and Department of Biomedical Engineering.

The catalysts used for Chapter 2 were provided by Dr. Wei-Chun Shih of the Department of Chemistry.

All other work conducted for the dissertation was completed by the student independently.

Funding Sources

This work was made possible in part by American Chemical Society Petroleum Research Fund under Grant Number 501813-ND7, National Science Foundation under Grant Number CHE-0840464, CHE-0846402, and CHE-1362691, as well as Welch Foundation under Grant Number A-1658.

NOMENCLATURE

BDPA	α,γ-bis-diphenylene-β-phenylallyl
D-DNP	Dissolution Dynamic Nuclear Polarization
DPPH	2,2-Diphenyl-1-picrylhydrazyl
EPR	Electron Paramagnetic Resonance
FID	Free Induction Decay
G2	Grubbs second generation catalyst
G3	Grubbs third generation catalyst
HMQC	Heteronuclear Multiple Quantum Coherence
HSQC	Heteronuclear single Quantum Coherence
NOE	Nuclear Overhauser Effect
NOESY	Nuclear Overhauser Effect Spectroscopy
OX63	tris-(8-carboxyl-2,2,6,6-tetrakis(2-hydroxyethyl)-1,3,5,7-tetrathia-2,6-dihydro-s-indacene-4-yl)methyl sodium salt
PAMAM	Polyamidoamine
ROMP	Ring-Opening Metathesis Polymerization
TEMPO	2,2,6,6-tetramethylpiperidine-1-oxyl
TEMPOL	4-hydroxy-2,2,6,6-tetramethylpiperidin-1-oxyl

TABLE OF CONTENTS

Page

LIST OF FIGURES

Page

LIST OF TABLES

LIST OF SCHEMES

Page

1. INTRODUCTION

Nuclear magnetic resonance (NMR) spectroscopy is a powerful analytical tool with widespread applications in all areas of synthetic chemistry, and polymer science is no exception.[1–3] High-resolution solution-state NMR not only provides accurate qualitative and quantitative information on the chemical structure from small molecules to macromolecules, but it is also capable of determining detailed local structures, *i.e.*, microstructure, which is not accessible by any other techniques. The microstructure of polymers are commonly characterized using ^{13}C NMR.[2,3] However, ^{13}C is a low sensitive nucleus and has low natural abundance. Signal averages and longer measurement time are often required for acquiring ^{13}C NMR spectra with high signal-to-noise ratio. The low sensitivity also limits the obtainable information when measuring an on-going reaction, where side products or reaction intermediates are present at low concentration. Notably, signal averaging is not applicable when analyzing transient reaction intermediates.

The low sensitivity of NMR stems from the low energies of a nuclear magnetic moment in magnetic field. The nuclear spin polarization, which is derived as the spin alignment on the energy levels, is generally small at thermal equilibrium. Hyperpolarization is a state, where nuclear spin polarization deviates strongly from thermal equilibrium. It has become an increasingly important means of improving the sensitivity of liquid- and solid-state NMR spectroscopy.[4–8] Methods for generating hyperpolarization include spin-exchange optical pumping (SEOP),[9] photochemically induced dynamic nuclear polarization (photo-CIDNP),[10] parahydrogen-induced

polarization (PHIP),[11] and microwave-driven dynamic nuclear polarization (DNP).[12] Among them, the microwave-driven DNP is a versatile method applicable to a variety of nuclei. For example, ^{1}H, ^{2}H, ^{19}F, ^{13}C, ^{15}N, ^{31}P, ^{89}Y, $^{107}Ag/^{109}Ag$ have been successfully polarized by DNP in the solid state.[13–15]

In 2003, Ardenkjaer-Larsen *et al.* invented the dissolution DNP (D-DNP) technique to generate several thousand-fold enhancements of NMR signals in the liquid state.[16] This method is accomplished by hyperpolarizing a solid sample using microwave driven DNP, and then transferring this sample via a dissolution process into a magnet for signal acquisition. The hyperpolarized signals of the dissolved sample can be measured using a NMR spectrometer or an MRI scanner.[17] Nuclear spins hyperpolarized by D-DNP have been developed as sensitive probes to monitor chemical and biochemical reactions *in vivo* and *in vitro*. For example, hyperpolarized HCO_3^- has been used as pH sensor for detecting tumor cells in mice.[18] Redox sensors for detecting reactive oxygen species (ROS) were developed using hyperpolarized ^{13}C-benzoylfomic acid and [^{13}C, $^{2}H_3$]-p-anisidine.[19–22] In our group, we have determined rate constants of an enzymatic reaction by combining D-DNP with stopped-flow instrumentation.[23] This method has been further extended to the study of polymerization. In 2013, Lee *et al.* first measured time-resolved spectra of anionic polymerization of styrene and identified the living propagating species.[24] These studies open the possibility of utilizing the D-DNP NMR method to characterize varieties of biochemical and chemical reactions.

1.1 D-DNP NMR Spectroscopy

1.1.1 DNP in Solid State

Microwave-driven DNP refers to the process of polarization transfer from electrons to nuclear spins by microwave irradiation. The possibility for increasing the polarization via DNP originates from the fact that the spin polarization of electrons is higher than of nuclei at the same temperature and magnetic field. The spin polarization is defined as the ratio of difference of spin population (n_α-n_β), which follows the Boltzmann distribution, over the total populations (n_α+n_β) among the Zeeman levels as described by equation (1-1). The n_α and n_β are the number of spins in α and β states. The spin polarization depends on the magnetic field B_0, the temperature T, the gyromagnetic ratio γ, Plank's constant h, and Boltzmann's constant, k_B.

$$P = \frac{n_A - n_B}{n_A + n_B} = \tanh\left(\frac{h}{2\pi}\frac{\gamma B_0}{2k_B T}\right) \quad (1\text{-}1)$$

The gyromagnetic ratio of the electron is about 660 and 2600 times larger than that of nuclear spins of ^{1}H and ^{13}C, respectively. When other parameters in equation (1-1) are equal, the theoretical increase in polarization through DNP is by the same factor.

The spin polarization is higher at low temperature as described in equation (1-1). A typical DNP sample hyperpolarized at low temperature contains the sample of interest and a polarizing agent, *i.e.*, the electron source, mixed in a glassy matrix. The glassy condition is to prevent sample crystallization, ensuring a homogeneous distribution of the polarizing agents. By irradiating the sample mixture with microwaves, spin polarization

transfer to the nucleus of interest occurs via solid effect,[25] cross effect,[26,27] or thermal mixing.[28–30] The solid effect occurs through polarization transfer from an isolated unpaired electron to a nucleus. Irradiation of the sample with microwaves frequency of $\omega_S \pm \omega_I$ triggers the polarization transfer process (ω_S and ω_I are the electron and nuclear Larmor frequencies, respectively). The cross effect takes place when two coupled electrons transfer the polarization to one nucleus. Finally, the thermal mixing mechanism involves the interactions of many dipolar coupled electrons with nuclear spins. The choices of the polarizing agents and the experimental conditions for hyperpolarization determines, which mechanism dominates.

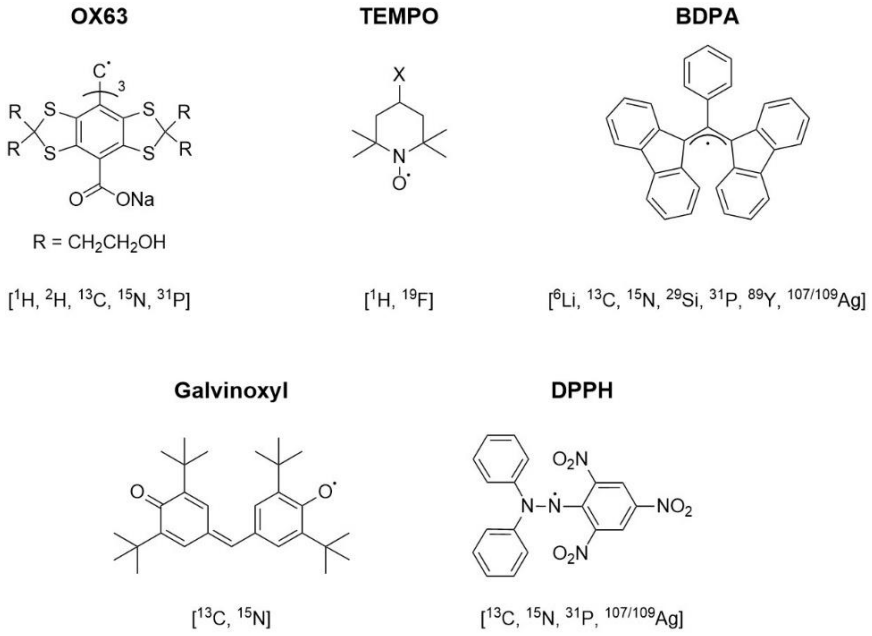

Figure 1-1. Examples of organic radicals used for the DNP process. The nuclei shown in the brackets have been hyperpolarized with these radicals using the dissolution DNP method.[31–33]

Figure 1-1 shows examples of chemical structures of radicals used in low-temperature DNP at ~ 1 K. The radical, OX63, is extensively used in biological experiments and is only applicable with hydrophilic compounds.[34] Radicals for hyperpolarizing organic molecules are BDPA, DPPH, and galvinoxyl. These radicals have been used to hyperpolarize multiple NMR active nuclei, as depicted in the bracket in Figure 1-1.[31–33] For $^{1}H/^{19}F$ hyperpolarization, nitroxide radicals such as TEMPO and TEMPOL are used for hydrophilic and hydrophobic compounds, respectively.[35]

Polarization transfer from electron to nuclear spins is just the initiation of the hyperpolarization process. A subsequent spin diffusion process is required to spread hyperpolarization to the entire sample.[29,36] For ^{1}H hyperpolarization, the polarization build-up completes in minutes. For ^{13}C hyperpolarization, the build-up can last for several hours. Polarizing ^{13}C nuclei in a shorter time can alternatively be achieved using cross-polarization from ^{1}H nuclei.[37–39] In this experiment, the TEMPO radical is used to polarize the ^{1}H nuclei, and then radio frequency (rf) pulses are given in the solid-state, causing polarization transfer from ^{1}H to ^{13}C.

1.1.2 Dissolution DNP

The dissolution DNP (D-DNP) is a method developed to acquire liquid-state NMR signals from sample hyperpolarized via DNP in solid-state. Specifically, the frozen hyperpolarized sample is dissolved using a hot solvent. Figure 1-2 shows a scheme of the D-DNP polarizer used in this thesis. The D-DNP polarizer is composed of a 3.35 T NMR magnet with a modified cryostat containing a variable temperature insert (VTI) (A in

Figure 1-2). The VTI controlls the temperature for the hyperpolarization at ~ 1 K. The DNP process occurs by irradiating microwave to the sample, which is pre-loaded in a cylindrical metal container (B in Figure 1-2). The dissolution starts with heating several milliliters of solvents, on the top of the DNP polarizer (blue box in Figure 1-2), to a set temperature of about 120 – 180 ^{o}C. The solvent is subsequently driven by pressurized helium gas to dissolve and flush out the sample from the cryostat in the NMR magnet.

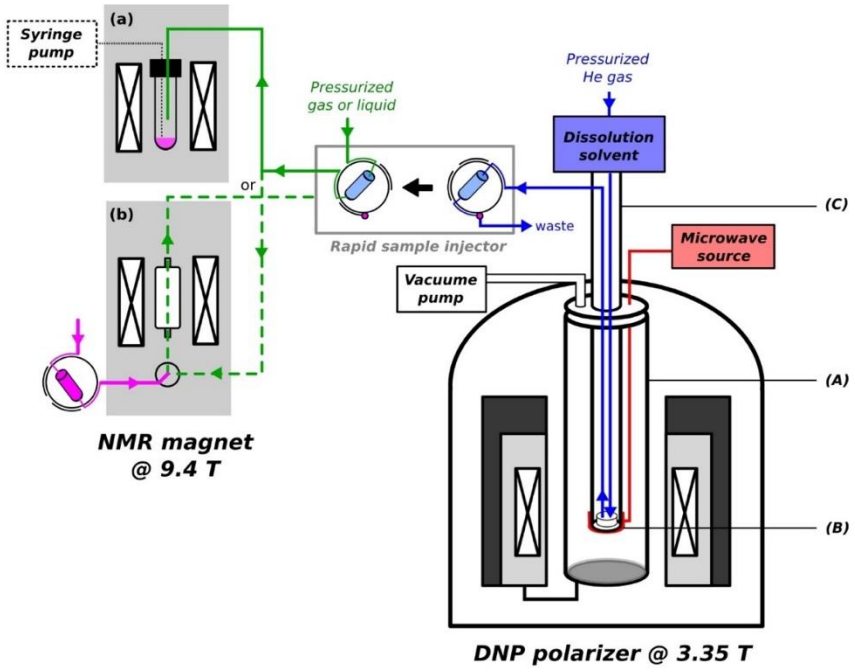

Figure 1-2. Scheme of dissolution DNP and rapid sample injector used for stopped-flow hyperpolarized NMR measurement in our lab. This setup is composed of a dissolution DNP (Hypersense, Oxford Instruments) at 3.35 T and the rapid sample injector connected with mixing vessels settle in the bore of NMR magnet at 9.4 T (Bruker). (A) Variable temperature insert (VTI) and (B) metal container where the DNP sample loads. (a) Sample mixing using gas-driven sample injection, and (b) sample mixing using liquid-driven injection.

1.1.3 Signal Enhancement in Liquid State

The substantial signal enhancement created by D-DNP is in part due to the temperature difference in the DNP polarizer and the NMR magnet. The relation of signal enhancement in the liquid state and solid state is equation (1-2).

$$\varepsilon_{D-DNP} = \varepsilon_s \cdot \frac{B_{DNP}}{B_{NMR}} \cdot \frac{T_{NMR}}{T_{DNP}} \quad (1\text{-}2)$$

In the above equation, ε_s is the actual solid-state DNP enhancement. B_{DNP} and B_{NMR} are the magnetic fields of DNP (3.35 T in Figure 1-2) and NMR (9.4 T in Figure 1-2), respectively. T_{DNP} and T_{NMR} are the temperature of DNP and NMR, respectively. Assuming that T_{DNP} = 1 K and T_{NMR} = 298 K, the signal enhancement in the D-DNP can be 80 times larger than in the solid-state DNP.

However, the actual signal enhancement in D-DNP experiment is reduced due to signal loss during sample transfer. This process occurs in a few seconds, on the time scale of nuclear spin relaxation. Because of the rapid signal decay, a short dead time between the DNP process and the liquid-state NMR measurement is important. Rapid sample injector developed in our lab allows for sample transfer in 1-2 seconds.[40,41] In addition, it is capable of measuring non-equilibrium chemical reactions by mixing the hyperpolarized sample with compounds pre-polarized at thermal equilibrium. Legget *et al.* have built a dual-isocenter magnet where the upper compartment (~3.35 T) is for DNP enhancement and a lower compartment (~ 9.4 T) is for NMR measurement.[42] The short distance between two compartments allows the sample transfer in 1 second.

1.1.4 Rapid Sample Injector

The rapid sample injector used in this thesis is driven by pressurized gas.[40] This design contains a two-position valve controlling the sample loading and the injection shown as the gray box in Figure 1-2. In the loading mode, the dissolved hyperpolarized sample fills a sample loop with a fixed volume. Subsequently, the sample is sensed by a photodiode triggering the switch between the loading and injection mode. In the injection mode, pressurized gas is applied for several hundred milliseconds to deliver this portion of the sample into the NMR tube for measurements. A small volume of reagents (< 50 μl) can be preloaded in the same NMR tube. These reagents are depicted as pink in Figure 1-2a. Forward and backward pressures are applied to carry the sample and to prevent outgassing, respectively. In this design, the mixing occurs in the NMR tube in which the turbulence during the injection ensures the sample homogeneity. The injection into the NMR tube results in a stopped-flow method where hyperpolarized sample and other compounds are mixed, followed by the start of measurement. Alternatively, the non-hyperpolarized reagent can be pre-loaded in a syringe pump and injected into the NMR tube after the arrival of the hyperpolarized sample. This setup was developed to characterize dormant species in a metallocene-catalyzed polymerization reaction described in Chapter 2.

Chen et al. have developed a rapid sample injector, where the sample is driven by pressurized liquid rather than gas.[41] In this method, the hyperpolarized sample is delivered into an NMR flow cell as drawn Figure 1-2b. This design helps to minimize sample turbulence during the injection, and it has been used in ultra-fast Laplace NMR for

investigating molecular diffusion and relaxation.[43] A reagent can be pre-loaded in a sample loop in another two-position valve. Both the reagent and the hyperpolarized sample are injected together with different delay time by a liquid pump. The mixed samples are delivered to an NMR flow cell and, after the NMR measurement, flow back into the rapid sample injector.

The mixing of the hyperpolarized sample with the non-hyperpolarized compound in both of rapid sample injectors can be adjusted using the pressure of carrier media, liquid or gas, and time of the sample injection. The mixing profile can be visualized by images acquired using pulsed field gradients.[44]

1.1.5 NMR Detection

NMR detection is performed after the sample injection. A single spectrum can be acquired by applying a rf pulse. Otherwise, series of rf flip angle pulses are applied to acquire time-resolved spectra using a hyperpolarized sample. The time window for NMR measurement after the dissolution is dependent on the spin-lattice relaxation of the nuclei in the liquid state. In general, the time window for common nuclei present in organic molecules such as ^{1}H and ^{13}C is several seconds, thus immediate NMR acquisition is required after the sample transfer. In addition, NMR signals of larger molecules decay more rapidly than of small molecules. Therefore, it is challenging to measure the NMR signals of macromolecules by directly hyperpolarizing them. In Chapters 2 to 4, we demonstrate that the NMR signal of synthetic polymers can be identified from *in-situ* polymerization using hyperpolarized monomers. This approach is applicable when the

polymerization is fast, so that polymers are generated within the time window determined by the signal decays of monomers.

1.2 Stopped-flow Hyperpolarized NMR

The D-DNP NMR spectroscopy is suitable for the study of chemical reactions when the reaction time scale is faster than the signal decay caused by the spin-lattice relaxation. Table 1-1 summarizes the spin-lattice relaxation time constants, T_1, of nuclei commonly observed in organic compounds. Among them, ^{13}C, ^{15}N, ^{29}Si have T_1 time constants much longer than the ^{1}H, ^{19}F, and ^{31}P. Besides, these nuclei have broad chemical shift dispersions allowing the identification of reactants, products, and species generated during the reactions. Therefore, these nuclei are excellent choices for chemical reaction study using hyperpolarization.

The rapid sample injector used in this thesis (Figure 1-2) provides for a quick mixing of samples. Radio frequency pulse is subsequently applied to acquire NMR signals. It is, therefore, suitable for the study of non-equilibrium chemical reactions such as enzymatic reactions, organic reactions, and polymerization in real-time.[24,44,48,49] Information that can be determined from stopped-flow hyperpolarized NMR spectroscopy includes reactions kinetics and the identity of transient species generated during the reactions, which are essential indications for characterizing the reaction mechanism. Methods for the kinetic measurements and the identification of unknown species using D-DNP NMR are discussed in the following sections.

Table 1-1. Chemical shift ranges and T_1 time constants for selected nuclei.[50]

Nuclei	Δδ /ppm	γ (relative to ^{1}H)	Common T_1 range
^{1}H	13	1	0.1 – 2 s
^{19}F	700	0.9409	0.1 – 1 s
^{13}C	250	0.2515	0.1 – 100 s
^{15}N	900	0.1013	0.1 – 400 s
^{29}Si	520	0.1987	0.1 – 150 s
^{31}P	430	0.4048	0.05 – 2 s

1.2.1 Kinetic Measurement

The D-DNP NMR method allows for kinetic measurements using low sensitive nuclei. With signal enhancement of several order of magnitude, the spin polarization from the thermal equilibrium is negligible. The time resolution between each successive measurement using the D-DNP NMR method can be much shorter than the conventional NMR method, which requires restoring the polarization between scans.

For signals acquired without the involvement of chemical reactions and polarization transfer, the time-evolution of hyperpolarized signals, $S(t)$, acquired from fixed small flip angle pulse, α, can be described as [48]

$$S(t) = S(0)e^{-\left(\frac{1}{T_1}+\lambda\right)t} \quad \text{with} \quad \lambda \cong \frac{-\ln(\cos(\alpha))}{t_d} \tag{1-3}$$

In the above equation, the first term in the exponential function is the signal loss due to the spin-lattice relaxation characterized by T_1. The second term, λ, in which t_d denotes the repetition duration between pulses, describes the signal depletion caused by the rf pulses.

The λ can be minimized if a small flip-angle pulse, α, or large time interval, t_d, is applied, although this also reduces the observable signal and time resolution. Alternatively, variable flip angle schemes can be applied to equalize signal intensity across all scans.[51,52]

When the hyperpolarized sample is mixed with a reactant and a chemical reaction occurs, additional signal depletion due to the reaction can be observed. For example, the observed hyperpolarized signal in a first-order reaction with a rate constant, *k*, can then be described as [48]

$$S(t) = S(0)e^{-\left(k+\frac{1}{T_1}+\lambda\right)t} \qquad \text{with} \qquad \lambda \cong \frac{-\ln(\cos(\alpha))}{t_d} \tag{1-4}$$

The rate constant, *k*, can be determined when other parameters are known. However, this method might not be suitable for a reaction with $k \ll \frac{1}{T_1} + \lambda$. The range of detectable rate constants is larger if the nuclear spin has slow spin-lattice relaxation, *i.e.*, $1/T_1$ is small. Therefore, nuclei with long T_1 are especially suitable for the study of reaction kinetics.

Equation (1-4) is also applicable in a pseudo first-order reaction. In this case, *k* is a pseudo first-order rate constant, which can be adjusted to fall within the observable time window through the concentration of reagents. Among other, the rate constants in an enzymatic reaction, Diels-Alder reaction, and a living polymerization reaction have been determined using equation (1-4). [24,44,48]

The measurement of kinetic rate constants using the D-DNP NMR method can also be applied to polymerization reaction catalyzed by transition metal complexes. In this case, the kinetic model can be more complicated, because the concentration of the active catalyst varies during polymerization. For example, active catalytic species can be generated *in-situ* in the polymerization, resulting in an increase in the initial reaction rate. During the propagation, the catalytic species gradually lose activity based on different mechanisms. Since many of these variations in the polymerization kinetics stem from the chemical properties of the active catalyst, the characterization of this species in a polymerization reaction becomes significant.

In Chapter 2, we derive equations used for calculating deactivation and propagation rate constants and characterize the deactivation of the active species in a metallocene-catalyzed polymerization. In Chapter 3, we investigate the initiation and propagation in ring-opening metathesis polymerization (ROMP) catalyzed by well-defined ruthenium catalysts. These two studies demonstrate the capability of the D-DNP method in characterizing the catalytic activity in the polymerization.

In addition to the homopolymerization, a kinetic study of copolymerization involving two hyperpolarized monomers using D-DNP method is demonstrated in Chapter 4. In this approach, we demonstrate the determination of individual rate constants of cross-propagation and self-propagation acquired by numerical fitting of the hyperpolarized monomer signals.

1.2.2 Correlation Experiments

In addition to the reaction kinetics, identification of unknown species is important to characterize a reaction mechanism. While ^{13}C NMR gives broad chemical shift dispersion, signal assignment of unknown species typically requires information from correlation NMR spectroscopy.

Heteronuclear chemical shift correlation can be reconstructed using a 1D NMR scheme with off-resonance decoupling. In these experiments, one of the nuclei is irradiated with the decoupling pulse while the other nucleus is detected. The decoupling pulse can be a continuous wave or designed through scaling of heteronuclear coupling by optimal tracking (SHOT).[53–55] In a recent study, the modified SHOT pulse scheme was applied in the measurement of a chemical reaction. [^{13}C, ^{1}H] chemical shift correlations of a carbon anionic active site from an on-going polymerization reaction species have calculated without prior knowledge of actual coupling constants.[55]

Temporal correlation of reactant and product species generated from a chemical reaction can be acquired using hyperpolarized NMR spectroscopy.[56] In this experiment, a shaped inversion pulse is applied before rf pulses for acquisition. Since nuclear spin state can be preserved, the spin encoding with the inversion pulse, either in reactants or products, shows the negative signals in the measured spectra.[49] The same method has been applied to identify a propagating anionic species in anionic polymerization.[24] In chapter 2, we characterize the dormant species generated from the on-going reaction using the temporal correlation NMR measurement. Another type of temporal chemical shift correlation experiment is by applying rf pulses implemented with acquisition to saturate unknown

species generated during the reaction. Kim and the author of this thesis have used this method to correlate a new signal from a ruthenium-alkylidene observed in hyperpolarized spectra to one of the products, ethylene, in a ring-closing metathesis reaction.[57]

Conventional multidimensional correlation NMR experiments are not directly applicable to D-DNP NMR, because the hyperpolarization is non-renewable. Methods to overcome this problem include ultrafast NMR experiments based on gradient encoding.[58–61] In this approach, the NMR detection volume is divided into several parts, in which different delay times are applied. These can then be reconstructed resulting a 2D spectrum making the single scan NMR measurement in D-DNP experiments possible. Alternatively, band Selective Optimized Flip-Angle Short Transient Heteronuclear Multiple Quantum Coherence (SOFAST-HMQC) experiments using very short inter-scan delays has been developed to acquire a 2D spectrum of macromolecules which is under chemical exchanges with water in seconds.[62,63] This method relies on the optimization of rf pulse and the T_1 relaxation delay in the HMQC-based pulse sequence to achieve high repetition rates of experiments. Szekely *et al.* have measured the 2D NMR of disordered proteins enhanced by hyperpolarized water using an HMQC-based experiment.[64]

1.2.3 Nuclear Overhauser Effect in ^{1}H D-DNP Measurement

The Nuclear Overhauser Effect (NOE) describes the polarization transfer from nuclei with spin populations being disturbed from the thermal equilibrium to nuclei close enough in space.[65] In a hyperpolarized experiment, the admixing of the hyperpolarized sample to a molecule which is initially under thermal equilibrium, introduces a non-

equilibrium spin population. The polarization transfer from hyperpolarized nuclear spins to the non-hyperpolarized spins generates indirect signal enhancement. For example, negative signals on a small-sized molecules were identified in a non-specific binding using hyperpolarized water.[66] Specific binding of a ligand to a protein results in positive signal enhancements on large-sized molecules.[67,68] For kinetic measurement using ^{1}H hyperpolarization, signal contributions from polarization transfer, for example from the hyperpolarized reactant to products or solvents, may need to be included. The polarization transfer is commonly described using cross-relaxation rates of the interacting spins. Zeng et al. have determined the cross-relaxation rates of intramolecular protons in products generated in a Diels-Alder reaction in ^{1}H hyperpolarized experiments. The determined apparent cross-relaxation rate is about ten times smaller than the auto relaxation of reactants.[48]

The reaction kinetics is not observable when a chemical reaction reaches to equilibrium within the dead time of the stopped-flow method. In this case, only auto-relaxation, cross-relaxation, and in some cases, exchange rates determine the evolution of hyperpolarized signals. Nonetheless, the polarization transfer using ^{1}H hyperpolarization can be used to characterize the molecular interaction in the time scale of the D-DNP method. Chemical reactions in this category, for example, are the protein and ligand/solvent interaction. In Chapter 5, we demonstrate the characterization of intermolecular interaction of ligand and polymer using D-DNP NMR method.

2. IN-SITU DETERMINATION OF TACTICITY, DEACTIVATION AND KINETICS IN METALLOCENE-CATALYZED POLYMERIZATION OF 1-HEXENE USING 13C HYPERPOLARIZED NMR[1]

2.1 Introduction

The physical properties of widely used plastics synthesized by olefin polymerization are modulated by the local structure of monomer linkage. Owing to the widespread application of these materials, precise understanding of the relationship between synthesis and properties of the final product is of high relevance. Metallocene catalysts are known for their tunability towards synthesizing polyolefins with different stereostructure, which is achieved by modifying the symmetry of the ligand (L) on an active catalyst, $[L_2MR^+X^-]$.[69–71] Polymerization takes place when the anion (X^-) is displaced by the incoming alkene. During the polymerization reaction, the active species exists in a complicated dynamic equilibrium with the counter anion, solvent, and probably other metal alkyl species.[69–72] Although metallocene catalyzed polymerization is efficient, it is subject to a decrease in catalytic activity through a number of side reactions, which vary depending on the type of ligand used.[69–71] Common side reactions include 2,1-misinsertion and β-hydride elimination.[70,73–75] Recently, evidence was found for a dormant

[1] Reproduced in part from "*In Situ* Determination of Tacticity, Deactivation, and Kinetics in [*rac*-(C_2H_4(1-Indenyl)$_2$)ZrMe][$B(C_6F_5)_4$] and [Cp_2ZrMe][$B(C_6F_5)_4$]-Catalyzed Polymerization of 1-Hexene Using ^{13}C Hyperpolarized NMR" by Chen, C.-H.; Shih, W.-C.; Hilty, C. *J. Am. Chem. Soc.* **2015**, *137*, 6965. Copyright [2015] by The American Chemical Society.

species, a Zr-allyl complex, which can be generated following β-hydride elimination. This complex may hinder propagation of the polymerization.[70,76–78] Such species are present in small amounts during the reaction and can undergo fast exchange between different coordinated structures, and hence have in the past been observed using ^{1}H NMR at low temperature.[76,79–81]

Here, we report a comprehensive characterization of the tacticity, kinetics and mechanisms of deactivation of two metallocene catalysts for olefin polymerization, [(EBI)ZrMe][B(C_6F_5)$_4$] and [Cp_2ZrMe][B(C_6F_5)$_4$], using highly sensitive *in-situ* ^{13}C NMR. Dissolution dynamic nuclear polarization (D-DNP),[82] a hyperpolarization technique to enhance NMR signal intensity by several orders of magnitude in a single scan, permits to detect analytes of sub-millimolar concentration and to follow a chemical reaction in real time within a time frame of seconds.[83–86] Using this technique, it becomes possible to observe the relevant species under room temperature reaction conditions, while making use of the large ^{13}C chemical shift dispersion for chemical identification. At the same time, the rate constants can be calculated by measuring the time evolution of signals stemming from the monomer, in the presence of the two different catalysts.

2.2 Results and Discussion

2.2.1 Time-Resolved Hyperpolarized NMR Spectra

For the metallocene-catalyzed polymerization reactions, 1-hexene was chosen as the monomer. Signal enhancements of >2000 were obtained for this molecule, when compared to single-scan ^{13}C spectra acquired without hyperpolarization in a 9.4 T NMR

magnet. This signal gain was sufficient to carry out NMR spectroscopy at natural ^{13}C isotope abundance. In order to allow the observation of catalyst-polymeryl species, a variable amount of catalyst between 0.8–6.7 mol % was used. During the observation window of 12.8 s, a short chain polymer representative of the early stage of the polymerization reaction is obtained. Figure 2-1 shows the time evolution of ^{13}C NMR signals obtained from 1-hexene in the presence of [(EBI)ZrMe][$B(C_6F_5)_4$] or [Cp_2ZrMe][$B(C_6F_5)_4$], respectively. The strongest observed signals in these spectra stem from a hyperpolarized monomer. Additionally, significant oligomer signals can be identified in the first hyperpolarized ^{13}C spectrum obtained 0.45 s after mixing of the monomer with the catalyst. A hyperpolarized ^{1}H coupled ^{13}C spectrum of the [(EBI)ZrMe][$B(C_6F_5)_4$] catalyzed reaction further shows the expected multiplet patterns in peaks between 14 and 41 ppm, confirming oligomer formation (Figure 2-2).

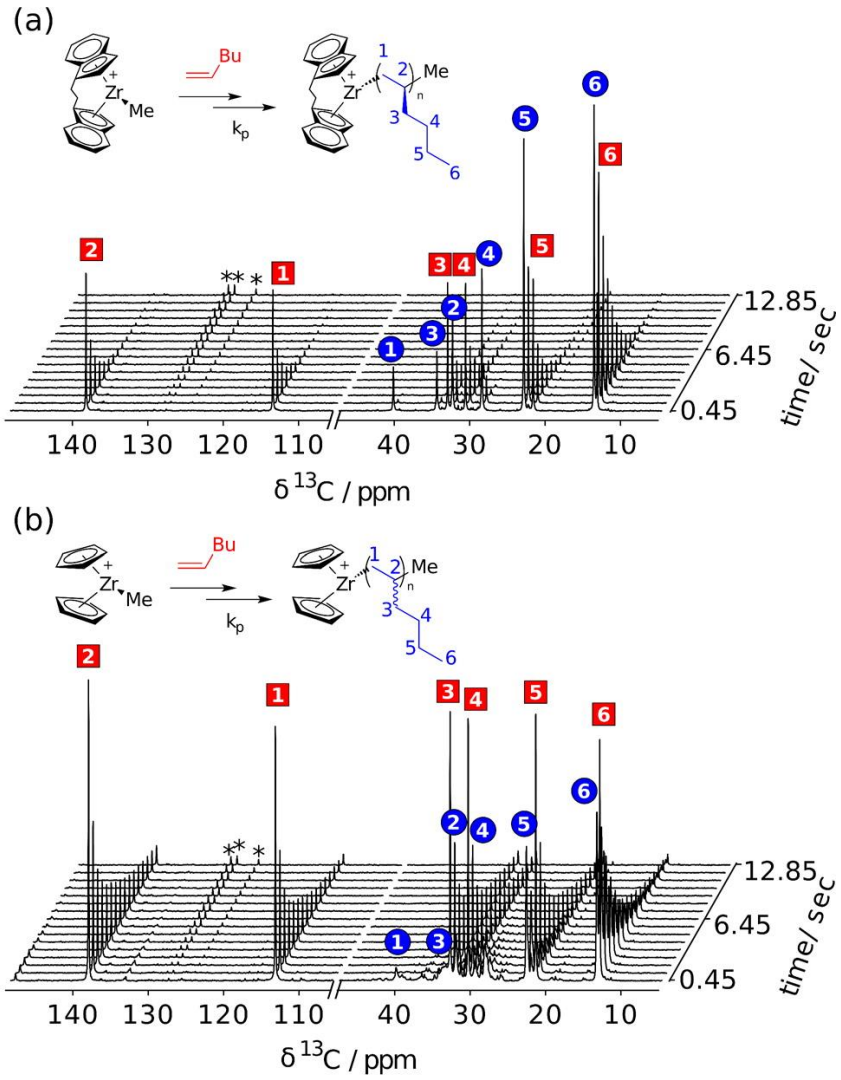

Figure 2-1. Regions from hyperpolarized ^{13}C NMR spectra acquired during the polymerization of 1-hexene in toluene, at 298 K, using 6.7 mol % of (a) [(EBI)ZrMe][$B(C_6F_5)_4$] and (b) [Cp_2ZrMe][$B(C_6F_5)_4$]. Numbers in square boxes indicate signals from 1-hexene, and numbers in circles indicate polymer signals. Signals from toluene are designated with *. The anion, $B(C_6F_5)_4^-$, is not shown in the reaction scheme.

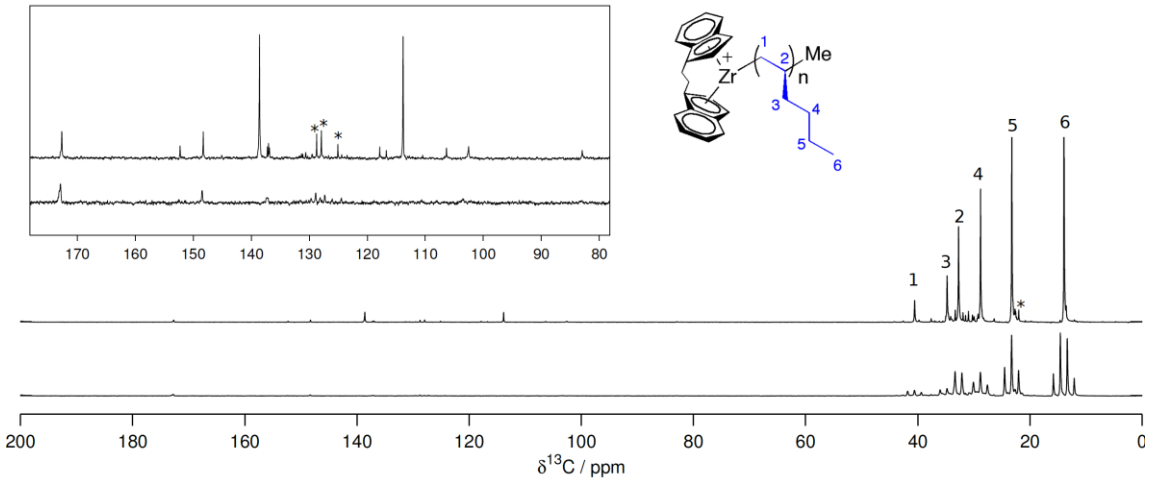

Figure 2-2. (a) ^{1}H-decoupled and (b) ^{1}H-coupled ^{13}C hyperpolarized NMR spectra of [(EBI)ZrMe][B(C_6F_5)$_4$] catalyzed 1-hexene polymerization. * designates toluene signals.

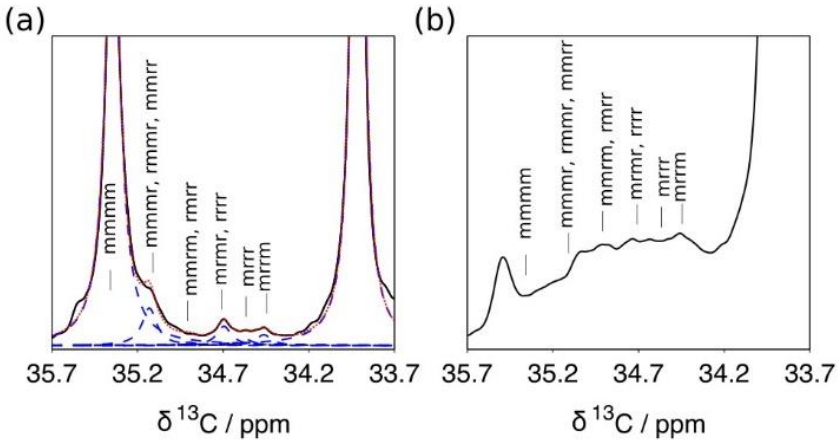

Figure 2-3. Regions from hyperpolarized ^{13}C NMR spectra acquired during the polymerization of 1-hexene in toluene, at 298 K, using 6.7 mol % of (a) [(EBI)ZrMe][B(C_6F_5)$_4$] and (b) [Cp_2ZrMe][B(C_6F_5)$_4$]. Figure 2-3 (a) and (b) are enlarged views of C3 signals of poly(-1-hexene) from the time points at 0.45 s from Figure 2-1. Pentad chemical shifts are labeled.[87] The red and blue dotted lines are results from Lorentzian line shape fitting.

Since the ^{13}C chemical shifts in the polymer are sensitive to the adjacent chemical structure, contributions to the signal from different elements of tacticity can be calculated from ^{13}C NMR.[70,87,88] An enlarged view of the spectral region containing the C3 signal from the hyperpolarized experiment is shown in Figure 2-3a,b. Under the assumption that spin–lattice relaxation affects the C3 atom in all pentads equally, the signal intensity of each peak in the hyperpolarized spectrum is proportional to the concentration of the respective isomer.

For the catalyst [(EBI)ZrMe][$B(C_6F_5)_4$], from the data in Figure 2-3a and three additional data sets, the relative intensity of the isotactic pentad mmmm was calculated to be 86–89% (Table 2-1) on the basis of the chemical shift assignments from ref. 87. Values for other pentads are given in Table 2-2. The catalytic environment of [(EBI)ZrMe][$B(C_6F_5)_4$], with C_2 symmetry in the ansa-metallocene, is expected to give rise to a high contribution from the isotactic form.[87,88]

Table 2-1. Experimental parameters and rate constants obtained from metallocene-catalyzed 1-hexene polymerization in toluene at 298 K. Rate constants were determined from the experimental data using the kinetic model described in the text. Isotacticity was determined from Lorentzian lineshape fitting.

Entry	Ligand	[Zr] /mM	[Zr] /mole %	$k_{p(obs)}$ /s^{-1}	k_d /s^{-1}	k_p /$M^{-1}s^{-1}$	r_p /s^{-1}	Isotacticity / %
1	EBI	19	6.7	0.56	0.15	29	0.90	86
2	EBI	19	6.7	0.36	0.13	19	1.01	88
3	EBI	10	3.4	0.62	0.14	65	1.08	88
4	EBI	10	3.4	0.65	0.12	68	1.04	87
5	EBI	5	1.7	0.30	0.10	63	1.06	86
6	EBI	5	1.7	0.30	0.08	63	1.02	89
7	EBI	2	0.8	0.08	0.13	34	0.98	N.A.
8	EBI	2	0.8	0.08	0.10	34	0.90	N.A.
9	Cp_2	19	6.7	1.73	0.90	97	0.88	N.A.
10	Cp_2	19	6.7	1.85	0.90	91	0.90	N.A.
11	Cp_2	10	3.4	0.97	0.93	102	0.94	N.A.
12	Cp_2	10	3.4	0.88	0.87	93	0.93	N.A.
13	Cp_2	5	1.7	0.43	0.88	91	0.98	N.A.
14	Cp_2	5	1.7	0.51	0.81	107	1.00	N.A.
15	Cp_2	2	0.8	0.03	0.99	13	0.87	N.A.
16	Cp_2	2	0.8	0.04	0.80	17	1.02	N.A.

[1-hexene]=0.283 M was determined from a conventional ^{1}H NMR spectrum without the addition of catalysts. Values of $k_{p(obs)}$ and k_d are obtained using methods described in section 2.2.3 Kinetic Analysis of Hyperpolarized NMR Signals and section 2.4.6 Analysis of Kinetic DataStandard deviations of $k_{p(obs)}$ and k_d determined from three set of $r_M + \lambda$ are shown in Figure 2-10.

Table 2-2. Relative pentad signal intensity and linewidth of the C3 of poly(-1-hexene) synthesized from [(EBI)ZrMe][B(C_6F_5)$_4$] in hyperpolarized and nonhyperpolarized measurement.

pentad	hyperpolarized ^{13}C at 298 K	nonhyperpolarized ^{13}C at 298 K	nonhyperpolarized ^{13}C at 368 K
mmmm	0.86	0.86	0.88
mmmr,rmmr,mmrr	0.07	0.07	0.06
mmrm,rmrr	0.01	0.02	0.01
mrmr,rrrr	0.04	0.03	0.03
mrrr	0.01	0.01	0.02
mrrm	0.02	0.02	0.01
Polymer linewidth[a]/Hz	5.3	5.1	3.7
Monomer linewidth[a]/Hz	1.7	-	-

[a] 5 Hz was subtracted from the measured line width to account for the window function.

For comparison, spectra of the products of the corresponding quenched reaction measured without hyperpolarization yielded a similar contribution of 88% mmmm (Table 2-2 and Figure 2-4). For polymers of short chain length, different chemical shifts from terminal units can potentially change the apparent contribution from isotacticity in both experiments. A polymer produced in a glovebox using a smaller amount of catalyst to obtain a longer chain length, however, also yielded an isotacticity of 85%. Therefore, under the present conditions, terminal effects do not appear to be dominant. For comparison, in the reaction with a catalytic environment of C_{2v} symmetry ([Cp_2ZrMe][B(C_6F_5)$_4$], Figure 2-3b) a broader distribution of polymer signals is observed. This distribution is a characteristic feature of atactic polymers due to the irregular sequence of side chain arrangements.[89,90]

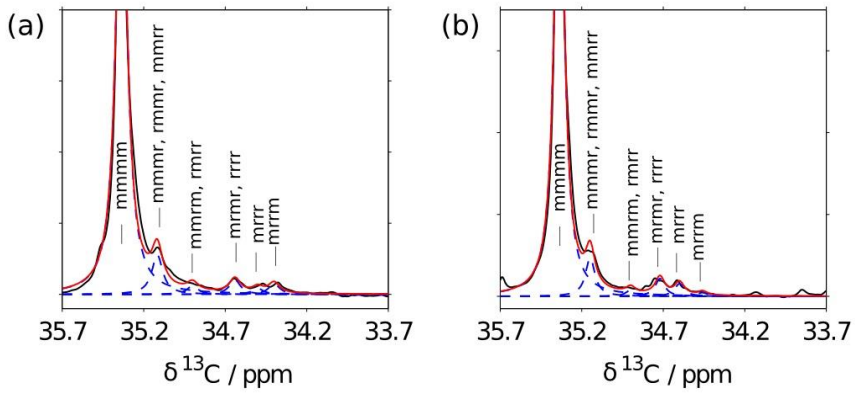

Figure 2-4. Lorentzian fitting of C3 signal intensity of quenched product from Figure 2-1a and Figure 2-3a. (a) $^{13}C\{^{1}H\}$ spectrum acquired at 298 K and (b) $^{13}C\{^{1}H\}$ spectrum acquired at 343 K. Data were acquired using 30 degree pulses with a field strength γB_1=20.83 kHz, acquisition time of 2.38 s, and 8000 transients by a Bruker 500 MHz spectrometer equipped with a triple resonance HCN cryoprobe with Z-gradient (Bruker Biospin, Billerica, MA).

2.2.2 Observation of Minor Species in Hyperpolarized Spectra

A closer viewing of the spectra from the *in situ* reaction reveals small signals in addition to those from a monomer or oligomer, which *prima facie* may stem from reaction intermediates or side products (Figure 2-5 and the inset in Figure 2-2). Commonly occurring side products are vinylidene-terminated polymer chains, which can form through β-hydride elimination.[70,73,74] ^{1}H NMR spectra acquired after the hyperpolarized experiment reveal the existence of unsaturated olefin species in the range of 4.1−6.3 ppm (Figure 2-6). Due to the presence of chemical shifts from the catalyst in the same spectral region (Figure 2-6a), the identification of signals in ^{13}C NMR would however, be preferred. In particular, the quaternary carbon of the vinylidene species should be favorable for observation by dissolution DNP, since its long T_1 relaxation time leads to reduced signal attenuation during the experiment. Hyperpolarized ^{13}C NMR spectra

acquired without ^{1}H decoupling indeed show two sets of singlet peaks stemming from carbon atoms not bonded to protons, at 148.8 and 173.3 ppm with [(EBI)ZrMe][$B(C_6F_5)_4$] and at 148.8 and 166.8 ppm with [Cp_2ZrMe][$B(C_6F_5)_4$].

The identity of the atoms giving rise to these peaks can be elucidated by an experiment designed to correlate chemical shifts between reactant and product species. This type of experiment, similar to exchange spectroscopy but applied to a nonreversible chemical reaction, is a unique option in the dissolution DNP experiment.[86,91] Such correlation experiments were performed by injecting the hyperpolarized monomer into the NMR spectrometer, applying a selective inversion pulse on a peak of interest from the reactant, admixing the catalyst using a syringe pump, and acquiring a series of NMR spectra (see section 2.4.4 Inversion Experiment with Dual Injection and Scheme 2-1). In the spectra obtained with inversion of the C2 signal of the monomer, all four of the above identified peaks were inverted, indicating that they originate from this atom. As the signals at 148.8 ppm are identical in the spectra with either of the two catalysts, they likely stem from the vinylidene group[92–94] (**1′** in Figure 2-5), which is not associated with the catalyst. Correlations to ^{1}H chemical shifts at 4.87 and 4.89 ppm in a nonhyperpolarized heteronuclear multibond correlation spectrum ([^{13}C,^{1}H]-HMBC) of the quenched product further support the identification of this species (Figure 2-6b and Figure 2-7).

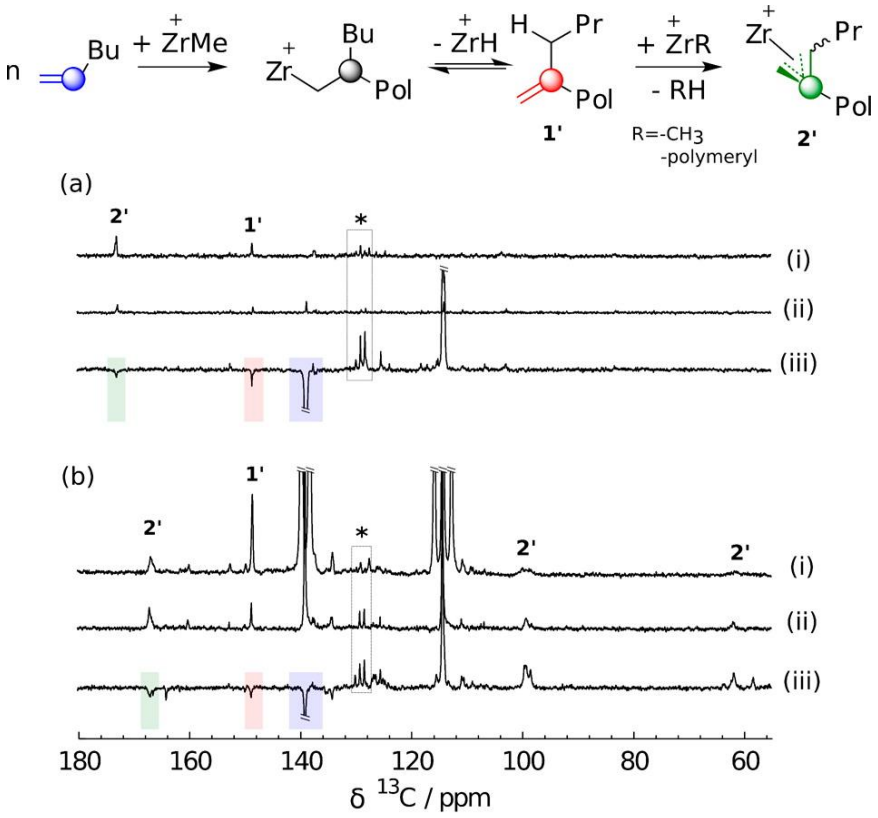

Figure 2-5. Spectra used for identification of different species in the reactions using (a) [(EBI)ZrMe][$B(C_6F_5)_4$] and (b) [Cp_2ZrMe][$B(C_6F_5)_4$], respectively. Both panels contain ^{13}C hyperpolarized spectra with *J*-coupling to ^{1}H (i), ^{1}H decoupled ^{13}C hyperpolarized spectra (ii), and ^{13}C hyperpolarized spectra with selective inversion of the C2 resonance of 1-hexene at the beginning of the reaction (iii). Peaks denoted with **1** are assigned to vinylidene, and those with **2** are assigned to the Zr-allyl complex. Signals from toluene are designated with *.

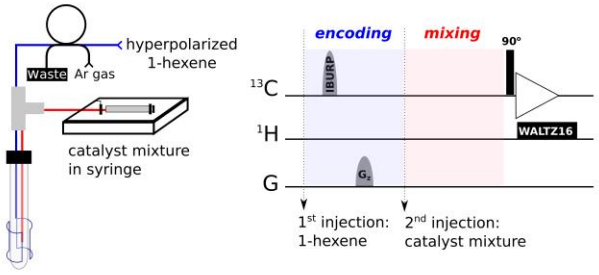

Scheme 2-1. Schematic illustration of two-component sample injection (left) and pulse sequence diagram (right) for selective inversion experiment.

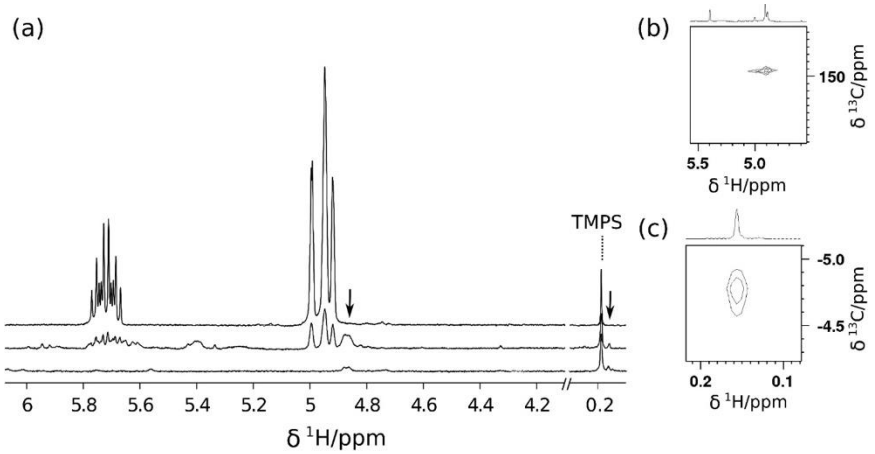

Figure 2-6. (a) Region of ^{1}H NMR spectra of 1-hexene polymerization acquired after hyperpolarized measurement without catalyst (top) or with $[Cp_2ZrMe][B(C_6F_5)_4]$ (middle) and $[(EBI)ZrMe][B(C_6F_5)_4]$ (bottom). Trimethylphenylsilane (TMPS) was used as internal standard. Arrows indicate peaks of interest, and the related cross peaks are shown in (b) [^{13}C,^{1}H]-HMBC spectrum from quenched 1-hexene polymerization catalyzed by $[(EBI)ZrMe][B(C_6F_5)_4]$ and (c) [^{13}C,^{1}H]-HSQC spectrum of $[Cp_2ZrMe][B(C_6F_5)_4]$-catalyzed 1-hexene polymerization prepared directly in the glovebox.

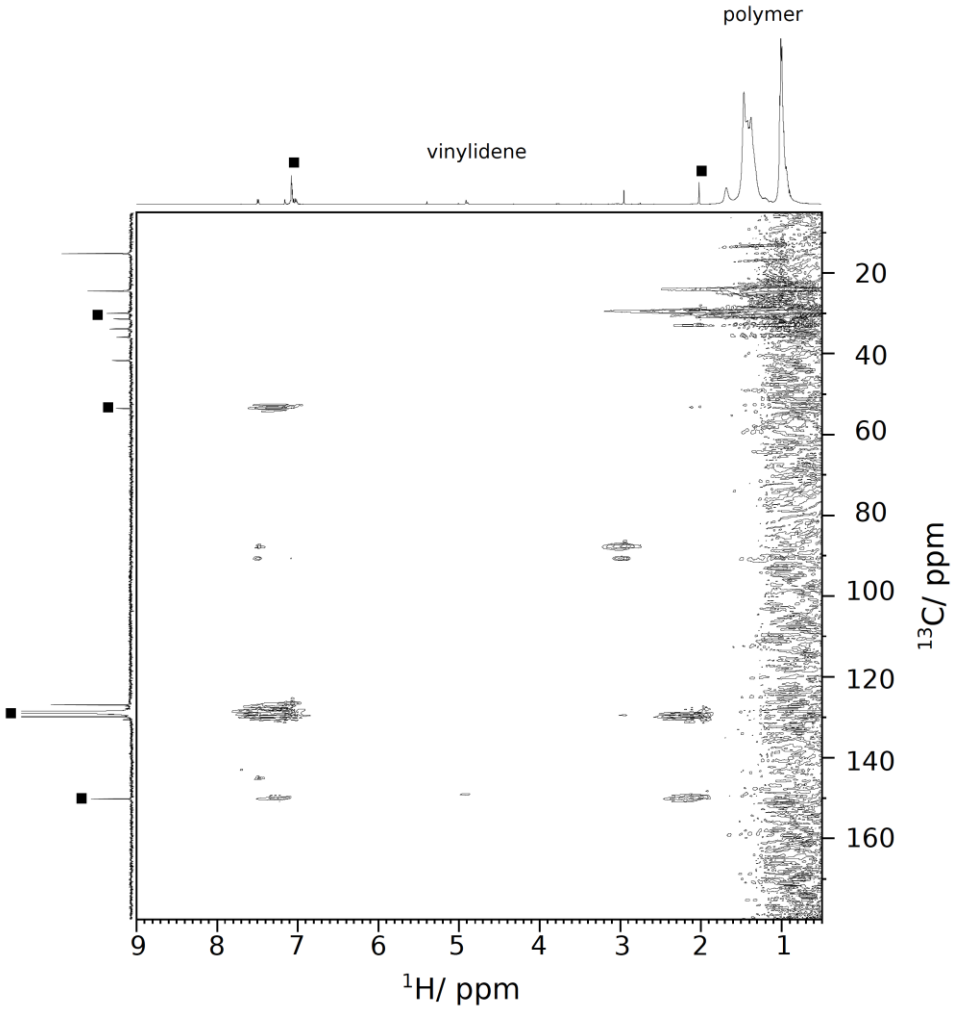

Figure 2-7. [^{13}C,^{1}H]-HMBC spectrum of quenched 1-hexene polymerization catalyzed by[(EBI)ZrMe][B(C_6F_5)$_4$] at 298 K. Peaks designated with (▪) are assigned as CPh_3Me.[95] The spectrum was obtained via heteronuclear zero and double quantum coherence optimized for long range coupling between 2 to 5 Hz using accordion with two-fold low-pass J-filter to suppress one-bond correlations with decoupling during acquisition. A detailed acquisition parameters are: 0.2 s acquisition time, a 10 ppm spectral window in ^{1}H, a 180 ppm spectral window in ^{13}C, a 1 s relaxation delay, and 160 transients. Benzene-d_6 was used as solvent.

The signals at 173.3 and 166.8 ppm, which are specific to the catalyst type, likely stem from a Zr-allyl complex (**2′**), which has been described,[76,79,80] but to our knowledge not previously been observed by NMR under typical reaction conditions at room temperature. A similar chemical shift of 162 ppm was reported for the quaternary carbon of [$Cp_2Zr^+(\eta^3\text{-}CH_2C(CH_2R)CH_2)$], a model complex stable at 0 °C.[79] Additional signals observed in the DNP spectra, also indicated in Figure 2-5b, appear to support the existence of the Zr-allyl complex in the polymerization reaction. These chemical shifts are within 7 ppm of the reported chemical shifts of [$Cp_2Zr^+(\eta^3\text{-}CH_2C(Me)CHR)$] at 57 ppm (allyl CH_2), 106 ppm (allyl CH) or [$Cp_2Zr^+(\eta^3\text{-}CH_2C(CH_2R)CH_2)$] at 67 and 68 ppm (allyl CH_2).[79] The Zr-allyl signal (allyl CH) from [(SBI)Zr(CH_2SiMe_3)][$B(C_6F_5)_4$] (SBI = *rac*-Me_2Si(indenyl)$_2$) has been observed at 80 and 84 ppm by Landis et al.[76] by using a ^1H–^{13}C HSQC and 1-^{13}C labeled 1-hexene at −40 °C. The hyperpolarized spectrum in Figure 2-2 also reveals a similar chemical shift at 83.6 ppm.

The existence of noncoordinated vinylidene during the polymerization suggests that the Zr-allyl complex was generated via the previously proposed mechanism, where the Zr-polymeryl complex undergoes β-hydride elimination to generate a vinylidene-terminated polymer, which further recoordinates with the active catalyst, a Zr-methyl cation, to form a Zr-allyl complex and results in the release of methane.[76] A signal at 0.16 ppm (^1H)/–4.8 ppm (^{13}C) in a nonhyperpolarized [^{13}C,^1H]-HSQC spectrum of the product from a reaction performed in the glovebox was assigned as methane and further supports the presence of this mechanism (Figure 2-6c and Figure 2-8).[69–71]

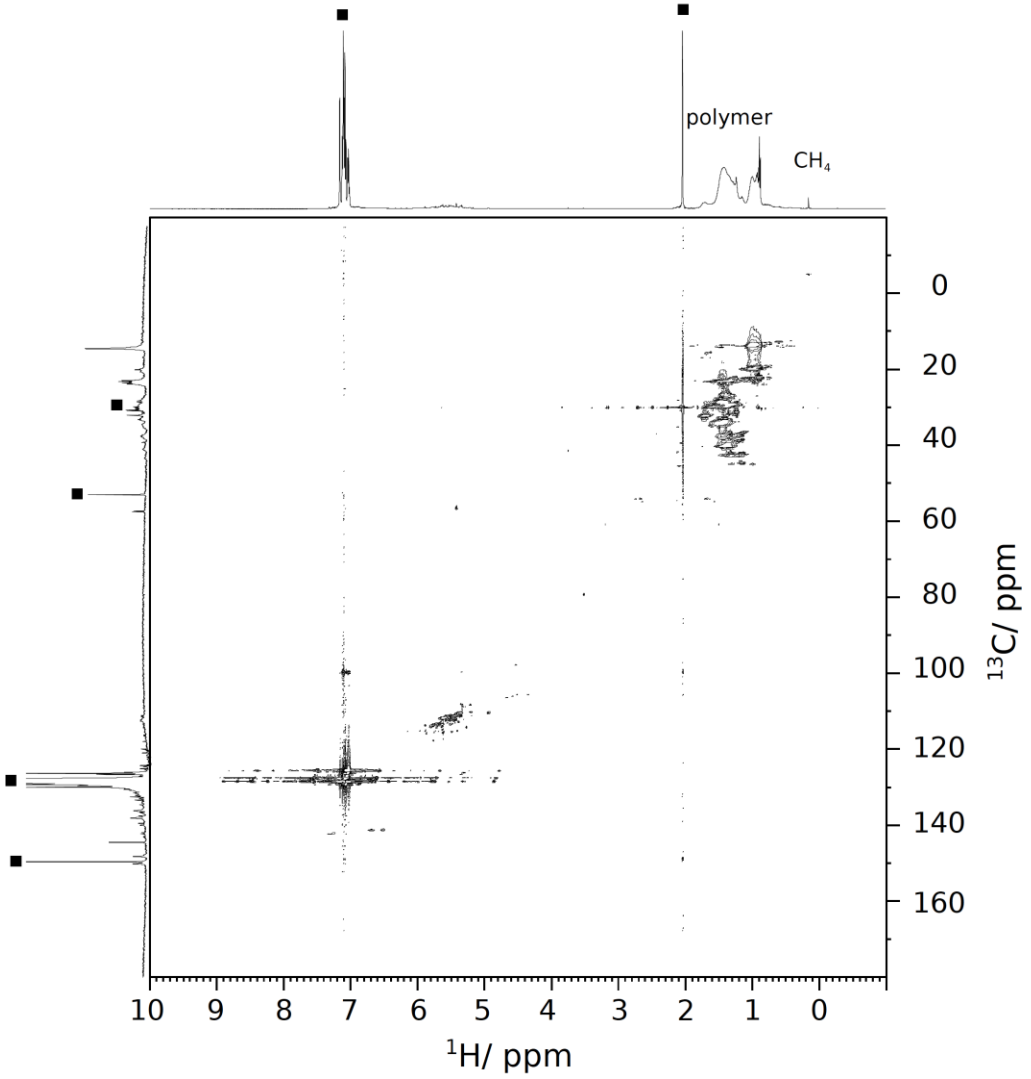

Figure 2-8. **[**^{13}C,^{1}H]-HSQC spectrum of [Cp_2ZrMe][$B(C_6F_5)_4$] catalyzed 1-hexene polymerization prepared directly in the glove box. Peaks designated with (▪) are assigned to CPh_3Me[2]. **S**pectrum was recorded at 298 K by 0.17 s acquisition time, a 12 ppm spectral window in ^{1}H, a 250 ppm spectral window in ^{13}C, 2 s relaxation delay, and 4 transients, and using enzene-d_6 as solvent.

2.2.3 Kinetic Analysis of Hyperpolarized NMR Signals

The Zr-allyl complex is considered a dormant species with low activity toward olefin insertion and low reinitiation probability.[70,76–78] Formation of this complex can be considered as a deactivation mechanism for the polymerization reaction. Kinetic rate constants pertaining to polymerization, as well as to deactivation by this or other mechanisms, can be determined from the time-resolved DNP-NMR spectra. In the absence of catalyst deactivation, such as in a living polymerization (Scheme 2-2a), the monomer consumption follows a pseudo-first-order rate law.

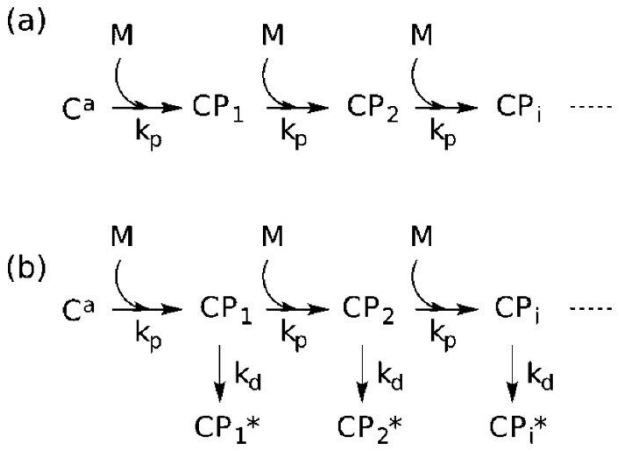

Scheme 2-2. Proposed kinetic pathways for the 1-hexene polymerization. (a) Living polymerization. (b) Polymerization with deactivation. C^a is the activated catalyst, CP_i is the catalyst-polymeryl species, and CP_i* is the deactivated catalyst-polymeryl species. k_p and k_d are second- and first-order rate constants, respectively.

Considering the spin up and spin down concentration, the monomer signal evolution in the hyperpolarized NMR experiment can be described by[84,86]

$$\frac{d}{dt}S_M = -(r_M + \lambda)S_M - k_{p(obs)}S_M \tag{2-1}$$

The first term originates from the intrinsic monomer spin–lattice relaxation, r_M, and the signal loss due to the application of small flip angle pulses ($\lambda = -\ln(\cos\alpha)/\Delta t$, with Δt as the time delay between scans and α as the flip angle of radio frequency excitation). The second term is due to the depletion of the monomer signal from the polymerization process by a rate constant, $k_{p(obs)} = k_p[C]_0$. The analytical solution of equation (2-1) can be written in logarithmic form:

$$ln\big(S_M(t)\big) - ln\big(S_M(0)\big) = -\big(r_M + \lambda + k_{p(obs)}\big)t \tag{2-2}$$

The above equation indicates a pseudo-first-order time dependence, characterized by a straight line with slope $r_M + \lambda + k_{p(obs)}$. The data from peak integration in Figure 2-9 however indicate that the rate constant for monomer consumption is larger at the beginning of the reaction, as evidenced by the nonlinear appearance of the plot of $\ln(S_M)$ against time. Hence, a modified kinetic model (Scheme 2-2b) is proposed to account for the decreasing catalytic activity. An assumption is made that the catalyst-polymeryl species, CP_i, undergoes a first-order deactivation process, with a rate constant k_d, to yield

a terminal species CP_i*. In this case, the time evolution of monomer signal can be described by

$$\frac{d}{dt}S_M = -(r_M + \lambda)S_M - k_{p(obs)}e^{-k_d t}S_M \tag{2-3}$$

where the rate of monomer signal decay is further affected by an exponential factor dependent on k_d. In logarithmic form, the time evolution of hyperpolarized monomer signal in the presence of this deactivation mechanism becomes

$$ln\big(S_M(t)\big) - ln\big(S_M(0)\big) = -(r_M + \lambda)t - \big(k_{p(obs)}/k_d\big)(1 - e^{-k_d t}) \tag{2-4}$$

(see also section 2.4.6 Analysis of Kinetic Data). This equation fits the hyperpolarized signal more closely than the simple exponential equation (2-2) supporting the presence of a deactivation mechanism in the present reaction. A comparison of the two data sets in Figure 2-9 shows a more significant deactivation (larger curvature) in $[Cp_2ZrMe][B(C_6F_5)_4]$. Although kinetic data cannot directly be used to identify the deactivation mechanism, notably this catalyst also gives rise to stronger signals identified as the Zr-allyl complex and vinylidene in the hyperpolarized ^{13}C spectra in Figure 2-5.

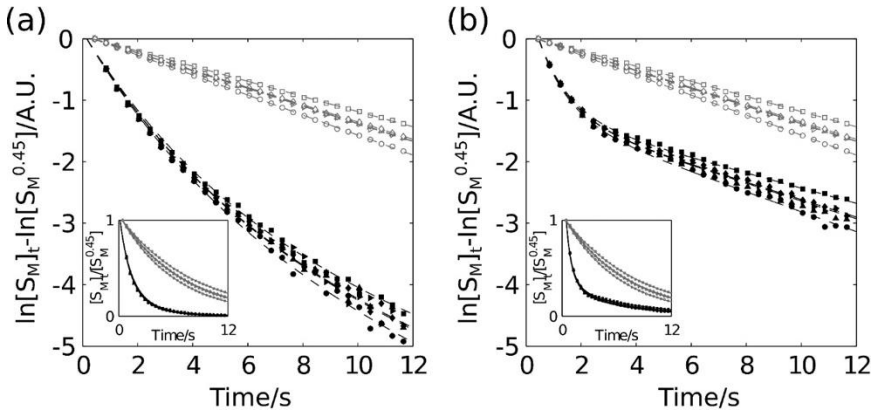

Figure 2-9. Time evolution of signal integrals (logarithmic scale) of monomer C1 to C5 from hyperpolarized NMR of polymerization reaction catalyzed by (a) [(EBI)ZrMe][$B(C_6F_5)_4$] and (b) [Cp_2ZrMe][$B(C_6F_5)_4$] from Figure 2-1 (filled symbols). In both panels, empty gray symbols are from measurements without the catalyst. The black fitted lines were obtained using equation (2-4), and the gray fitted lines were obtained using an exponential time dependence. The insets show the integrals on a linear scale.

2.2.4 Dependence of Observed Rates on Catalyst Concentration

A series of experiments were performed to determine the influence of catalyst concentration, starting from 0.8 mol %. Representative signals from these experiments are shown in Figure 2-10a and Figure 2-10b. A decrease in catalyst concentration reduces the relative contribution of the second term in equation (2-4). Hence, the signal intensities decrease less rapidly, and the curvature becomes less pronounced. Eventually, the time course of the monomer signal approaches the straight line obtained in the absence of catalyst. This behavior is observed at the catalyst concentration of 0.8 mol %, which is close to the lower limit of the concentration range that can be investigated with this method.

The rate constants calculated from the hyperpolarized ^{13}C NMR data sets at all concentrations are summarized in Table 2-1. These values were determined by

simultaneously fitting all signals from C1 to C5 of the monomer, as shown in Figure 2-9, Figure 2-11, and Figure 2-12 using the parameter $r_M + \lambda$ found from experiments in the absence of catalyst (Table 2-3).

Table 2-3. Calculated $r_M + \lambda$ from replacing the catalyst solution to pure fluorobenzene. Values were calculated using equation (2-1).

Entry	$r_M + \lambda(C_1)/s^{-1}$	$r_M + \lambda(C_2)/s^{-1}$	$r_M + \lambda(C_3)/s^{-1}$	$r_M + \lambda(C_4)/s^{-1}$	$r_M + \lambda(C_5)/s^{-1}$
1	0.160	0.122	0.141	0.142	0.139
2	0.163	0.124	0.144	0.145	0.142
3	0.162	0.123	0.142	0.144	0.142

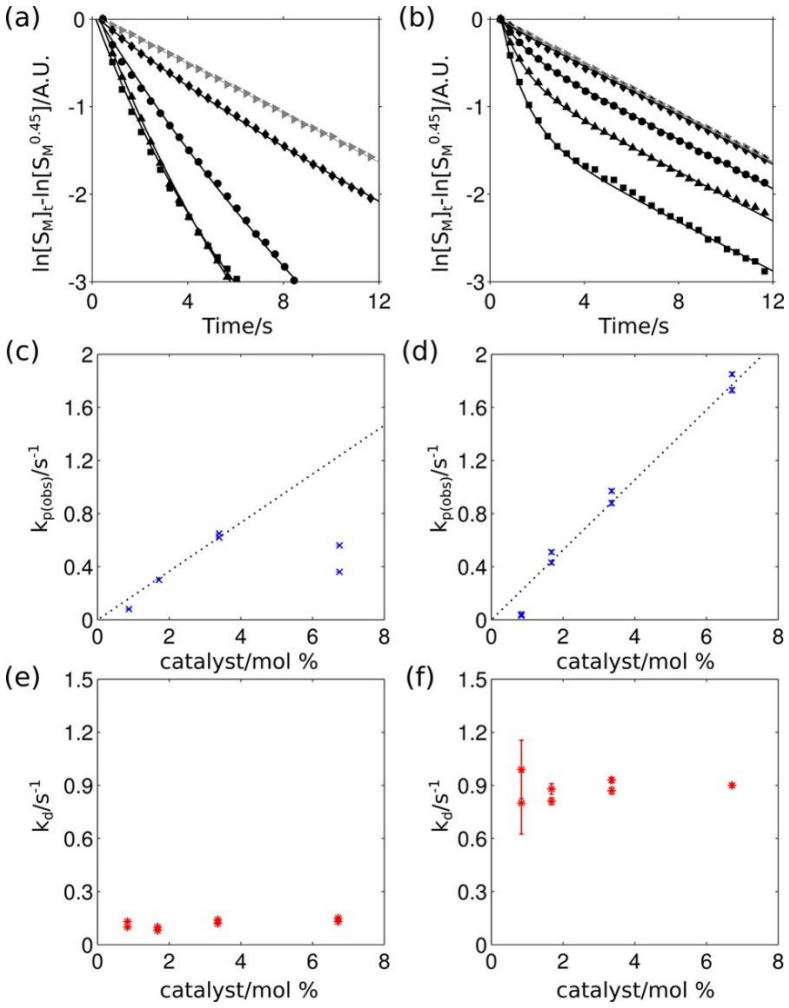

Figure 2-10. (a,b) Time evolution of signal integrals of C5 and (c–f) rate constants $k_{p(obs)}$ and k_d, determined from hyperpolarized ^{13}C NMR at different catalyst concentrations of (a,c,e) [(EBI)ZrMe][$B(C_6F_5)_4$] and (b,d,f) [Cp_2ZrMe][$B(C_6F_5)_4$]. The $k_{p(obs)}$ and k_d were calculated from the solid lines in (a) and (b), which were obtained using equation (2-4). Error bars represent the standard deviation from three separate reference sets of $r_M + \lambda$. The dotted line is a linear fit of the $k_{p(obs)}$ with respect to concentration.

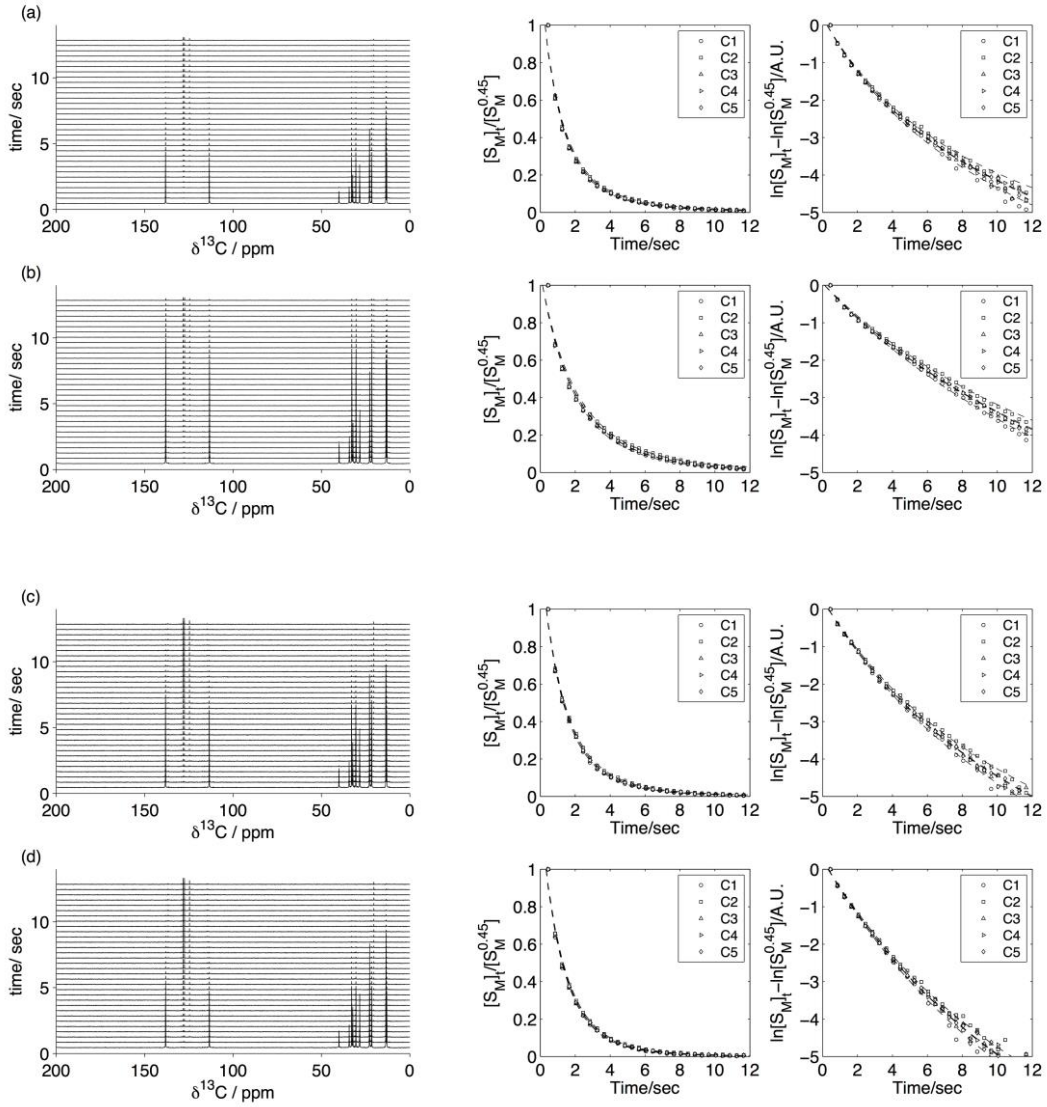

Figure 2-11. Hyperpolarized ^{13}C NMR spectra (left), time evolution signal on logarithmic scale fitted with equation (2-18) (right), and on linear scale (middle) of 1-hexene polymerization catalyzed by [(EBI)ZrMe][$B(C_6F_5)_4$] in toluene at 298 K. Data are from (a-h) entry 1 to entry 8 of Table 2-1.

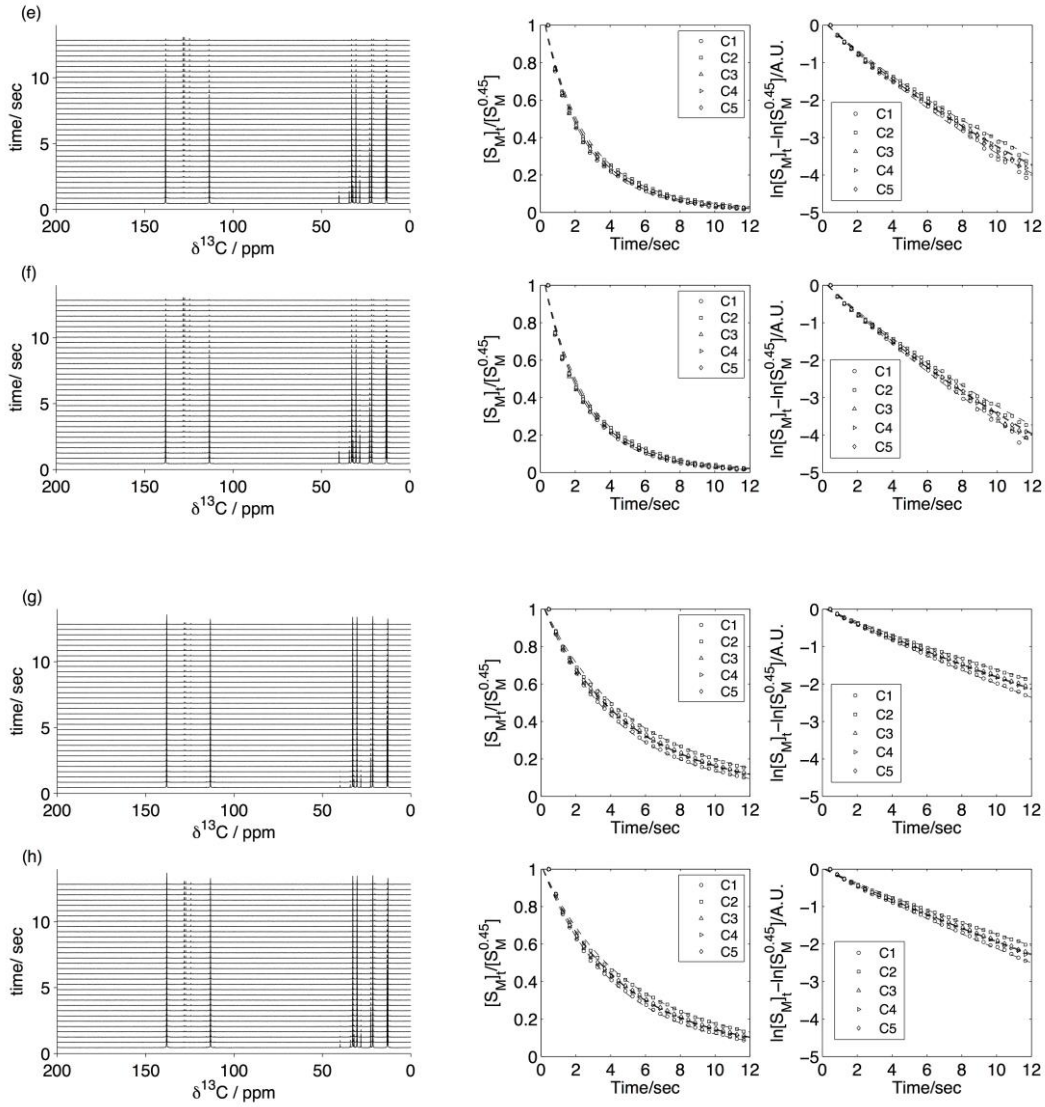

Figure 2-11. Continued.

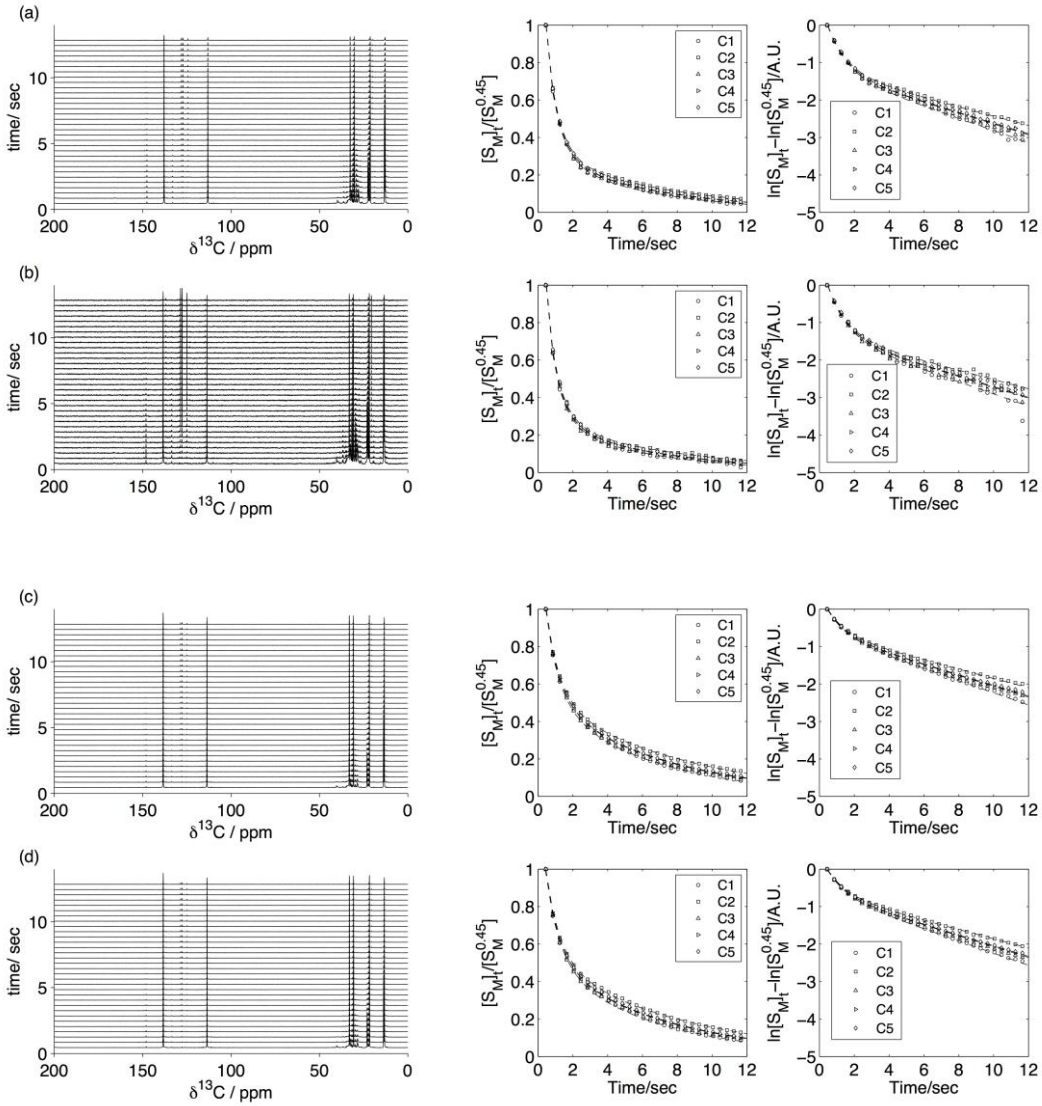

Figure 2-12. Hyperpolarized ^{13}C NMR spectra (left), time evolution signal on logarithmic scale fitted with equation (2-18) (right), and on linear scale (middle) of 1-hexene polymerization catalyzed by $[(Cp)_2ZrMe][B(C_6F_5)_4]$ in toluene at 298 K. Data are from (a-h) entry 9 to entry 16 of Table 2-1.

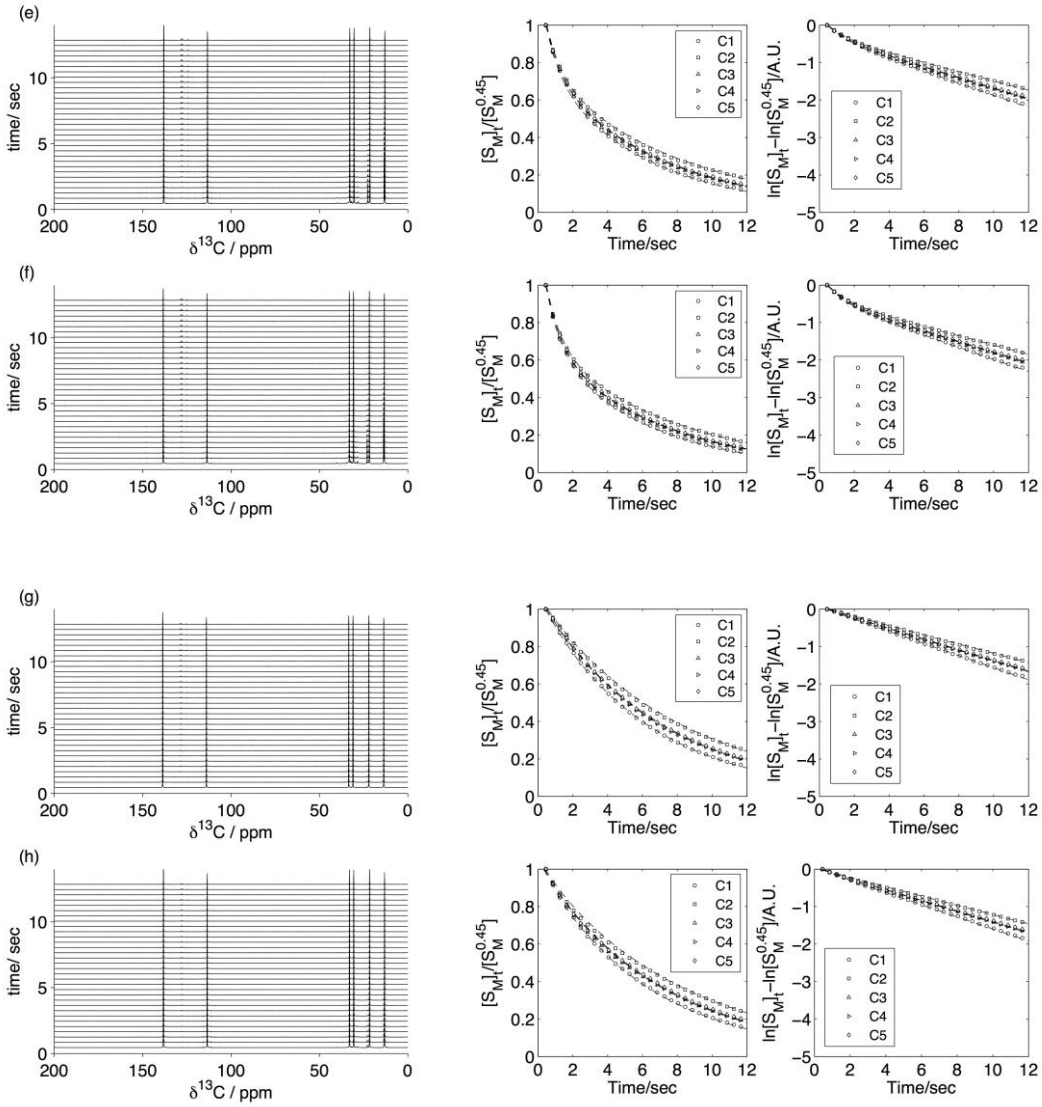

Figure 2-12. Continued.

The concentration dependence of the determined rate constants is plotted in Figure 2-10c−f. The data points in general follow a linear trend, with a positive slope for $k_{p(obs)}$ indicating a second-order process for the polymerization reaction. At the highest catalyst concentration, 6.7 mol %, the $k_{p(obs)}$ determined using [(EBI)ZrMe][$B(C_6F_5)_4$] fluctuates and falls below the linear trend. We attribute this behavior to low solubility of the activated catalyst in toluene, supported by visual observation of a precipitate, which can lead to an underestimated k_p value. At the lowest catalyst concentration of 0.8 mol % of [Cp_2ZrMe][$B(C_6F_5)_4$], the time course of the signal approaches that without catalyst. This results in a larger variation of the $k_{p(obs)}$ and k_d calculated on the basis of three independently measured values for $r_M + \lambda$, as shown in Figure 2-10d,f.

The averaged k_p from the linear fit is 65 M^{-1} s^{-1} for [(EBI)ZrMe][$B(C_6F_5)_4$] and 95 M^{-1} s^{-1} for [Cp_2ZrMe][$B(C_6F_5)_4$]. The rate constant k_p is 4 times higher than that observed in a study by Christianson et al.,[96] which was obtained using stopped-flow NMR of 1-hexene polymerization with nonhyperpolarized ^1H NMR. The higher k_p in the present study may be due to the use of $[B(C_6F_5)_4]^-$ as a weaker counteranion, which is believed to increase the reactivity.[72] In contrast to the rate constant for polymerization, the observed rate constant for the deactivation process, k_d, is independent of catalyst concentration. This property indicates that the dominant deactivation mechanism under these conditions is a first-order reaction and supports the idea that an extrapolation to even lower catalyst concentrations may be valid. Concomitantly with the curvature in the time course of monomer signal intensities due to deactivation, signals pertaining to Zr-allyl species are

observed in spectra acquired after a single 90° pulse at all but the lowest catalyst concentrations (Figure 2-13).

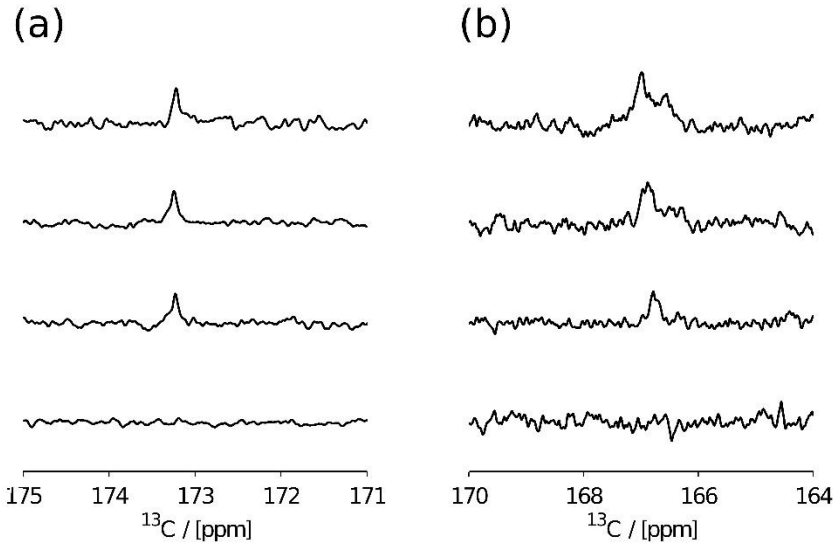

Figure 2-13. Selected region of Zr-allyl species measured from hyperpolarized NMR in the presence of 6.7, 3.4, 1.7, 0.8 mole % (from top to bottom) of (a) [(EBI)ZrMe][$B(C_6F_5)_4$] and (c) [Cp_2ZrMe][$B(C_6F_5)_4$].

A comparison of rate constants between two catalysts show a smaller k_p value for the ansa-metallocene [(EBI)ZrMe][$B(C_6F_5)_4$] to [Cp_2ZrMe][$B(C_6F_5)_4$], despite the larger access space to the coordination site of the former. While for a monomer such as propylene the ansa-metallocene catalyst would be expected to be more active, the interaction of the ligands on the catalyst with monomers can significantly influence the rate of catalysis.[97] For 1-hexene, Soga et al. found a lower activity in $Et(IndH_4)_2ZrCl_2$ compared to Cp_2ZrCl_2.[98] These two catalysts are similar in structure to those employed here and give rise to the same trend as seen in Figure 2-10c,d.

2.2.5 Observed Polymer Signals

The proposed model also allows calculation of the time dependence of signals from the polymer. Here, the relaxation rates of the polymer and deactivated polymeryl species are assumed to be identical and are denoted as r_P. The rate expression of the signal intensity of polymer can be described as

$$\frac{d}{dt}S_p = -(r_p + \lambda) * S_p + k_{p(obs)} * e^{-k_d * t} * S_M \qquad (2\text{-}5)$$

(see also section 2.4.6 Analysis of Kinetic Data). This time dependence was further examined with a numerical calculation, using $r_M + \lambda$ from Table 2-3, and $k_{p(obs)}$, k_d, $S_M(0)$ determined from the previous fitting step (equation (2-4)). The curves found by fitting with the remaining unknowns, r_P and $S_P(0)$, are shown in Figure 2-14 and Figure 2-15. As may be expected, the ratio of S_M/S_P at t = 0.45, i.e. the first acquired data point, is approximately proportional to the catalyst amount (Figure 2-14b,d), except for the highest concentration of [(EBI)ZrMe][B(C_6F_5)$_4$], which deviates due to solubility. Further, the obtained r_P values (Table 2-1) are within the expected range for the polymer size obtained, supporting the validity of the numerical values.

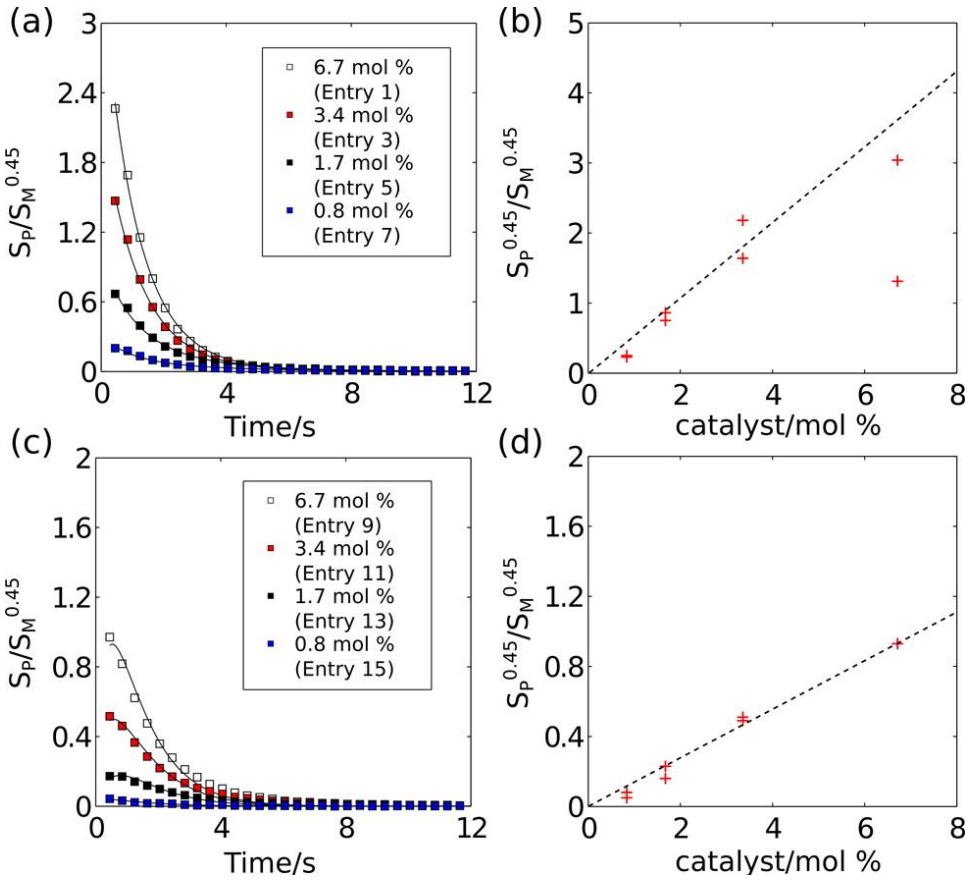

Figure 2-14. (a,c) Time evolution of signal integrals of polymer C5 from hyperpolarized ^{13}C NMR measurements. Solid lines are from the numerical fit based on equation (2-5). (b,d) Calculated ratio of polymer signal to monomer signal, S_P/S_M, at t = 0.45 s. (a) and (b) are from [(EBI)ZrMe][$B(C_6F_5)_4$]-catalyzed and (c) and (d) from [Cp_2ZrMe][$B(C_6F_5)_4$]-catalyzed 1-hexene polymerization.

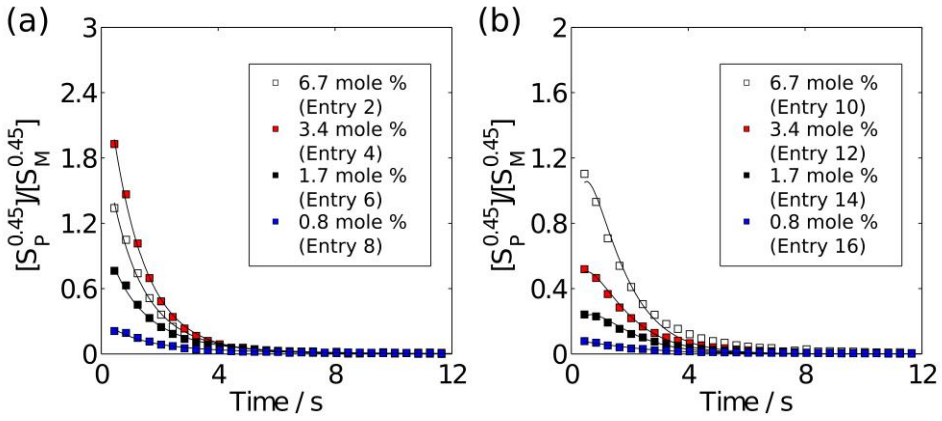

Figure 2-15. (a, c) Time evolution of signal integrals of polymer C5, from hyperpolarized ^{13}C NMR measurement. Solid lines are from the numerical simulation based on equation (2-4). (b, d) The result of calculated ratio of polymer signal to monomer signal at t = 0.45 sec. (a, c) [(EBI)ZrMe][$B(C_6F_5)_4$]-catalyzed and (b, d) [$(Cp)_2$ZrMe][$B(C_6F_5)_4$]-catalyzed 1-hexene polymerization. Other data are shown in Figure 2-14.

2.3 Conclusion

In summary, dissolution DNP-NMR permitted the simultaneous characterization of product tacticity, measurement of rate constants, and identification of deactivation processes in metallocene-catalyzed 1-hexene polymerization reactions. The stopped-flow DNP-NMR apparatus provided a sufficiently inert environment to enable study of the reactions with an air and moisture sensitive organometallic catalyst. Hyperpolarized 1-hexene, at natural isotope abundance, was used to detect the influence of a chiral and an achiral catalytic environment on the polymerization, without the need for postreaction quenching and separation processes. Reactive species such as a Zr-allyl complex difficult to capture under ambient temperature were readily detectable in the real-time NMR spectra. A quantitative model yielded rate constants for polymerization in the presence of a deactivation process. The dissolution DNP-NMR method is likely applicable to a broad

range of polymerization reactions and may provide valuable information for the design of catalysts yielding polymers with specific properties.

2.4 Experimental Section

2.4.1 Polymerization Reactions

Bis(cyclopentadienyl)dimethylzirconium(IV) and trityltetra(pentafluorophenyl) borate (cocatalyst) were purchased from Strem Chemicals, Inc., Newburyport, MA. *rac*-Ethylenebis(indenyl)dimethylzirconium(IV) was prepared according to literature procedures.[99] Toluene and fluorobenzene were dried over and distilled from NaK/Ph_2CO/18-crown-6 and stored in an Ar-filled glovebox. 1-Hexene was dried over and distilled from NaK/18-crown-6. All polymerization experiments were performed with 1.1 equiv of a cocatalyst and 1 mM trimethylphenylsilane (TMPS) as an internal standard. The catalyst activation was examined by the signal of [CPh_3Me] in ^{1}H NMR (δ 2.03, Me). Bridge complexes were also found in the spectrum at 298 K; those structures were omitted for clarity. Before the dissolution of the hyperpolarized sample, the activated catalytic ion pair was prepared by mixing the catalyst and the cocatalyst in 50 μL of fluorobenzene in an Ar-filled glovebox with subsequent transfer to a 5 mm NMR tube. Before installation of the NMR tube into the NMR instrument, the transfer line was purged with Ar gas to avoid moisture and oxygen from room air. After the hyperpolarized NMR measurement, the polymerization reaction was quenched with acidified methanol. The volatiles were removed by a rotary evaporator, and the generated polymer was extracted using a hexane and methanol mixture.

2.4.2 Dynamic Nuclear Polarization

A sample of 5 mM α,γ-bis-diphenylene-β-phenylallyl (BDPA; Sigma-Aldrich, St. Louis, MO; concentration is chosen for solubility) in 50 μL of neat 1-hexene (Alfa Aesar, Ward Hill, MA) was hyperpolarizd in a HyperSense system (Oxford Instruments, Abingdon, U.K.) at 1.4 K under the irradiation of microwaves at $\omega_e - \omega_N$ = 93.965 GHz and a power of 60 mW. After 4 h, the hyperpolarized sample was dissolved in 4 mL of hot toluene 800 kPa(g) and transferred into the rapid injection system by He gas.[100] A photodiode sensed the arrival of the hyperpolarized sample, at which point the hyperpolarized sample was rapidly injected by Ar gas into the NMR tube where the activated catalyst was preloaded (preloading was done in a glovebox before the experiment). The injection was accomplished with a forward pressure of 214 psi applied against a back pressure of 150 psi for 355 ms, followed by stabilization for 400 ms. The time t = 0 was defined as the midpoint between start and end of injection and mixing, and the first data point was acquired at t = 0.45 s. The final temperature was 298 K. Injection parameters were optimized using a ^{19}F pulsed field gradient experiment to ensure a homogeneous mixture,[85] and a Diels–Alder reaction was used as a stopped-flow control experiment.[86]

2.4.3 NMR Spectroscopy

The hyperpolarized ^{13}C NMR spectra were acquired using a Bruker 400 MHz NMR spectrometer equipped with a broad-band probe containing three pulse field gradients (Bruker Biospin, Billerica, MA) at a temperature of 298 K. The time evolution

NMR signal is measured with a pulse sequence, $[G_z\text{-}\alpha_x\text{-acquire}]_{x32}$. The NMR measurement was triggered after the hyperpolarized 1-hexene was delivered to the NMR tube. For each experiment, a data set with a total acquisition time of 12.8 s includes 32 transients separated by 400 ms. A randomized pulsed field gradient, G_z (35.5 G/cm, 1 ms), was applied to remove the residual coherence from the previous scan. A small flip angle, $\alpha = 16.65°$, with pulse strength $\gamma B_1 = 31.25$ kHz was applied after the G_z. During the acquisition, WALTZ-16 ^{1}H decoupling was applied with field strength $\gamma B_1 = 2.78$ kHz. In each scan, 15 924 data points were acquired. The temporal correlation experiment (Figure 2-5) is measured with a two-step injection process (see section 2.4.4 Inversion Experiment with Dual Injection) and a single transient pulse sequence, (shaped π)-G_z-(π/2)-acquire. An IBURP2 shaped pulse of flip angle π and 10 ms duration at the resonance frequency of C1 or C2 of 1-hexene was applied. A pulsed field gradient, G_z (35.5 G/cm, 1 ms), and a 90 deg pulse with field strength $\gamma B_1 = 31.25$ kHz were also applied. During the acquisition, WALTZ-16 ^{1}H decoupling was applied with field strength $\gamma B_1 = 2.78$ kHz. The acquisition time was 2.38 s, and 95 964 data points were collected. Nonhyperpolarized ^{1}H NMR spectra (Figure 2-6a) were acquired by using 30 degree pulses with field strength $\gamma B_1 = 22.87$ kHz, an acquisition time of 1 s, and 4 transients. The toluene resonance was saturated with continuous rf irradiation. Chemical shifts were referenced to the solvent resonance of toluene. The chemical shift of toluene was calibrated against tetramethylsilane (TMS) using a separate sample according to the IUPAC recommendations. Trimethylphenylsilane (TMPS) was used as an internal standard. Other nonhyperpolarized NMR spectra (Figure 2-4, Figure 2-6bc, Figure 2-7, and Figure 2-8)

were acquired using a 500 MHz NMR spectrometer equipped with a triple resonance TCI cryoprobe with a Z-gradient (Bruker Biospin), at 298 K.

2.4.4 Inversion Experiment with Dual Injection

Experiments to correlate the signals from reactant and product were performed by applying an inversion pulse to the monomer signal before the start of the polymerization reaction in the NMR spectrometer. For this purpose, the rapid injection system was modified to incorporate a 2nd injector containing activated catalyst solution. A syringe pump, Nexus 6000 (Chemyx Inc., Stafford, TX), was used to inject the activated catalyst solution into the NMR tube after the arrival of hyperpolarized 1-hexene and application of the inversion pulse. 0.06 M of activated catalyst in toluene/fluorobenzene=1/1 mixture was prepared in the glove box, and transferred into a stainless steel syringe with a manual switch valve (Scheme 2-1, left). Before assembling into the rapid injection system, the transfer line attached to the NMR tube was purged with argon gas. The catalyst solution was then filled into the transfer line. The experimental setup and pulse sequence with two triggers is shown in Scheme 2-1 (right). The first trigger signal was connected into the NMR spectrometer and initiated after the injection of hyperpolarized 1-hexene. After 50 ms, the second trigger signal was sent to the Nexus 6000 syringe pump to start the injection of the activated catalyst solution of 0.1 ml with an injection rate of 12 mL/min.

2.4.5 Microstructure Analysis

The microstructure of the oligomer produced in the reaction was analyzed by fitting the hyperpolarized and non-hyperpolarized ^{13}C NMR signal intensities of the C3 of

poly(-1-hexene) in the MATLAB program. A linear combination of six Lorentzian functions was used:

$$f(ppm) = \frac{a_1}{(b/2)^2 + (ppm - c_1)^2} + \frac{a_2}{(b/2)^2 + (ppm - c_2)^2} + \ldots \quad (2\text{-}6)$$

Here, the parameter *a* refers to the signal intensity from six pentad peaks, *b* is the line width of the signal, and *c* refers to the optimized chemical shifts of pentads in ppm. The pentad sets were referred from Asakura *et al.*[87] For data containing the monomer signal, for example the hyperpolarized spectra, a further Lorentzian term was added. The fitting was performed using a non-linear least square method, and the result is shown in Figure 2-3c, Figure 2-4, and Table 2-2.

2.4.6 Analysis of Kinetic Data

For processing of the time dependent DNP-NMR spectra, the raw NMR data were zero filled to 65536 complex data points, and an exponential window function with 5 Hz line broadening was applied before Fourier transform. Fourier transform and quantitative fitting were done using the MATLAB program (MathWorks, Natick, MA). The NMR signal at different time points is influenced by the spin-lattice relaxation and the polymerization reaction. The spin-lattice relaxation of hyperpolarized 1-hexene, r_M, was determined from an experiment, where the catalyst solution was replaced to pure fluorobenzene. For NMR signals measured by fixed small flip angle pulses, the time-resolved longitudinal magnetization can be described by:[84,86]

$$S_M(t) = S_M(0)e^{-(r_M+\lambda)t} \quad (2\text{-}7)$$

where λ=-ln(cosα)/Δt and Δt is the time delay between scans. λ is 0.1074 s^{-1} in this study. Alternatively, a logarithmic function can be used:

$$ln\big(S_M(t)\big) - ln\big(S_M(0)\big) = -(r_M + \lambda)t \quad (2\text{-}8)$$

The determined $r_M+\lambda$ are reported in Table 2-3. The sample motion generated during the instantaneous sample mixing can affect the observed rate constant.[86] Hence, three set of monomer relaxation without the addition of catalyst are used for the data fitting described below.

To describe the data acquired with catalyst, a convenient way is to derive a function that accounts for the consumption of monomer and consider the effect from the relaxation afterwards. Several kinetic models have been proposed in the study of metallocene-catalyzed olefin polymerization.[73,74] In general, the polymerization includes the activation, initiation, and propagation processes:

Activation: $C + A \rightarrow C^a$

Initiation: $C^a + M \rightarrow CP_1$

Propagation: $CP_i + M \rightarrow CP_{i+1}$

The kinetic model was based on the proposed mechanism as shown in Scheme 2-2. First, we omit the activation process, as C^a is generated ex situ before the olefin insertion. Second, we assume all of the C^a is converted into the CP_i in the presence of large amount

of catalyst. It can be further confirmed from the hyperpolarized ^{13}C spectrum that significant amount of polymer signals are observed. Third, a deactivated process is introduced to account for the decreasing catalytic activity. Due to the difficulty of observing all of the intermediate signals, we approximate the deactivation process as a first order reaction, where the amount of CP_idecreases with rate constant, k_d. Based on above assumptions, two differential equations are postulated:

$$\frac{d[M]}{dt} = -k_p * [M] * \sum_{i=1}^{n} [CP_i] \tag{2-9}$$

$$\frac{d\sum_{i=1}^{n}[CP_i]}{dt} = -k_d * \sum_{i=1}^{n} [CP_i] \tag{2-10}$$

The solutions of the two differential equations can be derived:

$$[M]_t = [M]_0 * e^{-\left(k_{p(obs)}/k_d\right)*\left(1-e^{-k_d t}\right)} \tag{2-11}$$

$$\sum_{i=1}^{n} [CP_i]_t = \sum_{i=1}^{n} [CP_i]_0 * e^{-k_d * t} \tag{2-12}$$

Here, we define$k_{p(obs)} = k_p * [C]_0$and $\sum_{i=1}^{n}[CP_i]_0 = [C]_0$

Following ref. 84, the time evolution of the spin-up and spin-down concentration is given by:

$$\frac{d[\hat{M}]}{dt} = \frac{r_M}{2} * \left([\check{M}] - [\hat{M}]\right) - k_p * \sum_{i=1}^{n} \left([\hat{CP}_i] + [\check{CP}_i]\right) * [\hat{M}] \quad (2\text{-}13)$$

$$\frac{d[\check{M}]}{dt} = \frac{r_M}{2} * \left([\hat{M}] - [\check{M}]\right) - k_p * \sum_{i=1}^{n} \left([\hat{CP}_i] + [\check{CP}_i]\right) * [\check{M}] \quad (2\text{-}14)$$

where $\sum_{i=1}^{n}\left([\hat{CP}_i] + [\check{CP}_i]\right) = \sum_{i=1}^{n}[CP_i]_t$. Here, the caret designates spin-up, and the inverted caret stands for spin-down. Combing equations (2-13) and (2-14) yields:

$$\frac{d\left([\hat{M}] - [\check{M}]\right)}{dt} = -r_M * \left([\hat{M}] - [\check{M}]\right) - k_p * \sum_{i=1}^{n}[CP_i]_t * \left([\hat{M}] - [\check{M}]\right) \quad (2\text{-}15)$$

since $S_M = \left([\hat{M}] - [\check{M}]\right)$, the solution of time resolved NMR signal is:

$$\frac{d}{dt}S_M = -r_M * S_M - k_{p(obs)} * e^{-k_d t} * S_M \quad (2\text{-}16)$$

$$S_M(t) = S_M(0)e^{-r_M * t - \left(k_{p(obs)}/k_d\right) * \left(1 - e^{-k_d t}\right)} \quad (2\text{-}17)$$

Finally, the signal intensity is scaled with $e^{-\lambda t}$, and the equation used in the data fitting is further treated by a logarithm:

$$ln\left(S_M(t)\right) - ln\left(S_M(0)\right) = -(r_M + \lambda)t - \left(k_{p(obs)}/k_d\right) * (1 - e^{-k_d t}) \quad (2\text{-}18)$$

where $k_{p(obs)} = k_p * [C]_0$. The hyperpolarized signal of 1-hexene was integrated as a function of time and plotted on a logarithmic scale. The data points are normalized over $S_M(0.45)$. The fitting parameter, $S_M(0)$, $k_{p(obs)}$ and k_d can be determined by a non-linear least square optimization over the 5 monomer signals (C1 to C5). The fitting curved are shown in Figure 2-9, Figure 2-10 a and b, Figure 2-11 and Figure 2-12. Values of $k_{p(obs)}$ and k_d are averaged by the three set of $r_M + \lambda$ values (Table 2-3), and the result are shown in Table 2-1.

The validity of proposed mechanism (Scheme 2-2) in describing the metallocene-catalyzed polymerization can also be demonstrated by simulating polymer signals. The polymer signal C5 is chosen as the signal of deactivated polymeryl species, CP*, is expected to be indistinguishable from the polymer signal, CP. Hence, the rate expression for polymer signal growth is simply given by:

$$\frac{d[P]}{dt} = k_p * [M] * \sum_{i=1}^{n} [CP_i] \tag{2-19}$$

Again, the time evolution of the spin-up and spin-down concentration is described as:

$$\frac{d[\hat{P}]}{dt} = \frac{r_p}{2} * \left([\check{P}] - [\hat{P}]\right) + k_p * [\hat{M}] * \sum_{i=1}^{n} \left([\hat{CP}_i] + [\check{CP}_i]\right) \tag{2-20}$$

$$\frac{d[\check{P}]}{dt} = \frac{r_p}{2} * \left([\hat{P}] - [\check{P}]\right) + k_p * [\check{M}] * \sum_{i=1}^{n} \left([\hat{CP}_i] + [\check{CP}_i]\right) \tag{2-21}$$

The differential equation of polymer signal is obtained by combing equation (2-20) and (2-21):

$$\frac{dS_p}{dt} = -r_p * S_p + k_p * S_M * \sum_{i=1}^{n} [CP_i]_t \qquad (2\text{-}22)$$

with equation (2-10), the following equation is derived for fitting the polymer signal:

$$\frac{dS_p}{dt} = -r_p * S_p + S_M * k_{p(obs)} * e^{-k_d * t} \qquad (2\text{-}23)$$

The small flip angle pulses cause extra signal decay with a factor of λ. Hence, the equation used in describing the signal evolution should be described as:

$$\frac{dS_p}{dt} = -(r_p + \lambda) * S_p + S_M * k_{p(obs)} * e^{-k_d * t} \qquad (2\text{-}24)$$

Here, we assume the relaxation rate of C5 of polymer and deactivated polymeryl species are the same and denoted as r_P. A simulation of polymer signal growth can be made using equation (2-24) where the $k_{p(obs)}$, k_d, and $S_M(0)$ are determined from equation (2-18). The resulting r_P values are listed in Table 2-1, and the fitted curves are shown in Figure 2-10 and Figure 2-13. The ratio of S_p/S_M at t=0.45 second is reported in Figure 2-14 b and d.

3. EARLY KINETICS OF RING-OPENING METATHESIS POLYMERIZATION MEASURED BY REAL-TIME HYPERPOLARIZED NMR SPECTROSCOPY

3.1 Introduction

Ring-opening metathesis polymerization (ROMP) has been proposed as a versatile method for polymerization because of the possibility to incorporate different functional groups and because of control over the architecture of final polymer when using modern catalysts.[101–105] Well defined complexes of Ru(II) can be created with organic ligands, such as [(H_2Mes)L_n($Cl)_2$Ru = CHPh] with the N-heterocyclic carbene H_2Mes = 1,3-(bis(mesityl)-2-imidazolidinyl-idene).[106,107] The mechanism of catalysis involves a [2+2] cycloaddition reaction of a cycloolefin with this complex, followed by cycloconversion and insertion into the polymer chain. The initiation of the ROMP is primarily controlled by another ligand L_n, which originally occupies the coordination site for the cycloolefin.[108] For example, the phosphine containing Grubbs second-generation catalyst, G2 (Scheme 1), exhibits slow dissociation,[109] whereas the pyridine ligand in Grubbs third-generation catalyst, G3, rapidly dissociates from pre-catalyst.[110] The ligand dissociation and resulting catalyst initiation causes specific molecular weight distributions and other properties of the final polymer. Knowledge of the kinetics and mechanisms of this process is important for the design of catalyst that allow control over polymer properties.

While the ligand dissociation rates of the pre-catalysts such as G2 and G3 can be estimated using model reactions,[111,112] kinetic measurements that include both initiation and propagation in an on-going polymerization reaction have not been reported. A

difficulty in measuring initiation kinetics and determining the corresponding mechanism is because due to the high reactivity of the active species.[113] The active species can react with the ligand dissociated from the pre-catalyst or the olefinic group on the in-situ generated polymer. These side reactions make the kinetic calculation of ROMP reaction in an on-going reaction complicated. For example, Walsh et al. have found that the apparent propagation rate constant in the G3-catalyzed reaction is independent to the catalyst concentration because of a reaction with dissociated pyridine ligand.[114] Also, the reaction of active species with the synthesized polymer that contains different chain lengths results in intermolecular or intramolecular chain transfers.[108,109]

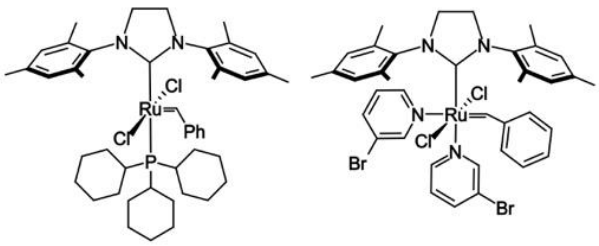

G2 G3

Scheme 3-1. Ruthenium catalysts used in this study. L_n = PCy_3 (n = 1; PCy_3 = tricyclohexylphosphine) for G2 and L_n = 3-Br-py (n = 2; py = pyridine) for G3.

3.2 Results and Discussion

Here, we use real-time NMR enabled by sensitivity enhancement from dissolution dynamic nuclear polarization (D-DNP)[16] to measure ROMP in the early time regime. Hyperpolarized ^{13}C NMR signals of unlabeled monomer, norbornene, and its *in-situ* reaction products are readily observable after a ~2000 fold signal enhancement provided

by DNP. Figure 3-1 shows the spectra from a time series acquired immediately following mixing of monomers with G2 or G3, as well as from a control data set without the reaction. Time points shown in the figure, t = 0.45 s for G3 and t = 1.65 s for G2, were chosen for maximun polymer signal. The polymer signal intensities in the entire time series first increase, then decay due to the combined effect of reaction kinetics and spin relaxation. In the figures, monomer signals from carbon atoms at positions 1 to 4 are labeled as M1 to M4, and the corresponding signals from polymers that formed during this time, are underlaid in gray and labeled as P1 to P4. Polymer signals specific to stereostructures, tt, cc, tc, and ct, originating from the combination of cis (c) and trans (t) configurations of the olefinic group, are readily identified in enlarged sections of the spectra (Figure 3-1c)

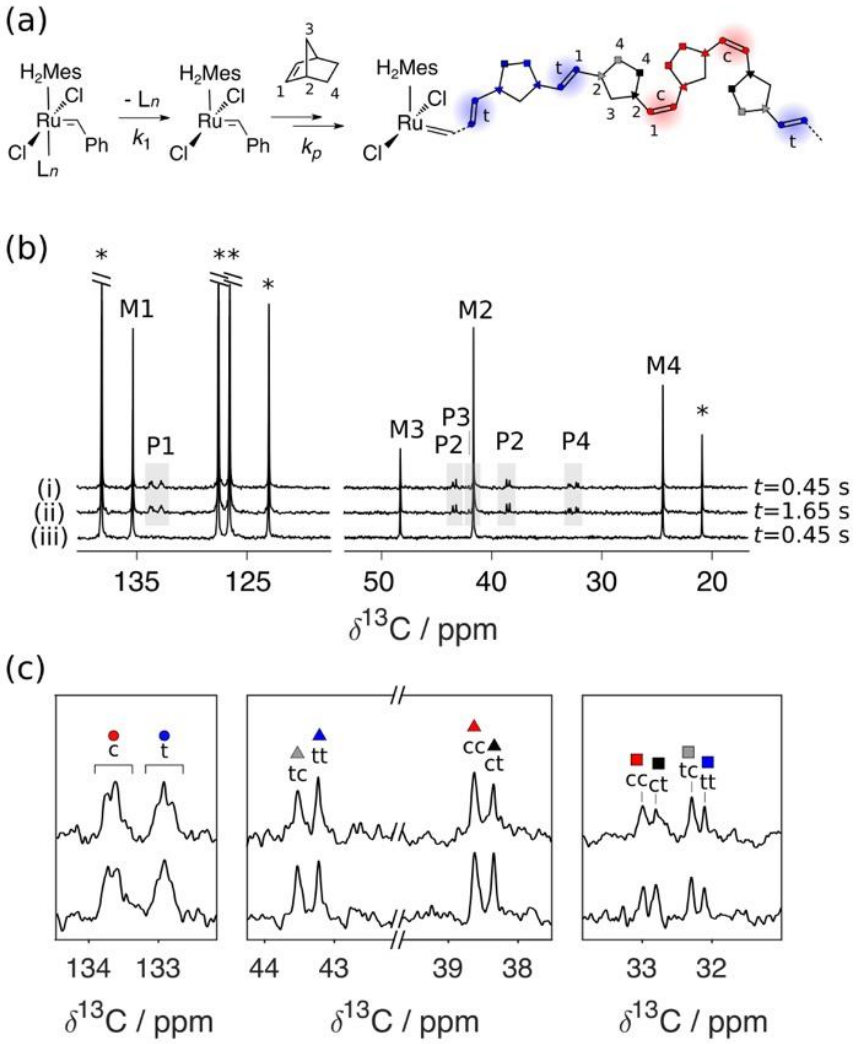

Figure 3-1. (a) Norbornene ROMP reaction scheme. (b) Hyperpolarized ^{13}C NMR spectra of the reaction in the presence of (i) 0.01 mM of G3 catalyst, (ii) 11.8 mM of G2 catalyst, and (iii) without the catalyst after mixing with catalysts. Spectra shown are from a time series of 64 acquisitions distributed over 25.65 s, employing small-flip angle excitation pulses of 13.5°. The numbering of carbon atoms in the reaction scheme corresponds to the labels M1 ~ M4 for monomer signals and P1 ~ P4 for polymer signals. Peaks from the glassing matrix and solvent, toluene, are labeled as *. (c) Enlarged spectral regions from (b), showing polymer signals. Olefinic carbon in cis or trans bond are indicated with letters 'c' and 't'. Aliphatic carbons are indicated with double letters designating nearest neighbor and second-neatest neighbor cis or trans bonds. Polymer signal assignments are from ref. 115.

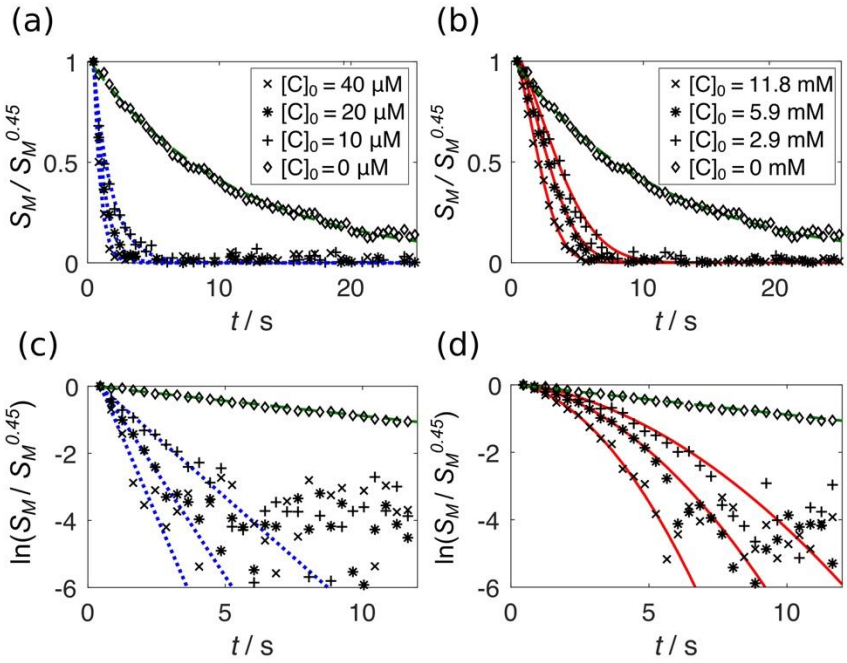

Figure 3-2. Time evolution of monomer signal integrals of M1 in (a) G3 and (b) G2 catalyzed ROMP reaction acquired from hyperpolarized ^{13}C NMR spectra. The same monomer signals are plotted on a logarithmic scale in (c) for G3 and in (d) for G2. Dashed and dotted lines indicate single exponential fitting. The solid lines are curves fitted using equation (3-4). All fits were on the linear scale. Data were measured using $[M]_0$ = 43 mM.

The difference in the initiation of the G2 and G3 ROMP can immediately be identified by comparing the time evolution of monomer signal integrals (Figure 3-2a and b). In the absence of catalysts, the monomer signal decay is exponential, characterized by the spin-lattice relaxation rate of the monomer, to which an additional signal depletion rate caused by the read-out pulses in each scan is added.[24,48,116] With catalyst, the signal decays more rapidly due to the depletion monomer in the reaction. The difference between the two catalysts can most easily be seen, when signal integrals are plotted on a logarithmic scale (Figure 3-2c and d). A straight line corresponding to a first order process for a controlled or living polymerization mechanism is seen for G3. In contrast, a non-linear

curve is observed for the slow initiation catalyst G2, indicating an increasing apparent rate constant, as catalyst becomes active.

3.2.1 Kinetic Analysis using Hyperpolarized Monomer Signals

Polymerization following the living polymerization mechanism can be characterized using a single exponential equation[24]

$$S_M = S_M(0)e^{-(k_p' + r_1^M + \lambda)t} \quad (3\text{-}1)$$

where k'_p is the pseudo-first-order rate constant of propagation ($k'_p = k_p$[CP]; [CP] is the concentration of active catalytic species), $r_1{}^M$ is the spin-lattice relaxation rate constant of the monomer, and λ describes the signal depletion by the radio-frequency (rf) pulses. Equation (3-1) is used to describe the monomer signals acquired from reactions with G3 catalyst (see dashed lines in Figure 3-2a and c and Figure 3-3). The calculated rate constants, k'_p, are summarized in a titration plot (Figure 3-4a).

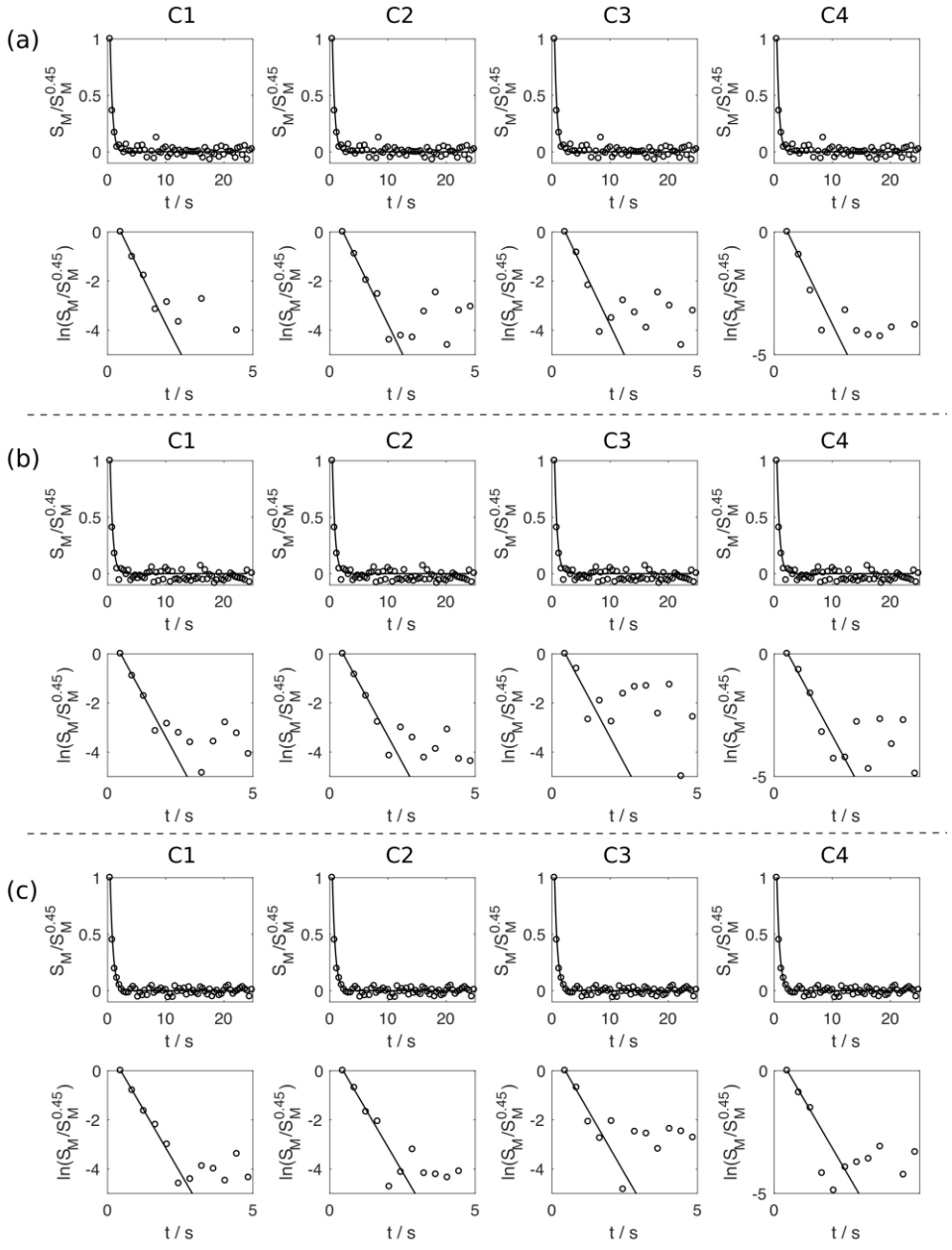

Figure 3-3. Time evolution of monomer signals in G3 catalyzed ROMP reaction acquired from hyperpoalrized ^{13}C spectra. Data in (a)-(h) correspond to the Entry 1 to 8 in Table 3-1. The solid lines are the fitting result using equation (3-1), and the calculated rate constants are summarized in Table 3-1.

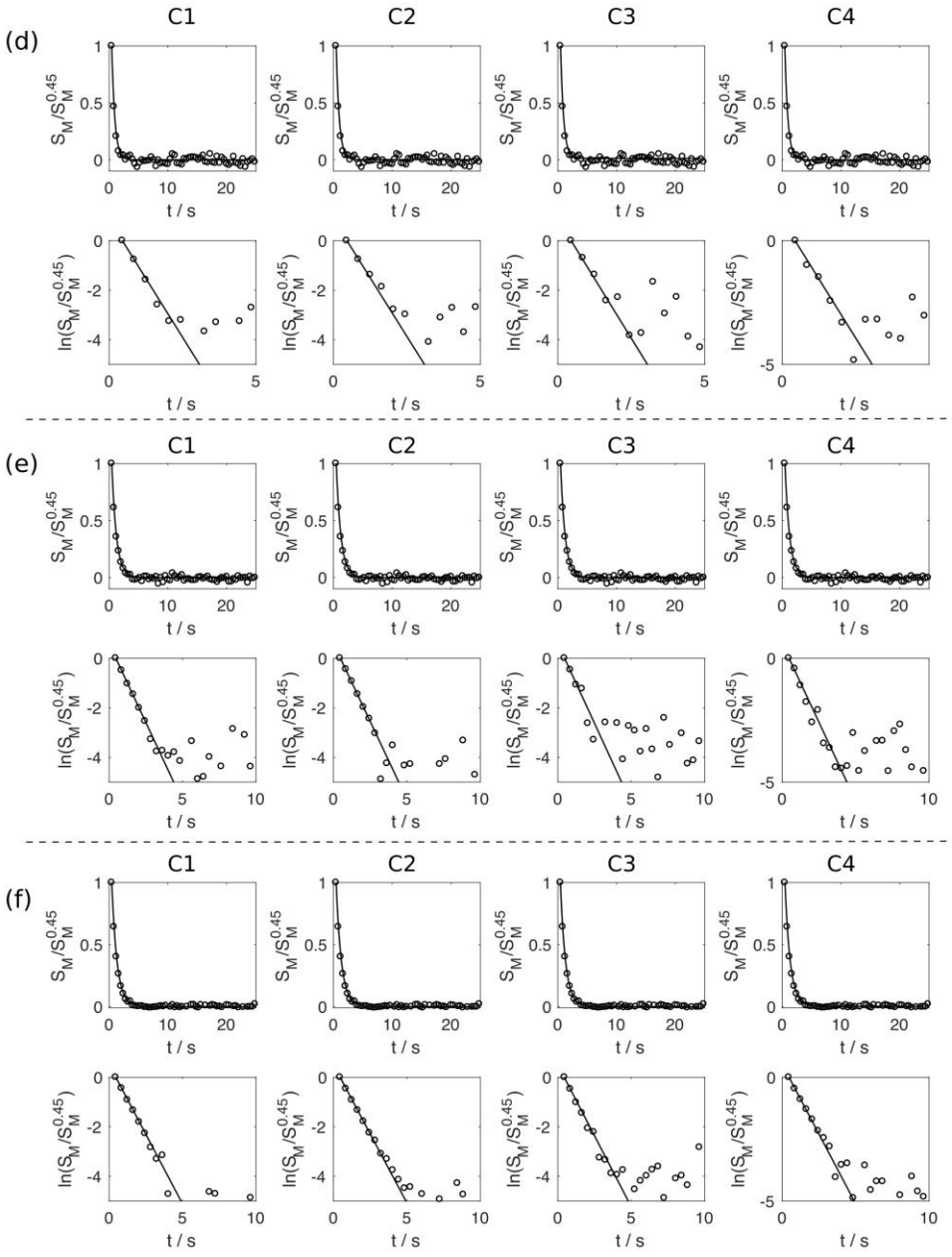

Figure 3-3. Continued.

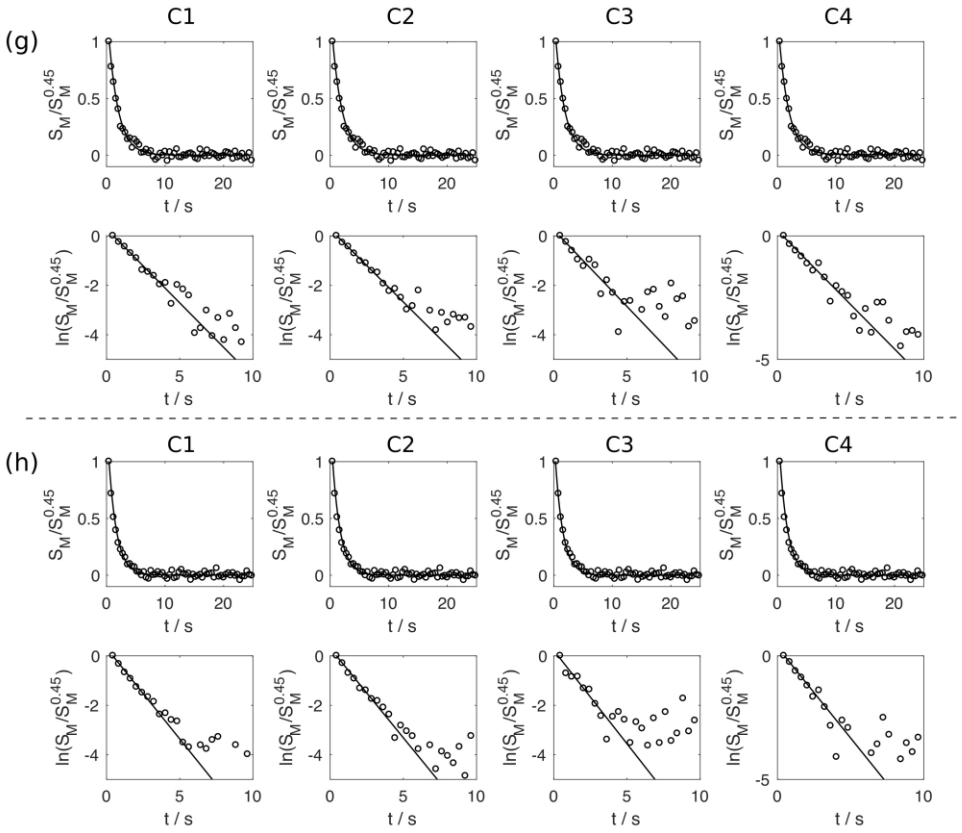

Figure 3-3. Continued.

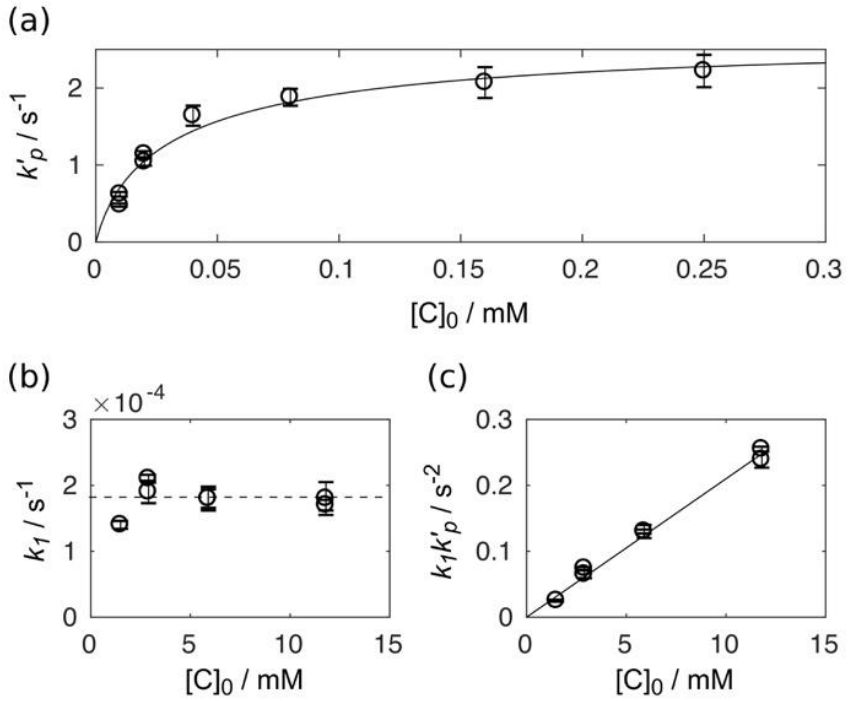

Figure 3-4. (a) k'_p, rate constants determined for G3-catalyzed ROMP using equation (3-1). (b) k_1, rate constants for G2 catalyzed ROMP using equation (3-4). (c) $k_1k'_p$, product of rate constants for G2 catalyzed ROMP using equation (3-5). The error bars represent the 95% confidence intervals from the data fitting. The solid lines in (a) is the result of data fitting using equation (3-3), and in (c) is the result of linear fitting.

Table 3-1. Experimental conditions and calculated parameters from G3 catalyzed ROMP in toluene at 298 K using ^{13}C hyperpolarization. Numbers inside the parenthesis indicate the 95% confidence interval derived from the data fitting. The monomer concentrations are 43 mM in all of the data sets.

Entry	C_0 / μM	k'_p / s^{-1}	$k'_{Pct} = k'_{Ptc}$ / s^{-1}	k'_{Ptt} / s^{-1}	k'_{Pcc} / s^{-1}
1	250	2.22 (± 0.21)	0.55 (± 0.02)	0.46 (± 0.03)	0.77 (± 0.03)
2	160	2.07 (± 0.20)	0.44 (± 0.04)	0.36 (± 0.05)	0.69 (± 0.06)
3	80	1.88 (± 0.11)	0.41 (± 0.02)	0.34 (± 0.03)	0.41 (± 0.04)
4	40	1.74 (± 0.13)	0.36 (± 0.03)	0.32 (± 0.04)	0.36 (± 0.05)
5	20	1.14 (± 0.04)	0.28 (± 0.02)	0.23 (± 0.03)	0.28 (± 0.03)
6	20	1.04 (± 0.05)	0.23 (± 0.01)	0.21 (± 0.01)	0.39 (± 0.02)
7	10	0.47 (± 0.02)	0.11 (± 0.02)	0.10 (± 0.02)	0.11 (± 0.03)
8	10	0.62 (± 0.05)	0.16 (± 0.02)	0.14 (± 0.02)	0.16 (± 0.02)

In Figure 3-4a, the k'_p is concentration dependent and appears to gradually reach a saturation at high catalyst concentration. Walsh *et al.* have observed the saturation at high catalyst concentration, which can be related to a reaction with the dissociated pyridine ligand, in a G3-catalyzed reaction using a norbornene derivative.[114] Here, we find that k'_p decreases when the catalyst concentration is lower than the previously reported values.[114] This observation suggests that an equilibrium reaction involving the active propagating species, CP, undergoes a reaction with the dissociated ligand, L, to generate the ligand-bound species, CP^b (see Scheme 3-3). Assuming that the equilibrium involves only a single ligand, as suggested in ref. 114, the corresponding equilibrium constant, *K*, can be written as:

$$K = \frac{[CP^b]}{[L][CP]} \tag{3-2}$$

The relationship of the observed propagation rate constant k'_p with the total catalyst concentration, $[C]_0$, then becomes

$$k'_p = k_p[CP] = k_p \frac{-(K[C]_0 + 1) + \sqrt{(K[C]_0 + 1)^2 + 4K[C]_0}}{2K} \tag{3-3}$$

Equation (3-3) is used to describe the titration curve in Figure 3-4a. The determined k_p and the K are $1.2(\pm 0.47)\cdot 10^5$ $M^{-1}s^{-1}$ and $4.7(\pm 2.4)\cdot 10^4$ M^{-1}, respectively.

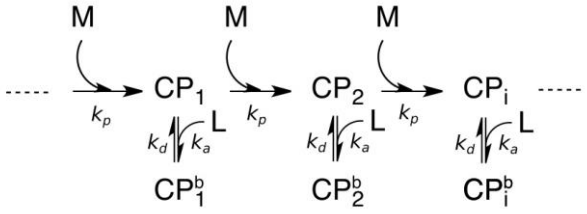

Scheme 3-2. Kinetic models used for characterizing the equilibrium of propagating species in G3-catalyzed ROMP at high catalyst concentration (0.25 – 2 mM).

For the G2-catalyzed ROMP, we consider initiation and propagation reactions, as drawn in scheme in Figure 3-1 and Scheme 3-3. In this model, the catalyst both undergo ligand dissociation with a first order rate constant k_1.[111,112] After dissociation, propagation involves the reaction of the active species with the monomer following a second-order

reaction with rate constant, k_p. The derived equation for describing the time-evolved monomer signal evolution is

$$S_M = S_M(0)e^{-(k_p'+r_1^M+\lambda)t-\frac{k_p'}{k_1}(e^{-k_1 t}-1)} \quad (3\text{-}4)$$

In equation (3-4), k_1 is the first order rate constant for ligand dissociation, and the other parameters are the same as in equation (3-1).

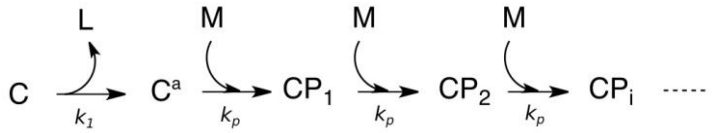

Scheme 3-3. Kinetic model of polymerization involving ligand dissociation via dissociative mechanism

Since the G2 and G3 catalysts both undergo initiation through a dissociative mechanism,[112,114] they generate the same propagating species. Therefore, the rate constants k_p are expected to be the same in both reactions. The propagation rate constant k_p obtained from G3 catalyst was included as a constant in the equation (3-4), to determine the rate constant k_1 for G2 catalyst. The determined k_1 is concentration independent, and the average of the calculated k_1 is $1.8(\pm 0.21)\cdot 10^{-4}$ s^{-1}. (see Figure 3-4b and Table 3-2)

Although the k_1 can be determined using the above method, the equilibrium of the active species and the dissociated ligand, which appears to occur in common ruthenium

alkylidene catalysts, cannot be easily identified. Here, we simplify equation (3-4) into equation (3-5). This approximation is true when the k_1 and the t are sufficiently small

$$S_M = S_M(0)e^{-(r_1^M+\lambda)t-\frac{k_1 k_p'}{2}t^2} \quad (3\text{-}5)$$

Notably, the product of rate constants $k_1k'_p$ in the second order coefficient of t characterizes the curvature observed in Figure 3-2d. When the data fitting is performed using equation (3-5), $k_1k'_p$ and $S(0)$ are the fit parameter. A linear relationship of the $k_1k'_p$ with the catalyst concentration is observed in a titration plot (Figure 3-4c). Since the initiation rate k_1 is concentration independent, the linear relationship in Figure 3-4c immediately indicates that k_p is a second order rate constant. The saturation caused by the ligand equilibrium as observed in the G3-catalyzed reaction in Figure 3-4a is not observed.

Using the k_p determined from G3-catalyzed reaction together with the slope of the line in Figure 3-4c, the initiation rate constant k_1 for G2 is determined as $1.8(\pm0.09)\cdot10^{-4}$ s^{-1}. The determined k_1 agrees well with that from using equation (3-4). The k_1 calculated from the on-going polymerization reaction using hyperpolarized ^{13}C NMR is on the same order as the initiation rate constants of several Grubbs-typed pre-catalysts determined using model reactions.[111,112] Based on the determined k_1 value, the fraction of the activated G2 catalyst is 0.09 % at a time point of 5 s after the start of the reaction, which is near the time point that the monomer signal disappears in the hyperpolarized spectrum measured using highest catalyst concentration ($[C]_0$=11.8 in Figure 3-2a). The calculated concentration of active catalytic species is similar to the lowest concentration in the Figure

3-4a. At this low catalyst concentration, the equilibrium with the phosphine ligand is not observed, resulting in the straight line in Figure 3-4c.

Table 3-2. Experimental conditions and calculated parameters from G2 catalyzed ROMP in toluene at 298 K using ^{13}C hyperpolarization. The rate constant k_1 were determined by simultaneously fitting the data of C1 to C4 using equation (3-4) in which the k_p is fixed as a constant determined from G3-catalyzed reaction. The product of rate constant $k_1 k'_p$ were determined by simultaneously fitting the data of C1 to C4 using equation (3-5). Numbers inside the parenthesis indicate the 95% confidence interval derived from the data fitting. The monomer concentrations are 43 mM in all of the data sets.

Entry	C_0 / mM	M_0 / mM	k_1 / s^{-1}	$k_1 k'_p$ / s^{-2}
1	11.8	43	$1.7(\pm 0.08)\cdot 10^{-4}$	0.24 (± 0.012)
2	11.8	43	$1.8(\pm 0.25)\cdot 10^{-4}$	0.26 (± 0.036)
3	5.9	43	$1.8(\pm 0.14)\cdot 10^{-4}$	0.13 (± 0.010)
4	5.9	43	$1.8(\pm 0.18)\cdot 10^{-4}$	0.13 (± 0.013)
5	2.9	43	$1.9(\pm 0.17)\cdot 10^{-4}$	0.07 (± 0.006)
6	2.9	43	$2.1(\pm 0.006)\cdot 10^{-4}$	0.07 (± 0.002)
7	1.5	43	$1.4(\pm 0.006)\cdot 10^{-4}$	0.03 (± 0.001)

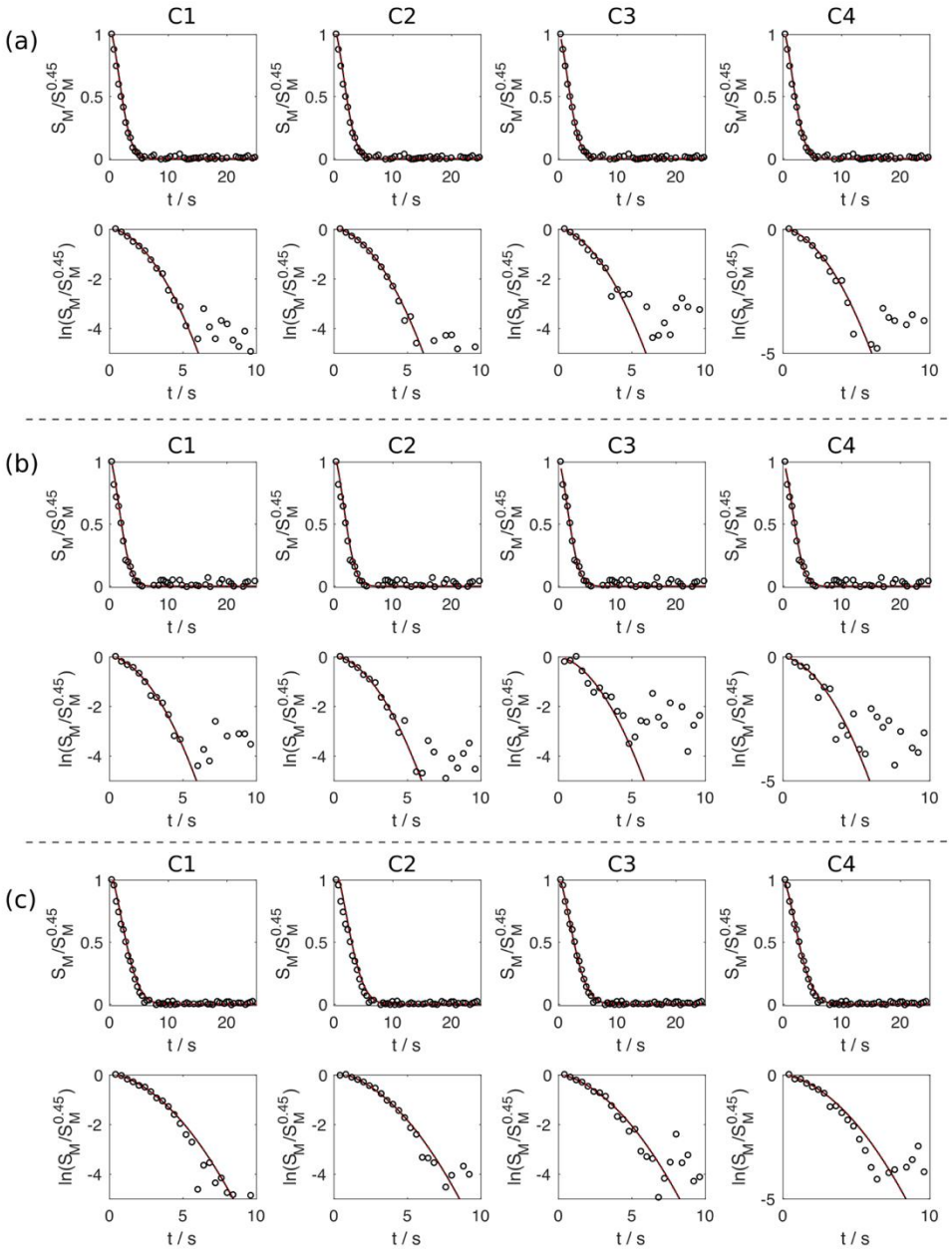

Figure 3-5. Time evolution of monomer signal in G2 catalyzed ROMP reaction acquired from hyperpoalrized ^{13}C spectra. Data in (a)-(g) are from Entry 1 to 7 in Table 3-2. The solid lines are the result from the data using equation (3-4) and the dotted lines are the results from the data fitting using equation (3-5). The calculated rate constants are summarized in Table 3-2 and Figure 3-4b.

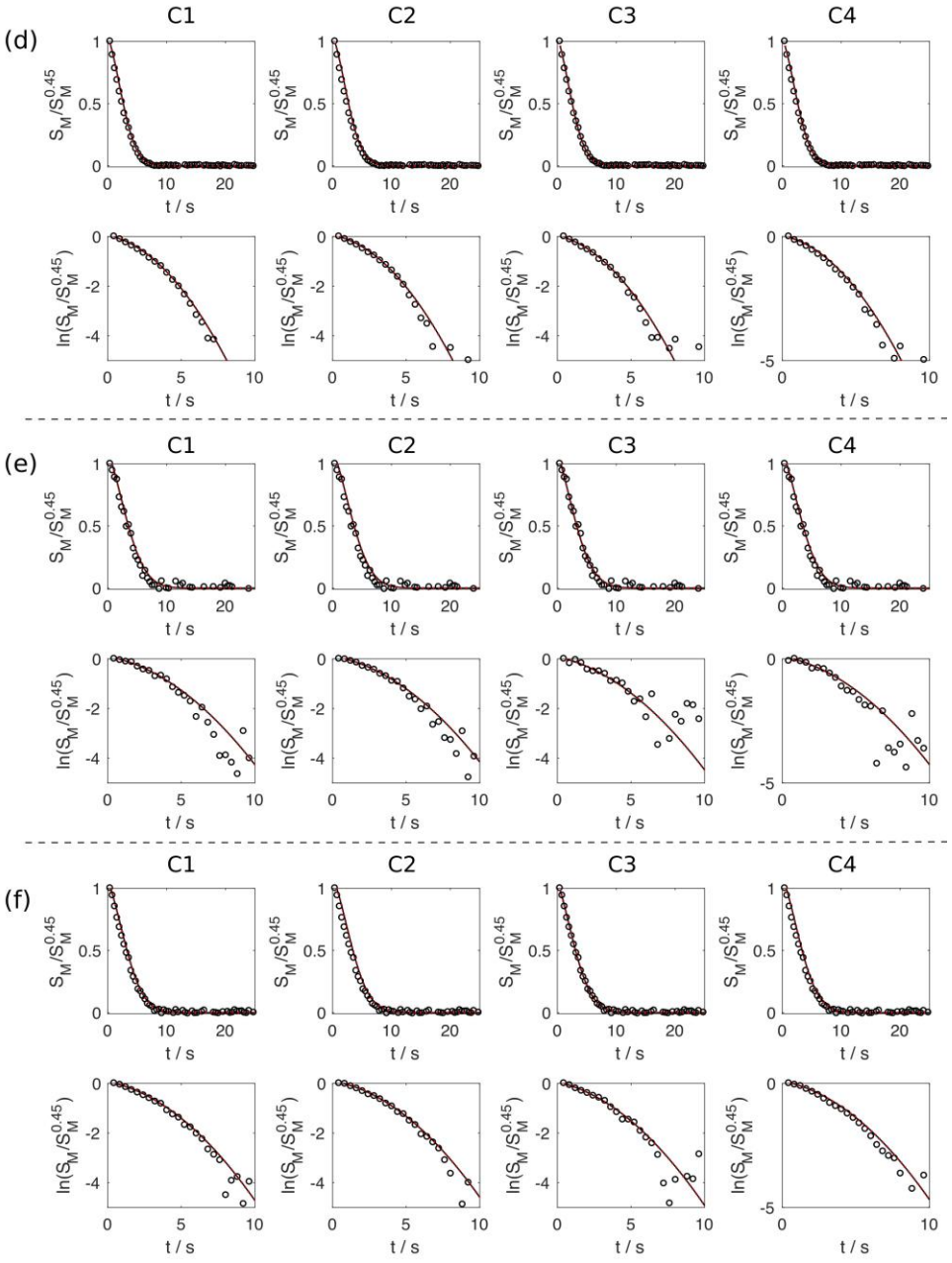

Figure 3-5. Continued.

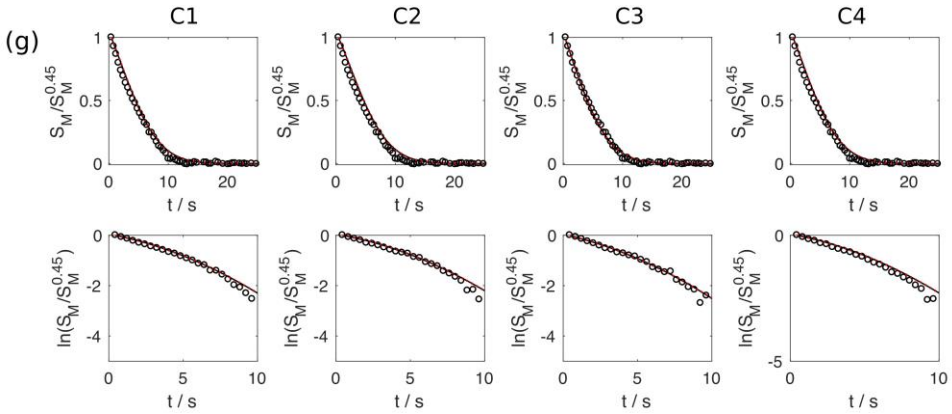

Figure 3-5. Continued.

3.2.2 Kinetic Analysis using Hyperpolarized Polymer Signals

In addition to monomer signals, the polymer signal build-up can be observed in the real-time hyperpolarized NMR experiments (Figure 3-6a to c). The signals from individual stereostructures, S_{Px} (x = cc, ct, tc, and tt), can be described by

$$\frac{dS_{P_x}}{dt} = k'_{P_x} S_M - r_1^{P_x} S_{P_x} \tag{3-6}$$

In equation (3-6), k'_{Px} is the pseudo-first-order rate constant for the formation of the individual polymer signal of sterestructure x (x = cc, ct/tc, or tt) and $k'_{Px} = k_{Px}$[CP]. Because the formation of tc is accompanied with the formation ct due to symmetry, the $k'_{Ptc} = k'_{Ptc}$. The r_1^{Px} is the spin-lattice relaxation rate of the polymer signal. Numerical fitting was performed simultaneously on the time-resolved signals of P_{1c}, P_{1t}, P_{2cc}, P_{2ct}, P_{2tc}, P_{2tt}, P_{4cc}, P_{4ct}, P_{4tc}, P_{4cc}, and M_1 to M_4 at different catalyst concentrations, as plotted in Figure 3-7 to Figure 3-15. Figure 3-6d to f show the resulting titration plots composed of calculated rate

constants k'_{Pcc}, $k'_{Pct/ct}$, k'_{Ptt}, in the G3-catalyzed reaction. The results show a similar concentration dependence as in Figure 3-4a, with the rate constants gradually reaching saturation at elevated catalyst concentration. The second-order rate constants specific to different polymer stereostructures, k_{Pcc}, $k_{Pct/ct}$, k_{Ptt}, were calculated using equation (3-43) and the K determined in Figure 3-4a. The calculated values are $4.0(\pm0.33)\cdot10^4$ $M^{-1}s^{-1}$, $2.7(\pm0.22)\cdot10^4$ $M^{-1}s^{-1}$, and $2.3(\pm0.21)\cdot10^4$ $M^{-1}s^{-1}$ for k_{Pcc}, $k_{Pct/ct}$, and k_{Ptt}, respectively. The summation of these rate constants, $k_{Pcc}+2k_{Pct/ct}+k_{Ptt}$, matched within the error ranges of the k_p determined from the monomer signals. The result shows P_{cc} is the most kinetically favorable structure in this reaction. These individual rate constants were subsequently fixed in the data fitting of the polymer signals acquired from G2-catalyzed reaction, yielding the dissociation rate constant $k_1 = 1.8(\pm0.05)\cdot10^{-4}$ s^{-1} (Figure 3-16). This result agrees with the same rate constant derived from the monomer signals, indicating self-consistency of the data.

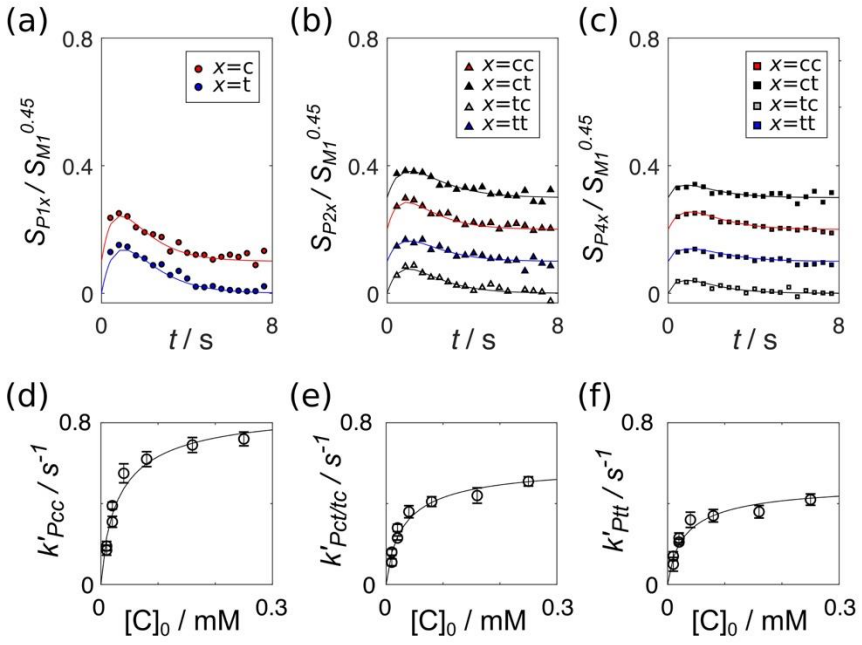

Figure 3-6. (a-c) Time evolution of polymer signals P1, P2 and P4 in G3-catalyzed ROMP using $[M]_0$ = 43 mM and $[C]_0$ = 0.01 mM. The data for each polymer stereostructure are separated by a factor of 0.1 in the y-axis. The solid lines are the results of the numerical fitting using equation (3-6). (d-f) Rate constant, k'_{Px}, determined in G3-catalyzed ROMP. Error bars represent the 95% confidence intervals from the data fitting. The solid line indicates the result of data fitting using equation (3-43).

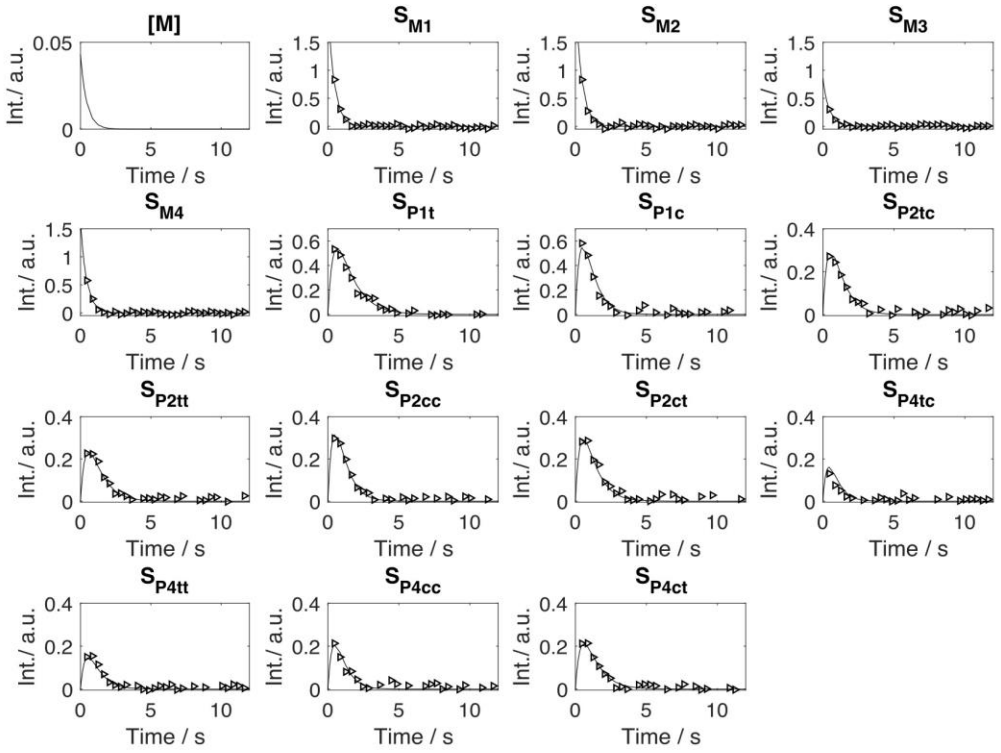

Figure 3-7. Numerical fitting of monomer and polymer signal of ROMP reaction using 2 mM G3 catalyst and 43 mM norbornene (Entry 1 in Table 3-1). The identities of the signals (S) are shown in the subscript, with "M" designating monomer, "P" designating polymer, the numbers indicating the carbon position, and the "c" and "t" letters the stereostructure.

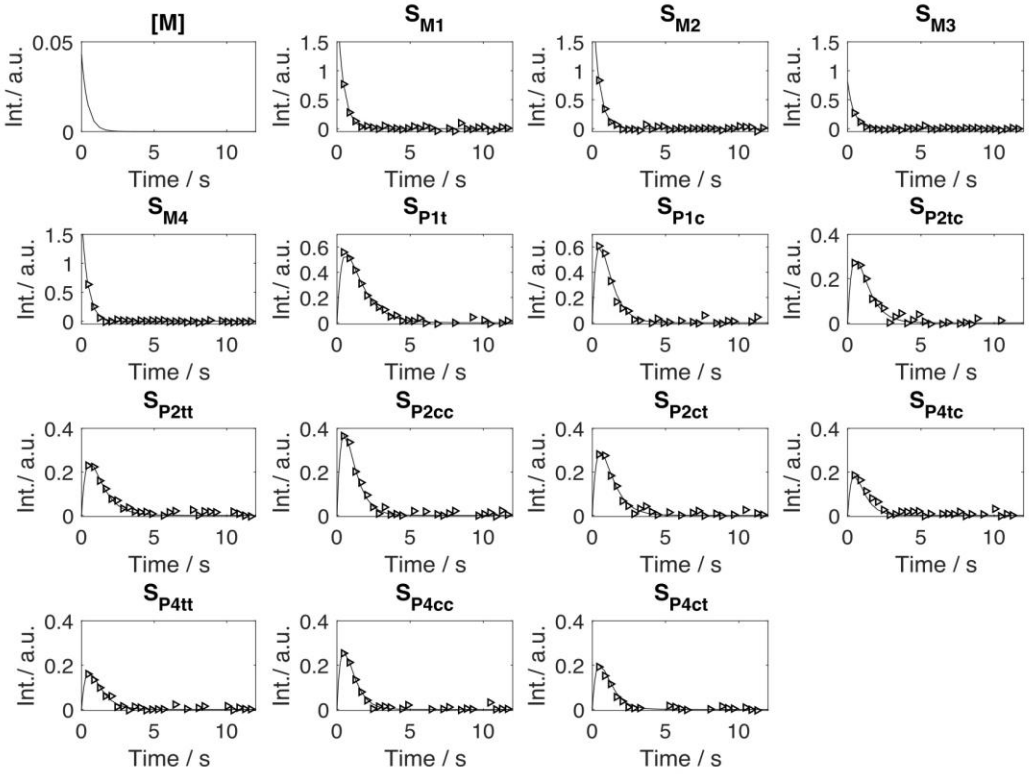

Figure 3-8. Numerical fitting of monomer and polymer signal of ROMP reaction using 0.16 mM G3 catalyst and 43 mM norbornene (Entry 2 in Table 3-1). The identities of the signals (S) are shown in the subscript, with "M" designating monomer, "P" designating polymer, the numbers indicating the carbon position, and the "c" and "t" letters the stereostructure.

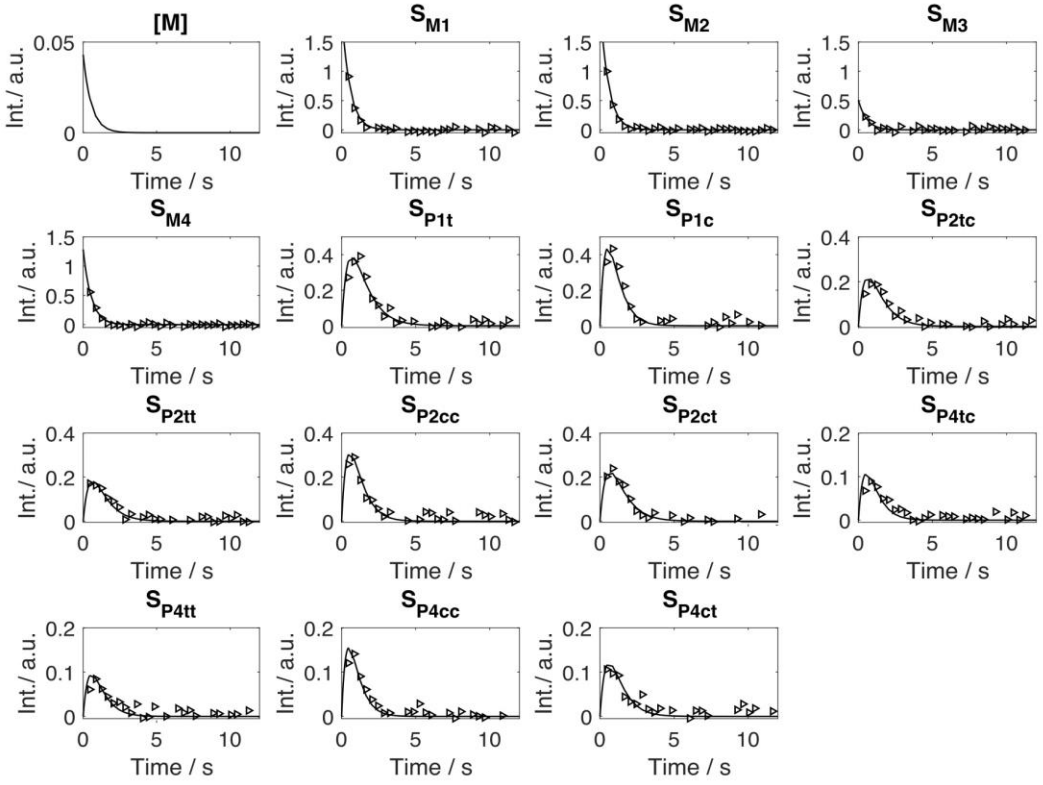

Figure 3-9. Numerical fitting of monomer and polymer signal of ROMP reaction using 0.125 mM G3 catalyst and 43 mM norbornene (Entry 3 in Table 3-1). The identities of the signals (S) are shown in the subscript, with "M" designating monomer, "P" designating polymer, the numbers indicating the carbon position, and the "c" and "t" letters the stereostructure.

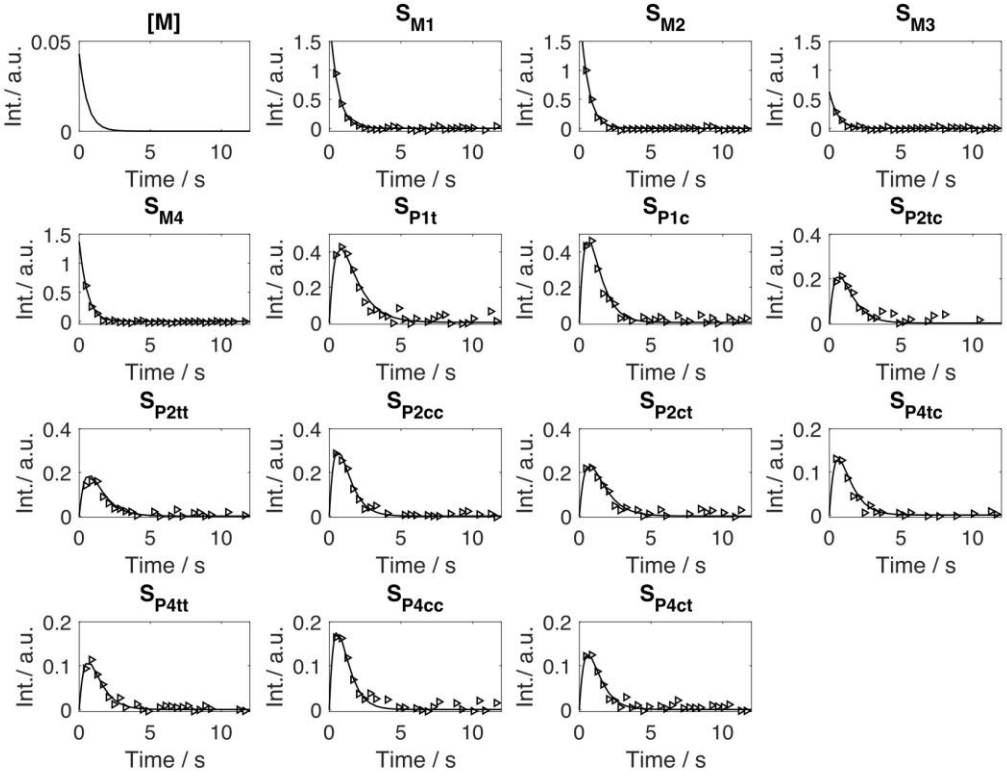

Figure 3-10. Numerical fitting of monomer and polymer signal of ROMP reaction using 0.08 mM G3 catalyst and 43 mM norbornene (Entry 4 in Table 3-1). The identities of the signals (S) are shown in the subscript, with "M" designating monomer, "P" designating polymer, the numbers indicating the carbon position, and the "c" and "t" letters the stereostructure.

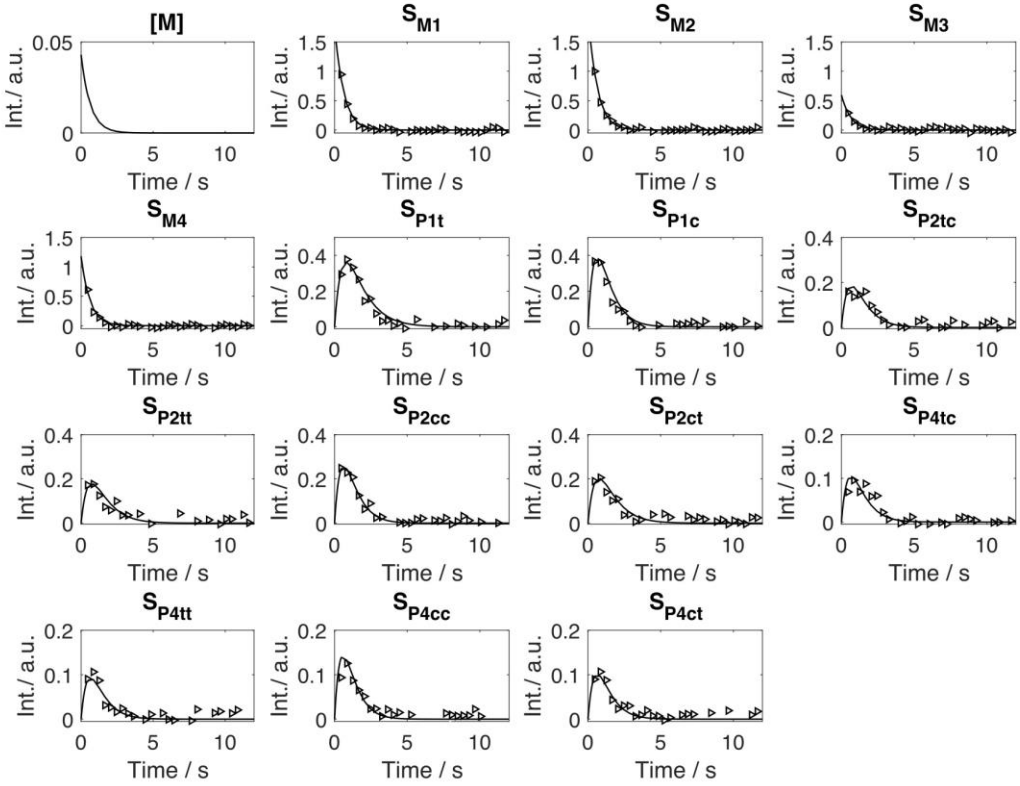

Figure 3-11. Numerical fitting of monomer and polymer signal of ROMP reaction using 0.04 mM G3 catalyst and 43 mM norbornene (Entry 5 in Table 3-1). The identities of the signals (S) are shown in the subscript, with "M" designating monomer, "P" designating polymer, the numbers indicating the carbon position, and the "c" and "t" letters the stereostructure.

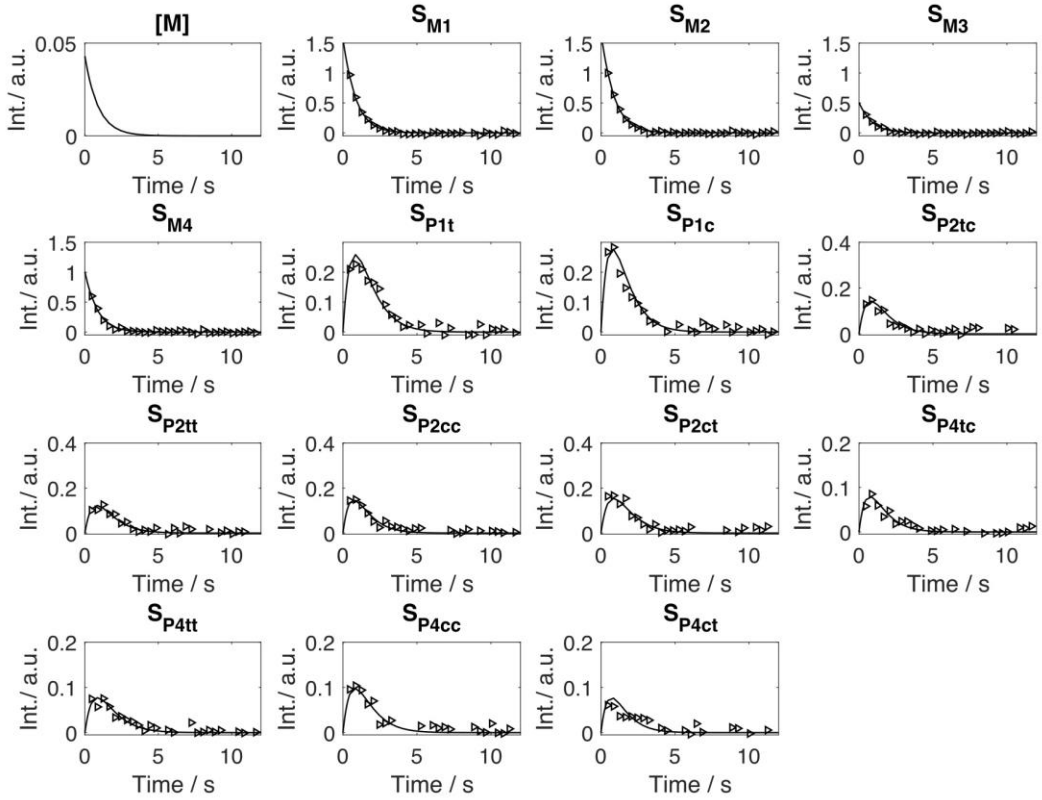

Figure 3-12. Numerical fitting of monomer and polymer signal of ROMP reaction using 0.02 mM G3 catalyst and 43 mM norbornene (Entry 6 in Table 3-1). The identities of the signals (S) are shown in the subscript, with "M" designating monomer, "P" designating polymer, the numbers indicating the carbon position, and the "c" and "t" letters the stereostructure.

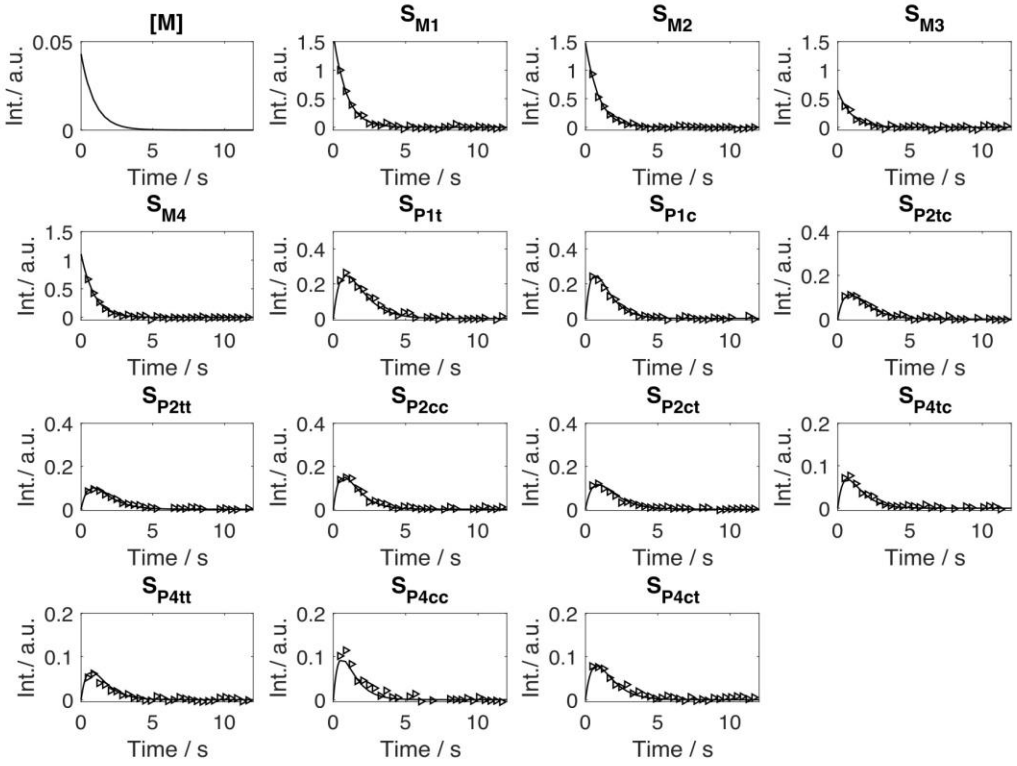

Figure 3-13. Numerical fitting of monomer and polymer signal of ROMP reaction using 0.02 mM G3 catalyst and 43 mM norbornene (Entry 7 in Table 3-1). The identities of the signals (S) are shown in the subscript, with "M" designating monomer, "P" designating polymer, the numbers indicating the carbon position, and the "c" and "t" letters the stereostructure.

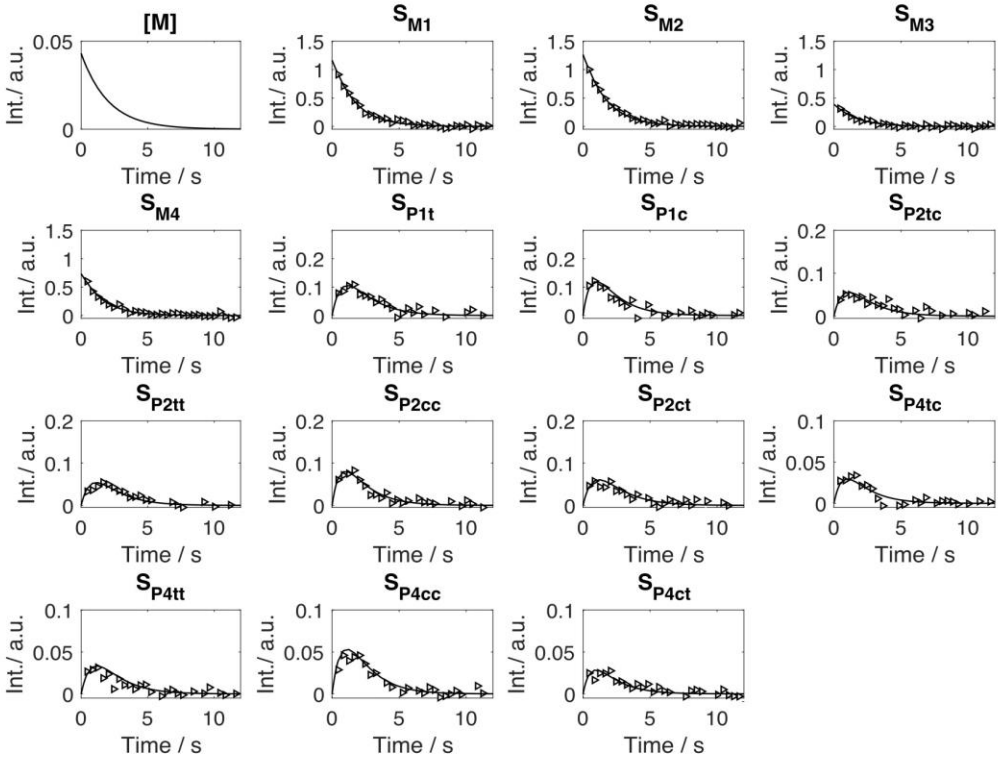

Figure 3-14. Numerical fitting of monomer and polymer signal of ROMP reaction using 0.01 mM G3 catalyst and 43 mM norbornene (Entry 8 in Table 3-1). The identities of the signals (S) are shown in the subscript, with "M" designating monomer, "P" designating polymer, the numbers indicating the carbon position, and the "c" and "t" letters the stereostructure.

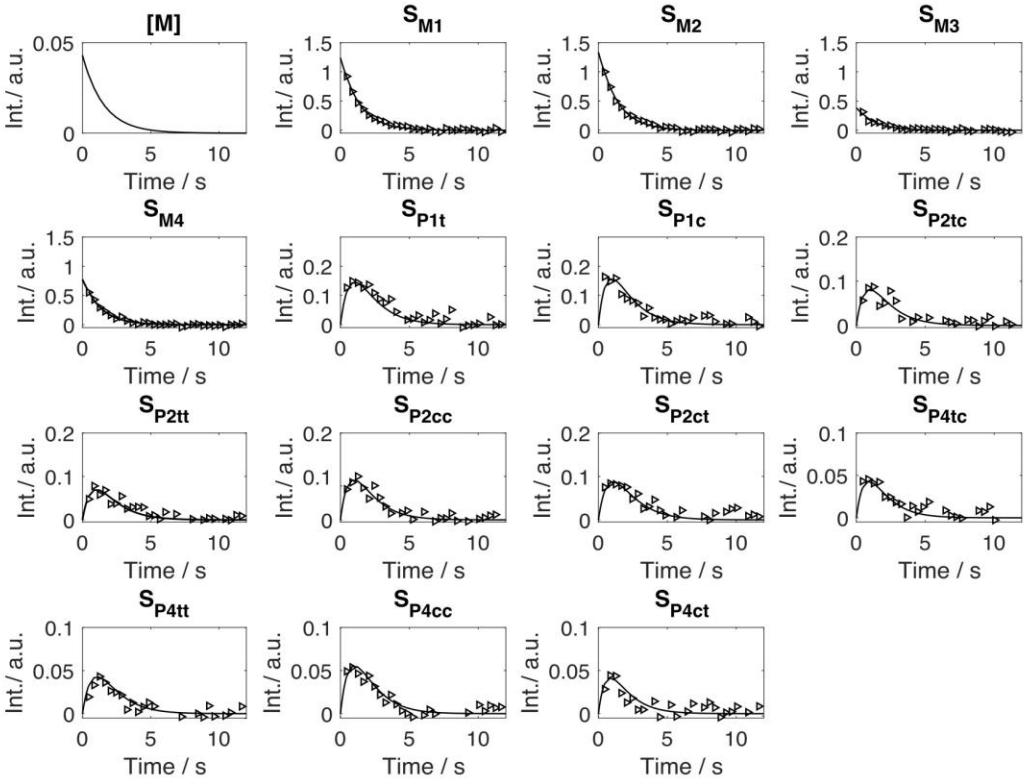

Figure 3-15. Numerical fitting of monomer and polymer signal of ROMP reaction using 0.01 mM G3 catalyst and 43 mM norbornene (Entry 9 in Table 3-1). The identities of the signals (S) are shown in the subscript, with "M" designating monomer, "P" designating polymer, the numbers indicating the carbon position, and the "c" and "t" letters the stereostructure.

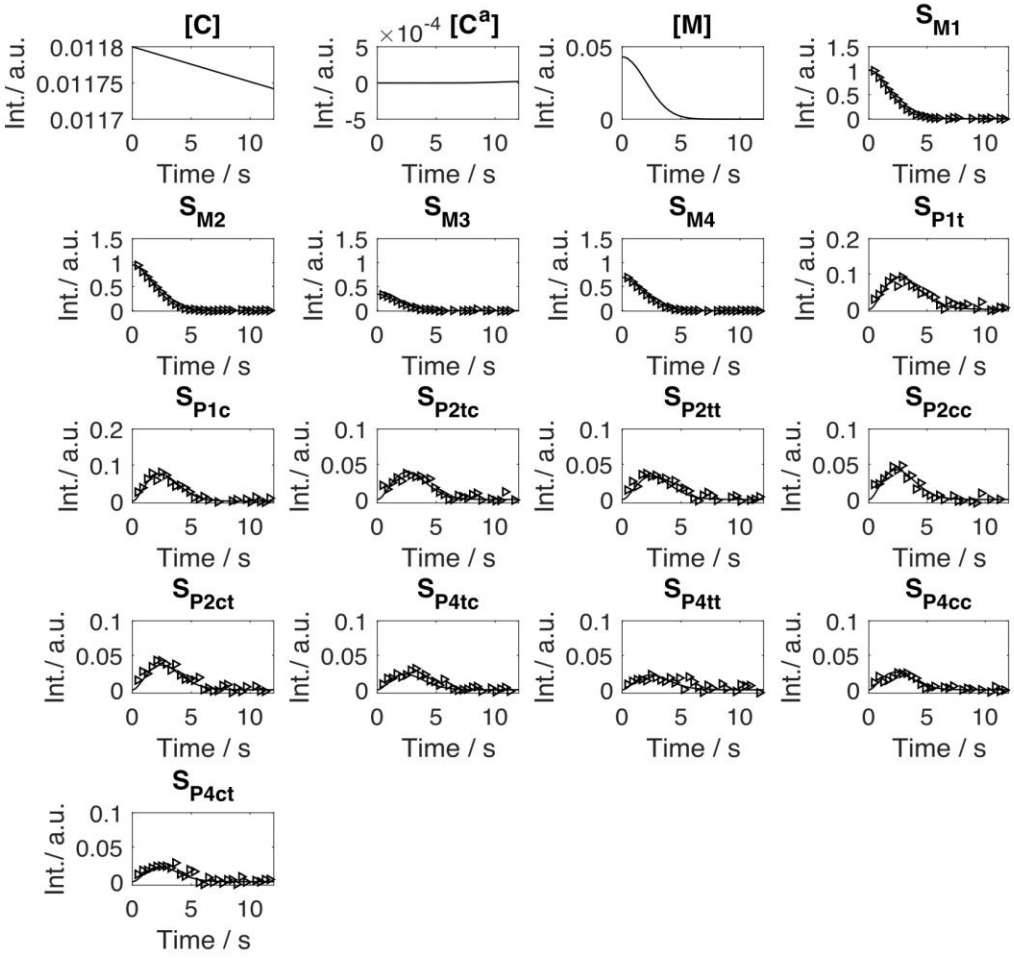

Figure 3-16. Numerical fitting of monomer and polymer signal of a reaction using 11.8 mM G2 catalyst and 43 mM norbornene (Entry 1 in Table 3-2). The identities of the signals (S) are shown in the subscript, with "M" designating monomer, "P" designating polymer, the numbers indicating the carbon position, and the "c" and "t" letters the stereostructure.

While ^{13}C hyperpolarization allows the determination of the individual rates for the formation of different polymer stereostructures during the on-going reaction, ^{1}H spectra only resolve cis or trans configuration. The G2-catalyzed ROMP reaction measured using ^{1}H non-hyperpolarized NMR shows changes of cis-to-trans ratio from 1.34 to 0.87 over the course of 25 min (Figure 3-17). A possible cause for this change on the longer time scale is a secondary cis to trans conversion process, which may occur due

to the chain transfer reaction. The G3-catalyzed ROMP, in contrast, is less affected by the chain transfer presumably due to the equilibrium reaction with the dissociated ligands (Figure 3-17). The observed difference demonstrates the ability of observing the initiation and propagation in the short time regime accessible by D-DNP-NMR, disregarding the influence of other processes.

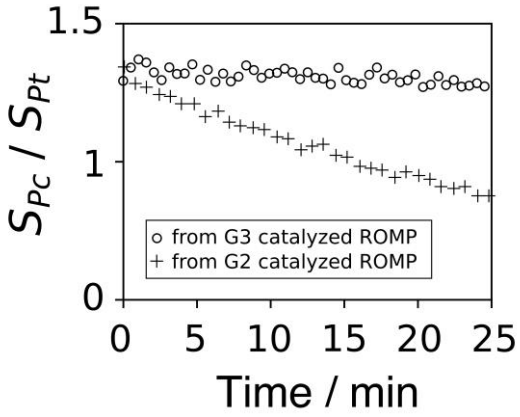

Figure 3-17. Ratio of cis to trans signals measured from non-hyperpolarized ^{1}H NMR of ROMP catalyzed by G2 or G3 with M_0 = 48 mM and C_0 = 2.4 mM.

3.3 Conclusion

In summary, we observed the initiation and propagation ROMP catalyzed by G2 and G3 using D-DNP NMR spectroscopy. The early time measurement enables the simplification of kinetics equations and calculation of the corresponding rate constants both for the overall process and for the formation of individual stereostructure. The equilibrium of the dissociated ligand with the active propagating species can be observed in titration curves composed from the rate constants. Measurement of polymerization kinetics on this time scale using D-DNP NMR therefore opens the possibility to access

intrinsic rate constants, for different chemical structures, that are not obscured by secondary processes.

3.4 Experimental Section

3.4.1 Polymerization Materials and Preparation

Norbornene (> 99.0 % GC) was purchased from TCI America. G2 catalyst, (1,3-bis(2,4,6-trimethylphenyl)-2-imidazolidinylidene)dichloro(phenylmethylene)(tricycle-hexylphosphine)ruthenium, and G3 catalyst, dichloro[1,3-bis(2,4,6-trimethylphenyl)-2-imidazolidinylidene](benzylidene)bis(3-bromopyridine)ruthenium(II), were purchased from Sigma-Aldrich. Toluene and isooctane was dried and distilled from NaK/Ph_2CO/18-crown-6 and stored in an Ar-filled glove box. Before the dissolution of hyperpolarized sample, the catalyst solution was dissolved in 50 μL toluene in an Ar-filled glove box and then transferred to a 5 mm NMR tube. Before installing the NMR tube into the NMR instrument, the transfer line for injection of the DNP sample was purged with Ar gas to avoid contamination of the sample with moisture and oxygen from room air. After the hyperpolarized NMR measurement, the polymerization reaction was quenched with diethyl ether.

3.4.2 Dynamic Nuclear Polarization

^{13}C Hyperpolarization: A sample of 15 mM α,γ-Bisdiphenylene-β-phenylallyl (BDPA; Sigma-Aldrich) in 15 μL of 5.2 M norbornene (Alfa Aesar) in toluene was hyperpolarizd in a HyperSense system (Oxford Instruments, Tubney Woods, U.K.) at 1.4

K under the irradiation of microwaves at $\omega_e - \omega_N$ = 93.965 GHz and a power of 60 mW, for 3 h. The hyperpolarized sample was dissolved in 4 mL of hot toluene 800 kPa and transferred into the rapid injection system by He gas.[100] The injection was accomplished with a forward pressure of 1450 kPa applied against a back pressure of 11030 kPa using Ar gas for 400 ms, followed by stabilization for 0.4 s. The hyperpolarized sample was mixed with catalyst in the NMR tube during injection. The final temperature was 298 K.

3.4.3 NMR Spectroscopy

The hyperpolarized NMR spectra were acquired using a Bruker 400 MHz NMR spectrometer equipped with a boradband probe containing three pulsed field gradients (Bruker Biospin, Billerica, MA) at a temperature of 298 K. A NMR experiment with the pulse sequence $[G_z\text{-}\alpha_x\text{-acquire}]_{\times 64}$, was triggered after hyperpolarized sample was delivered to the NMR tube. For each experiment, a data set with total acquisition time of 25.6 s included 64 transients separated by 400 ms. A randomized pulsed field gradient, G_z (35.5 G·cm^{-1}, 1 ms) was applied to remove residual coherences from the previous scan. For ^{13}C experiments, a pulse with small flip angle, α = 13.5º, and pulse strength γB_1 = 31.25 kHz was applied after G_z. During the acquisition, WALTZ-16 ^{1}H decoupling was applied with a field strength γB_1 = 32.78 kHz. In each transients, 15924 data points were acquired. Chemical shifts of ^{13}C of both the hyperpolarized and non-hyperpolarized experiments were referenced to the solvent resonance of toluene. The chemical shift of toluene was calibrated against tetramethylsilane (TMS) using a separate sample, following the IUPAC recommendations.[117]

3.4.4 Kinetic Model

The NMR signal at different time points is influenced by the spin-lattice relaxation and the polymerization reaction. For NMR signals measured by fixed small flip angle pulses, the time-resolved monomer signal, S_M, can be described by:[24,86]

$$S_M = S_M(0)e^{-((r_1^M+\lambda)t} \quad (3\text{-}7)$$

where $\lambda = -\ln(\cos\alpha)/\Delta t$ and Δt is the time delay between scans.

The kinetic model is based on the dissociative mechanism[118] as shown in Scheme 3-2a. The pre-catalyst, C, undergoes a first order reaction with rate constant, k_1, to dissociate a ligand, L, and becomes the "activated" catalyst, C^a. Subsequently, it reacts with monomer, M, via a second order process with rate constant k_p, to generate the catalyst polymeryl species, CP_i.

Based on the above scheme, differential equations for the concentrations $[C]$, $[C^a]$, $[M]$, as well as $[CP_i]$, can be written as:

$$\frac{d[C]}{dt} = -k_1[C] \quad (3\text{-}8)$$

$$\frac{d[C^a]}{dt} = k_1[C] - k_p[C^a][M] \quad (3\text{-}9)$$

$$\frac{d[M]}{dt} = -k_p(C_0 - [C])[M] \quad (3\text{-}10)$$

$$\frac{d[CP_1]}{dt} = k_p[M][C^a] - k_p[M][CP_1] \tag{3-11}$$

$$\frac{d[CP_i]}{dt} = k_p[M][CP_{i-1}] - k_p[M][CP_1] \text{ for } i > 1 \tag{3-12}$$

The total concentration of catalyst polymeryl species is the sum of $[CP_i]$, *i.e.* $\sum_{i=1}^{\infty}[CP_i]$, which follows

$$\frac{d}{dt}\sum_{i=1}^{\infty}[CP_i] = k_p[C^a][M] \tag{3-13}$$

The concentration of monomer unit in catalyst polymeryl species is $\sum_{i=1}^{\infty} i[CP_i]$

$$\frac{d}{dt}\sum_{i=1}^{\infty} i[CP_i] = k_p[M]\left([C^a] + \sum_{i=1}^{\infty}[CP_i]\right) \tag{3-14}$$

The mass conservation of catalyst can be written as

$$C_0 = [C] + [C^a] + \sum_{i=1}^{\infty}[CP_i] \tag{3-15}$$

Then equation (3-14) becomes

$$\frac{d}{dt}\sum_{i=1}^{\infty} i[CP_i] = k_p[M](C_0 - [C]) \tag{3-16}$$

We define the concentration of monomer unit in catalyst polymeryl species excluding the directly bound monomer unit as [P], from which follows

$$\frac{d}{dt}[P] = \frac{d}{dt}\left(\sum_{i=1}^{\infty} i[CP_i] - \sum_{i=1}^{\infty}[CP_i]\right) = k_p[M](C_0 - [C] - [C^a]) \tag{3-17}$$

The directly bound monomer unit is excluded from [P], because of the different chemical shift of the spins near the carbon-metal bond.

Differential equations for hyperpolarized monomer signal, S_M, are dependent on both the concentrations, and the spin polarization of each species. Equations for the change in monomer signal can be found by considering the concentrations of each species in the spin-up and spin-down state separately, combining equation (3-10) with the relaxation terms.[84,116]

$$\frac{d[M^+]}{dt} = \frac{r_1^M}{2}([M^-] - [M^+]) - k_p(C_0 - [C])[M^+] \tag{3-18}$$

$$\frac{d[M^-]}{dt} = \frac{r_1^M}{2}([M^+] - [M^-]) - k_p(C_0 - [C])[M^-] \tag{3-19}$$

The NMR signal is proportional to the difference of the concentration of spin-up and spin-down concentrations, while the total concentration of monomer is equal to the sum. The equation for the signal evolution S_M can be found by combining equation (3-18) and (3-19):

$$\frac{dS_M}{dt} = -r_1^M S_M - k_p(C_0 - [C])S_M \tag{3-20}$$

Using equation (3-8) and equation (3-20), the analytical solution for S_M is:

$$S_M = S_M(0)e^{-(C_0 k_p + r_1^M)t - \frac{C_0 k_p}{k_1}(e^{-k_1 t} - 1)} \tag{3-21}$$

The $C_0 k_p$ can be considered as a pseudo-first order rate constant, k'_p. Under the effect of fixed small flip angle pulses, the signal further is depleted on average by a single exponential with rate constant, λ.[24,48]

Equation (3-21) then becomes

$$S_M = S_M(0)e^{-(k'_p + r_1^M + \lambda)t - \frac{k'_p}{k_1}(e^{-k_1 t} - 1)} \tag{3-22}$$

When the k_1 and the t are sufficiently small, the above equations can be expended into equation (3-23)

$$S_M = S_M(0)e^{-(r_1^M+\lambda)t-\frac{k_1 k_p'}{2}t^2} \quad (3\text{-}23)$$

When the ligand dissociation is fast enough, the pre-catalyst is fully activated and becomes the catalyst polymeryl species. In this case $[C]$ and $[C_a]$ are zero. Monomer signal is then described by a single exponential equation:[24]

$$S_M = S_M(0)e^{-(k_p'+r_1^M+\lambda)t} \quad (3\text{-}24)$$

For every monomer insertion, a cis or trans bond in the polymer is generated. The newly generated double bond connects the previous unit (i-1) with the new monomer unit (i) in the polymer chain. Hence, equation (3-17) can be split into two equations with individual rate constants for formation of cis or trans bonds, k_{Pc} and k_{Pt}:

$$k_p = k_{Pt} + k_{Pc} \quad (3\text{-}25)$$

$$\frac{d[P_c]}{dt} = k_{Pc}(C_0 - [C] - [C^a])[M] \quad (3\text{-}26)$$

$$\frac{d[P_t]}{dt} = k_{Pt}(C_0 - [C] - [C^a])[M] \quad (3\text{-}27)$$

The hyperpolarized polymer signal can then be calculated for each case. The spin-lattice relaxation rates of cis and trans polymer are denoted as r_1^{Pc} and r_1^{Pt}.

$$\frac{d[P_c{}^+]}{dt} = \frac{r_1^{P_c}}{2}([P_c^-] - [P_c^+]) + k_{P_c}(C_0 - [C] - [C^a])[M^+] \quad (3\text{-}28)$$

$$\frac{d[P_c{}^-]}{dt} = \frac{r_1^{P_c}}{2}([P_c^+] - [P_c^-]) + k_{P_c}(C_0 - [C] - [C^a])[M^-] \quad (3\text{-}29)$$

The hyperpolarzed cis polymer signal can be written as:

$$\frac{dS_{P_c}}{dt} = -r_1^{P_c} S_{P_c} + k_{P_c}(C_0 - [C] - [C^a])S_M \quad (3\text{-}30)$$

Likewise,

$$\frac{dS_{P_t}}{dt} = -r_1^{P_t} S_{P_t} + k_{P_t}(C_0 - [C] - [C^a])S_M \quad (3\text{-}31)$$

The polymer signal from C1 directly generate cis and trans double bond. Therefore, equations (3-30) and (3-31) are used for describing carbon or proton polymer signal from C1.

Rate equations representing the stereopeaks from C2 and C4 are considered in a similar way. Polymer signals of tt, tc, ct, and cc can be identified in the ^{13}C spectrum. Following definition of the stereopeaks from Ivin et al,[119–121] the first letter represents the nearest cis/trans double bond and the second letter represents the second nearest cis/trans double bond. The relationship between the rate constant for the formation of cis/trans double bond and the rate constants for the formation of structures pertaining to different

stereopeaks can be derived by considering the monomer addition process. The i^{th} monomer can be added to an existing cis or trans double bond in CP_{i-1}. The generation of a new cis double bond next to an existing cis double bond results in cc structure. Also, the generation of a new cis double bond next to an existing trans double bond gives half ct and half tc structure. Therefore, the following equation must be satisfied:

$$k_{P_c} = k_{P_{cc}} + (1/2)k_{P_{ct}} + (1/2)k_{P_{tc}} \quad (3\text{-}32)$$

Similarly,

$$k_{P_t} = k_{P_{tt}} + (1/2)k_{P_{ct}} + (1/2)k_{P_{tc}} \quad (3\text{-}33)$$

where k_{Pcc}, k_{Ptc}, k_{Pct}, k_{Ptt} are the second order rate constants for the formation of P_{cc}, P_{tc}, P_{ct}, $P_{tt.}$ Due to the symmetry of each polymer unit, the formation of a ct sereostructure is accompanied with the formation of a tc sereostructure. Therefore, the formation rate of polymer peaks of ct and tc are the same, i.e. $k_{Ptc} = k_{Pct}$.

Rate equations representing four stereostructures from C2 and C4 can be derived as:

$$\frac{d[P_{cc}]}{dt} = k_{P_{cc}}(C_0 - [C] - [C^a])[M] \quad (3\text{-}34)$$

$$\frac{d[P_{tc}]}{dt} = k_{P_{tc}}(C_0 - [C] - [C^a])[M] \quad (3\text{-}35)$$

$$\frac{d[P_{ct}]}{dt} = k_{P_{ct}}(C_0 - [C] - [C^a])[M] \quad (3\text{-}36)$$

$$\frac{d[P_{tt}]}{dt} = k_{P_{tt}}(C_0 - [C] - [C^a])[M] \quad (3\text{-}37)$$

Following a similar procedure as in equation (3-28) and equation (3-29), the hyperpolarized polymer signal from different stereostructures, S_{Pcc}, S_{Ptc}, S_{Pct}, S_{Ptt}, can be written as:

$$\frac{dS_{P_{cc}}}{dt} = -r_1^{P_{cc}} S_{P_{cc}} + k_{P_{cc}}(C_0 - [C] - [C^a])S_M \quad (3\text{-}38)$$

$$\frac{dS_{P_{tc}}}{dt} = -r_1^{P_{tc}} S_{P_{tc}} + k_{P_{tc}}(C_0 - [C] - [C^a])S_M \quad (3\text{-}39)$$

$$\frac{dS_{P_{ct}}}{dt} = -r_1^{P_{ct}} S_{P_{ct}} + k_{P_{ct}}(C_0 - [C] - [C^a])S_M \quad (3\text{-}40)$$

$$\frac{dS_{P_{tt}}}{dt} = -r_1^{P_{tt}} S_{P_{tt}} + k_{P_{tt}}(C_0 - [C] - [C^a])S_M \quad (3\text{-}41)$$

where the r_1^{Pcc}, r_1^{Ptc}, r_1^{Pct}, r_1^{Ptt} represent the spin-lattice relaxation rates of polymer. When the ligand dissociation is fast enough, $[C]=[C^a]=0$. The C_0k_{Px} (x=c, t, cc, tt, ct, and tc) in equation (3-30), equation (3-31), and equations (3-38)-(3-41) can be written as a pseudo-first order rate constant, k'_{Px} (x=c, t, cc, tt, and ct/tc).

To describe the titration curve in Figure 3-4b, we assume that the catalyst polymeryl species, CP, is in an equilibrium with the dissociated ligand. This equilibrium involves an inactive, singly coordinated pyridine species, Cp^b, and the active species Cp that is not coordinated to a pyridine.[114] Concentration of these species is the sum of the individual CP_i or CP_i^b in the Scheme 3-2. The equilibrium constant, K, is assumed to be independent of the polymer length, and is written as equation (3-2)

Based on the mass conservation, $[CP^b] = C_0 - [CP]$ and $[L] = L_0 - [CP^b]$ where $L_0 = 2C_0$. The concentration of the active propagating species, $[CP]$, can be

$$[CP] = \frac{-(K[C]_0 + 1) + \sqrt{(K[C]_0 + 1)^2 + 4K[C]_0}}{2K} \tag{3-42}$$

The k'_p in equation (3-24) is then written as equation (3-3), and the observed polymer signal build-up rate constants in equation (3-30), equation (3-31), and equation (3-38) to equation (3-41), $k_{px}(C_0-[C]-[C^a])$ where x denotes the c, t, cc, tc/ct, or tt, becomes

$$\begin{aligned} k'_{Px} &= k_{Px}[CP] \\ &= k_{Px}\frac{-(K[C]_0 + 1) + \sqrt{(K[C]_0 + 1)^2 + 4K[C]_0}}{2K} \end{aligned} \tag{3-43}$$

3.4.5 Analysis of Kinetic Data

The raw NMR data were zero filled to 65536 complex data points, and an exponential window function with 3 Hz line broadening was applied before Fourier

transform. Fourier transform was done using Topspin Software (Bruker Biospin). Peaks were integrated using Matlab (The Math Works, Natick, MA). Integration included subtraction of a linear baseline defined by baseline regions on both sides of each peak. The spin-lattice relaxation of hyperpolarized monomer, r_1^M, was determined from an experiment using pure toluene instead of the catalyst solution with equation (3-7) and λ=0.07.

In the ^{13}C experiment, monomer relaxation from C1 to C4 were determined as 0.03 s^{-1}, 0.01 s^{-1}, 0.04 s^{-1}, and 0.04 s^{-1}. Spin lattice relaxation of polymer, r_1^{Px} (x=c, t, cc, tc, ct, tt) were measured using quenched sample after the D-DNP experiment.

Monomer signal from C1 to C4 were analyzed for calculating rate constants k'_p in G3-catalyzed ROMP or $k'_p k_1$ in G2-catalyzed ROMP. The rate constant k'_p in G3-catalyzed ROMP reaction was determined by simultaneously fitting the data of C1 to C4 using equation (3-1). The second order rate constant k_p was then calculated from the titration plot in Figure 3-4b using equation (3-3). The rate constant k_1 in G2-catalyzed ROMP reaction is determined using two methods. In the first method, the dissociation rate constant k_1 were determined by simultaneously fitting the data of C1 to C4 using equation (3-4) in which the k_p is fixed as a constant determined from G3-catalyzed reaction. In the second method, the rate constant $k_1 k'_p$ in G2-catalyzed ROMP reaction were determined by simultaneously fitting the data of C1 to C4 using equation (3-5). The dissociation rate constant k_1 in G2-catalyzed ROMP reaction was calculated by dividing the slope in the titration plot (Figure 3-4a) over the k_p derived in G3 catalyzed ROMP. The results are summarized in Figure 3-4, Table 3-2, and Table 3-1.

The calculation of k'_{Pcc}, $k'_{Ptc/ct}$, and k'_{Ptt} was done by numerically fitting monomer C1 to C4, and polymer C1, C2 and C4. In the case of the G3 catalyzed ROMP reaction, four equations (3-20) representing the monomer signals and ten sets of equation (3-30), equation (3-31), and equation (3-38) to equation (3-41) representing the polymer signals from different stereostructure were applied. The concentrations of unreacted catalyst, [C], and activated catalyst, [C^a], were set to zero. The fitting procedure included successive numerical solution of the differential equations followed by multiplication with cos(α) to account for the signal depletion due to each rf pulse.[114] The residual sum of squares was minimized using a multi-start algorithm in Matlab. In the case of the G2 catalyzed ROMP reaction, the fitting procedure was the same, but the [C] and [C^a] in equation (3-8) to equation (3-10) were also included in the numerical fitting. The k_i and the initial monomer signals, $S_M(0)$, are the only parameters for calculating the k_1. The fitting results are shown in Figure 3-7 to Figure 3-16, and Table 3-1.

4. KINETICS AND REACTIVITY RATIOS OF COPOLYMERIZATION MEASURED BY ^{13}C HYPERPOLARIZED NMR SPECTROSCOPY

4.1 Introduction

Polymers with different physical and mechanical properties can be affected by the local linkages of the repeating units in the polymer chain. In homopolymerization, the type of monomer and the polymer microstructure determine the properties of polymers. In the presence of the second monomer, a variety of copolymers with different compositions can be synthesized based on the difference in the reactivity of two monomers. Random, blocky, alternating, and gradient copolymers can be synthesized. Each of them displays a different property from those of the corresponding homopolymer.[105,122–127]

One indicator to predict the copolymer composition is by the monomer reactivity ratio, *r*. The reactivity ratio is the ratios of the self-propagation to the cross-propagation rate constant for the active site derived from each respective monomer.[128–130] Thus, if $r > 1$ for a given monomer, it indicates a preference to the homopolymerization. Whereas, if $r < 1$ for a given monomer, it tends to copolymerize with the other monomer. The difference in reactivity ratio of two monomers used in a copolymerization determines its instantaneous composition.

Traditionally, the Mayo-Lewis equation describing the relationship between ratios of feed monomer and ratios of the instantaneous polymer composition is used to determine the reactivity ratios.[128,129] This method is applied under the assumption that the compositional drift in the copolymer chain is negligible at low polymerization conversion.

This assumption can usually be satisfied by quenching the reaction at early time. The reactivity ratios are then determined using linear or non-linear data fitting based on the Mayo-Lewis equation.[130]

A more direct way to determine the reactivity ratio is to acquire individual rate constants in the polymerization measured in real-time. In general, these rate constants can be measured by monitoring the time-dependent monomer or product concentration using the quenched-flow method where the reactants are mixed quickly followed by discharging into a quenching solution.[131] This method is laborious because single data set requires multiple quenched sample. Alternatively, a stopped-flow method can be applied, in which the reaction mixture is measured immediately following the mixing without quenching. Common detectors used with stop-flow methods are UV-Vis, FT-IR, Mass and NMR spectroscopy. Among them, NMR spectroscopy has advantages in elucidating the structure of small molecules and macromolecules at atomic resolution. Conventional stopped-flow NMR relies on acquiring high sensitive ^{1}H NMR signals.[132,133] However, due to a low chemical shift dispersion, structural information from ^{1}H spectra alone is limited.

Dissolution dynamic nuclear polarization (D-DNP)[16], a hyperpolarized technique, allows for the NMR signal enhancement of several thousand fold in the liquid state. This technique can be used to boost the signals from other NMR active nuclei such as ^{13}C. In the D-DNP NMR measurement, a mixture of molecules of interest with free radicals is first hyperpolarized in a DNP polarizer at temperature of ~1 K under microwave irradiation. After the hyperpolarization, a hot solvent is used to dissolve the frozen sample

and transfer into a high-resolution NMR magnet for liquid state NMR spectroscopy. The pre-polarized sample initially yield a strong signal, which hen decay as spin-lattice relaxation establishes the polarization at thermal equilibrium.

Hyperpolarized ^{13}C NMR is suitable for study of the fast reaction because his nucleus exhibits a broad chemical shift dispersion and an extended spin-lattice relaxation time.[134] After mixing the hyperpolarized sample with substrates in a reaction, signals generated during the reaction can be acquired. We have previously studied a metallocene-catalyzed polymerization reaction using ^{13}C hyperpolarized NMR. The signal enhancement allows for the observation of polymer microstructure generated from the *in-situ* reaction along with and the calculation of kinetic rate constants.[116]

We have previously also studied the norbornene ring-opening metathesis polymerization (ROMP) catalyzed by Grubbs third generation (G3) catalyst. It is known for a controlled or living polymerization mechanism.[110] A fast catalyst initiation process generates the active species almost instantaneously upon the addition of monomer. Termination and chain transfer in G3 catalyzed is not significant. The second-order propagation rate constants were determined when the catalyst concentration is low.[135]

Here, we demonstrate the use of D-DNP NMR for characterizing instantaneous kinetic properties of co-polymerization reactions, using ROMP catalyzed by G3 catalyst as example. We show that real-time 3C NMR spectroscopy uniquely allows the determination of cross-propagation and self-propagation rate constants in the time regime following initiation of the reaction. The ratio of these rate constants determines the

reactivity ratios of monomers, allowing the estimation of the instantaneous composition of the copolymer.

4.2 Result and Discussion

Hyperpolarized monomer mixtures composed of cyclooctene (COE) and norbornene (NOE) were mixed in different proportions, $f = [COE]_0 / [NOE]_0 = 100: 0, 80: 20, 50: 50, 20: 80, 0: 100$. Figure 4-1a shows the ^{13}C spectra acquired at $t = 0.45$ s after these hyperpolarized monomer were mixed with the G3 catalyst. Monomer signal from carbon C1 to C4 are labeled in Figure 4-1a. Signal enhancement of the monomer signals is over 1500. This magnitude of signal enhancement is sufficient to observe polymer signals specific to different stereostructure generated from the *in-situ* reaction. Figure 4-1b,c show the expanded ^{13}C hyperpolarized spectra acquired at $t = 1.65$ s after the mixing. The selected time point is for showing the stronger polymer signals in the hyperpolarized spectra. The polymerization of cyclooctene itself generates poly(1-octenylene), and these polymer signals are as labeled in Figure 4-1b,c. New signals at 30.46 ppm and 28.00 ppm start to appear when the reaction dopes with norbornene as seen in Figure 4-1b. These signals are neither from the poly(1-octenylene) nor the poly(1,3-cyclopentylenevinylene), the polymer generated from the pure norbornene. They are from the doping of norbornene into the poly(1-octenylene). Since the incorporation of the second monomer alters the local microstructures of the generated polymers, the chemical shifts corresponding to the main polymer chain changes accordingly. We have identified the signal at 30.46 ppm is from $^{c}P_{3c}$, and the signal at 28.00 ppm is from $^{c}P_{2c}$. The changes of these chemical shifts

before and after the addition of norbornene are identical as has been reported in metathesis copolymerization using tungsten based catalysts.[136] Similarly, the incorporation of cyclooctene into the poly(1,3-cyclopentylenevinylene) also induce the chemical shift changes. Characteristic peaks are at 44.13 ppm, 43.86 ppm, 38.80 ppm, and 38.52 ppm in Figure 4-1c. They are originated from the signals of $^{N}P_{2tc}$, $^{N}P_{2tt}$, $^{N}P_{2cc}$, and $^{N}P_{2ct}$, respectively.[136] We have found the cis related polymer signals are in general have large differences in the chemical shifts indicating they are more sensitive to the occupation of the second monomer.

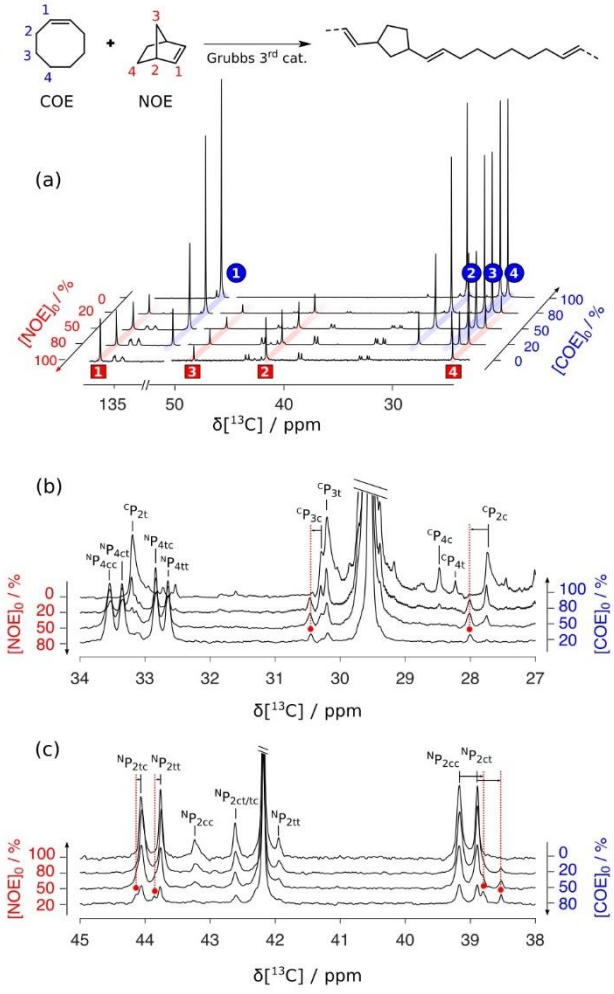

Figure 4-1. Reaction scheme of ring opening metathesis copolymerization using cyclooctene and norbornene and (a) ^{13}C hyperpolarized spectra acquired at t = 0.45 s after mixing the hyperpolarized monomers with the G3 catalyst. Each spectrum is acquired using a different monomer concentration ratio, as indicated along the axis at the left and right. The monomer signals from cyclooctene and norbornene are labeled with circles and squares, respectively. Enlarged regions of the ^{13}C hyperpolarized spectra from measured 165s after mixing are in (a) and (c). The polymer signals generated from the monomer are denoted as $^{y}P_{xz}$ (y = c or n stands for cyclooctene or norbornene; x = 1 – 4 stands for the carbon number; z stands for the stereostructure as defined in ref. 136). • are the characteristic peaks from the copolymer of cyclooctene and norbornene. All spectra were acquired using a flip angle of α = 13°.

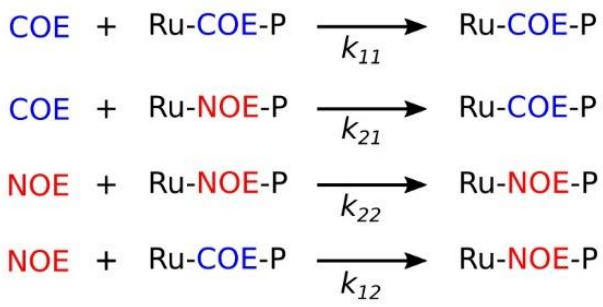

Scheme 4-1. The propagation reaction in ring opening metathesis copolymerization. P stands for the polymer.

The observation of signals from copolymer lead us to propose a kinetic model of copolymerization. For homopolymerization following a controlled/living polymerization mechanism, only one propagating site is generated and responsible for the propagation. In copolymerization, the presence of the second monomer split the propagation into four reactions, in which two active propagating sites appear, as shown in Scheme 4-1. Since the mechanism of ROMP involves the [2+2] cycloaddition of the monomer to the metal alkylidene (Ru=CHR), the reactivity of propagating species can be assumed to be dependent only on the nearest opened monomer unit next to the ruthenium *i.e.*, Ru-COE-polymer and Ru-NOE-P. The assumption similar to the chain growth copolymerization where the reactivity of an active center depends only upon the terminal monomer unit on which is located.

The propagation reactions in ring-opening metathesis copolymerization involve the reaction of COE and NOE react with Ru-COE-polymer and Ru-NOE-P as depicted in Scheme 4-1. The k_{11} and k_{22} are the second-order self-propagation rates for homopolymerization of COE or NOE respectively. The k_{12} and k_{21} are the second-order

cross-propagation rates representing the addition of NOE or COE into the Ru-COE-polymer or Ru-NOE-P respectively. Differential Equations for describing the concentration changes of each substance in Scheme 4-1 can then address as equation(4-4) to equation (4-7). Equations for describing hyperpolarized COE and NOE signal is by combining the spin-lattice relaxation of monomer, r_1^{COE} or r_1^{NOE}, with the kinetics:

$$\frac{dS_{COE}}{dt} = -(k_{11}[Ru - COE - P] + k_{21}[Ru - NOE - P] - r_1^{COE})S_{COE} \quad (4\text{-}1)$$

$$\frac{dS_{NOE}}{dt} = -(k_{22}[Ru - NOE - P] + k_{12}[Ru - COE - P] - r_1^{NOE})S_{NOE} \quad (4\text{-}2)$$

The equation (4-1) and equation (4-2) can be expanded to describe the individual monomer signals of C1 ~ C4 for both monomers.

Series of small flip angle pulses is applied to obtain the time-resolved monomer signals over the time courses of about 26 s after the mixing of catalyst and the monomers. Figure 4-2 presents the signal integration of C1 ~ C4 from both COE and NOE and the results of the data fitting using equation (4-1) and equation (4-2). The concentration of Ru-COE-P and Ru-NOE-P are numerically calculated using equation (4-4) to equation (4-7). The monomer signal after a pulse was computed using the polarization before the pulse multiplied with cos(α), where α is the flip angle.[66] Data sets acquired with f = 80: 20, 50: 50, and 20: 80 are used to calculate self-propagation and cross-propagation rate constants. The determined rate constants, k_{11}, k_{22}, k_{12}, and k_{21} in copolymerization are in Figure 4-3.

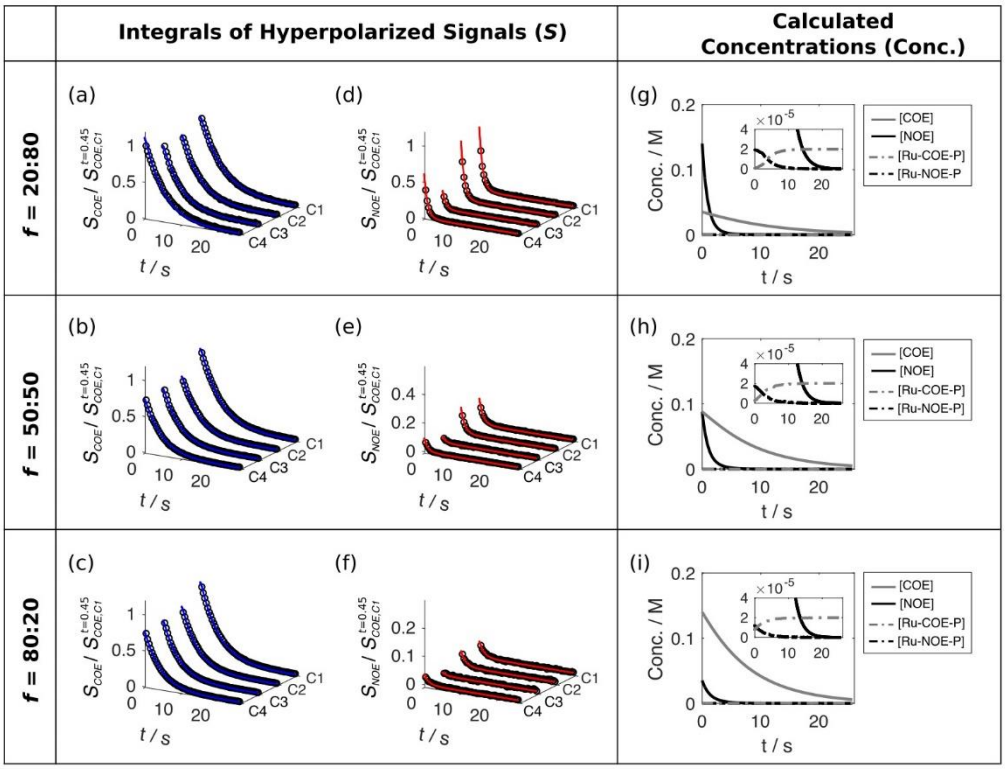

Figure 4-2. Time-evolution of hyperpolarized signal integrals of (a)-(c) cyclooctene and (d)-(e) norbornene in the copolymerization experiments. The solid lines indicate the result of the data fitting as described in 4.4.5 Data Analysis. (g)-(i) are the numerically calculated concentration changes over the time scale of the D-DNP experiments.

The determined rate constants shown in Figure 4-3 shows the reactions involve NOE (k_{22} and k_{21}) are faster than the reactions involving COE (k_{11} and k_{12}). It results in a quicker decay in the NOE signal and a larger error from the data fitting especially when the concentration of NOE is small (f = 80: 20 in Figure 4-3). Averaged values from the three data set are determined as $k_{11} = 0.56(\pm0.09)\cdot10^4$ $M^{-1}s^{-1}$, $k_{22} = 5.2(\pm0.35)\cdot10^4$ $M^{-1}s^{-1}$, $k_{12} = 2.3(\pm0.19)\cdot10^4$ $M^{-1}s^{-1}$, $k_{21} = 0.42(\pm0.06)\cdot10^4$ $M^{-1}s^{-1}$. The errors indicate the standard deviation of the three data. The calculated k_{11} and k_{22} are further compared with that determined in the data set collected using f = 100: 0 and f = 0: 100. In this case, a single

exponential equation containing the self-propagation rate constant can be used to describe the monomer signal evolution.[24]

$$S_M = S_{M(0)} e^{-(k_p[C]_0 + r_1 + \lambda)t} \tag{4-3}$$

In equation (4-3), the decay rate is the sum of spin-lattice relaxation of monomer, r_1, the second-order self-propagation rate constant, k_p for COE or NOE, the concentration of catalyst, $[C]_0$, and the $\lambda = \frac{-\ln(\cos(\alpha))}{\Delta t}$ with Δt indicating the time resolution between each scan. The last term describes the signal depletion by the rf pulses.[24] The results of data fitting are in Figure 4-4. The calculated rate constants are $k_p = 0.62(\pm 0.01)\cdot 10^4$ $M^{-1}s^{-1}$ for COE polymerization and $k_p = 5.7(\pm 0.15)\cdot 10^4$ $M^{-1}s^{-1}$ for NOE polymerization. These rate constants matched within error range with those determined in copolymerization.

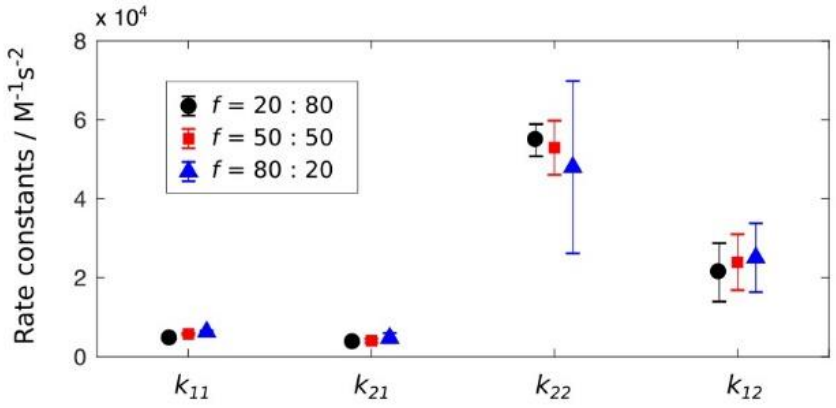

Figure 4-3. Self-propagation rate constants (k_{11} and k_{22}) and cross-propagation rate constants (k_{12} and k_{21}) determined from the numerical fitting as described in 4.4.5 Data Analysis. The error bars indicate the 95% confidence interval from the data fitting.

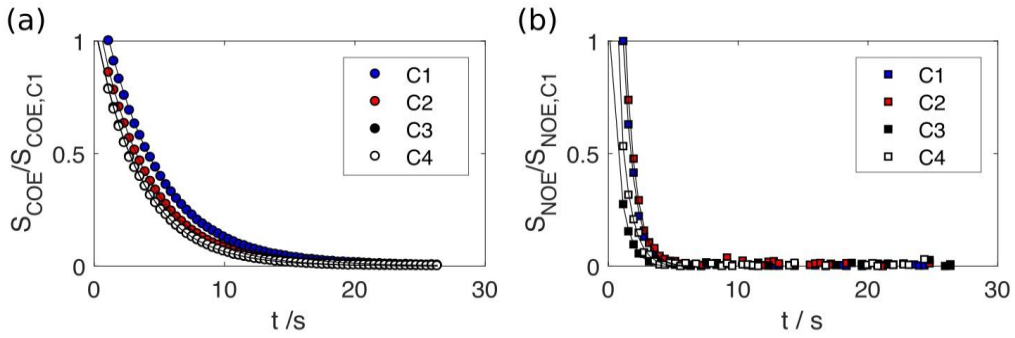

Figure 4-4. Time evolution of hyperpolarized monomer signal acquired from (a) f = 100: 0 and (b) f = 0:100. The solid lines are from the data fitting using equation (4-3).

The reactivity ratio for COE and NOE (r_{COE} and r_{NOE}) are 0.24(±0.02) and 13(±2.5), which are calculated using the determined rate constants. The errors indicate the standard deviation of three data sets. The result indicates NOE prefers the self-propagation (r_{NOE} > 1), and COE prefers the cross-propagation (r_{COE} < 1). Similar results have been found in the ring opening metathesis copolymerization using NOE and cycloalkane.[136] In the situation of r_{NOE} > 1and r_{COE} < 1, the instantaneous composition shift can occur as identified in the calculated concentration changes of Ru-COE-polymer and Ru-NOE-P in Figure 4-2(g)-(i). The Ru-NOE-P is quickly formed initially in all case, and the Ru-COE-polymer grow up after the consumption of the NOE.

4.3 Conclusion

In summary, we have demonstrated the kinetics of copolymerization can be determined using ^{13}C hyperpolarized NMR enabled by the dissolution DNP. The observed characteristic peaks in the time-resolved hyperpolarized spectra signify the doping of the second monomer. The self-propagation, cross-propagation, and the reactivity ratio can be

determined using a single data set acquired from hyperpolarized monomer mixtures. This real-time hyperpolarized method shortens the time needed for acquiring the same information using conventional methods. The ^{13}C hyperpolarization is applicable in the copolymerization containing monomers and polymers showing similar ^{1}H NMR signals. It opens the possibility to use the D-DNP method in the study of copolymerization with a broad range selection of monomers.

4.4 Experimental Section

4.4.1 Materials and preparation

Norbornene (> 99.0 % GC) was purchased from TCI America. Cyclooctene (analytical standard) and G3 catalyst, dichloro[1,3-bis(2,4,6-trimethylphenyl)-2-imidazolidinylidene](benzylidene)bis(3-bromopyridine)ruthenium(II), and α,γ-Bisdiphenylene-β-phenylallyl (BDPA) were purchased from Sigma-Aldrich. Toluene was dried over and distilled from NaK/Ph_2CO/18-crown-6 and stored in an Ar-filled glove box. Before the dissolution of the hyperpolarized sample, the 160 mM catalyst in toluene was prepared in an Ar-filled glove box, and then 50 μL of a solution is transferred to a 5 mm NMR tube. Before installing the NMR tube into the NMR instrument, the transfer line for injection of the DNP sample was purged with Ar gas to avoid contamination of the sample with moisture and oxygen from room air. After the hyperpolarized NMR measurement, the polymerization reaction was quenched with diethyl ether.

4.4.2 Dynamic Nuclear Polarization

The hyperpolarized monomer samples are prepared using 5.2 M cyclooctene (COE) and 5.2 M norbornene (NOE) both containing 15 mM BDPA in toluene mixed in a volume ratio (*f*) of 100: 0, 80: 20, 50: 50, 20: 80, and 0: 100. An aliquot of 15 μL of monomer sample was hyperpolarized in a HyperSense system (Oxford Instruments, Tubney Woods, U.K.) at 1.4 K under the irradiation of microwaves at $\omega_e - \omega_N$ = 93.965 GHz and a power of 60 mW, for 3 h. The hyperpolarized sample was dissolved in 4 mL of hot toluene 800 kPa and transferred into the rapid injection system by He gas.[100] The injection was accomplished with a forward pressure of 1450 kPa applied against a back pressure of 11030 kPa using Ar gas for 400 ms, followed by stabilization for 0.4 s. The hyperpolarized sample was mixed with the catalyst in the NMR tube during injection. The final temperature was 298 K.

4.4.3 NMR spectroscopy

The hyperpolarized NMR spectra were acquired using a Bruker 400 MHz NMR spectrometer equipped with a broadband probe containing three pulsed field gradients (Bruker Biospin, Billerica, MA) at a temperature of 298 K. A NMR experiment with the pulse sequence $[G_z\text{-}\alpha_x\text{-acquire}]_{\times 64}$, was triggered after hyperpolarized sample was delivered to the NMR tube. For each experiment, a data set with a total acquisition time of 25.6 s included 64 transients separated by 400 ms. A randomized pulsed field gradient, G_z (35.5 G·cm^{-1}, 1 ms) was applied to remove residual coherences from the previous scan. For ^{13}C experiments, a pulse with a small flip angle, α = 15.52º, and pulse strength γB_1 =

31.25 kHz was applied after G_z. During the acquisition, WALTZ-16 ^{1}H decoupling was applied with a field strength γB_1 = 32.78 kHz. In each transient, 15924 data points were acquired. Chemical shifts of ^{13}C of both the hyperpolarized and non-hyperpolarized experiments were referenced to the solvent resonance of toluene. The chemical shift of toluene was calibrated against tetramethylsilane (TMS) using a separate sample, following the IUPAC recommendations.[117]

4.4.4 Kinetics Equations

The rate equation used for describing the copolymerization of norbornene and cyclooctene in ring opening metathesis reaction based on Scheme 1 can be written as:

$$\frac{d[COE]}{dt} = -(k_{11}[Ru - COE - P] + k_{21}[Ru - NOE - P])[COE] \quad (4\text{-}4)$$

$$\frac{d[NOE]}{dt} = -(k_{22}[Ru - NOE - P] + k_{12}[Ru - COE - P])[NOE] \quad (4\text{-}5)$$

$$\frac{d[Ru-COE-P]}{dt} = -k_{12}[Ru - COE - P][NOE] + k_{21}[Ru - NOE - P][COE] \quad (4\text{-}6)$$

$$\frac{d[Ru-NOE-P]}{dt} = -k_{21}[Ru - NOE - P][COE] + k_{12}[Ru - COE - P][NOE] \quad (4\text{-}7)$$

Differential equations for describing hyperpolarized monomer signal are dependent on both the concentrations and the spin polarization of each species. Equations for the change in monomer signal can be found by considering the concentrations of each species in the spin-up and spin-down state separately, combining equation (4-4) with the relaxation terms.[84]

$$\frac{d[COE^+]}{dt} = -(k_{11}[Ru - COE - P] + k_{21}[Ru - NOE - P])[COE^+] - \frac{r_1}{2}([COE^-] - [COE^+]) \quad (4\text{-}8)$$

$$\frac{d[COE^-]}{dt} = -(k_{11}[Ru - COE - P] + k_{21}[Ru - NOE - P])[COE^-] - \frac{r_1}{2}([COE^+] - [COE^-]) \quad (4\text{-}9)$$

The NMR signal is proportional to the difference of the concentration of spin-up and spin-down sates, while the total concentration of monomer is equal to the sum. The equation for the signal evolution of COE, S_{COE}, can be found by combining equation (4-8) and equation (4-9):

$$\frac{dS_{COE}}{dt} = -(k_{11}[Ru - COE - P] + k_{21}[Ru - NOE - P])S_{COE} - r_1 S_{COE} \quad (4\text{-}10)$$

Similarly, the equation for the signal evolution of NOE, S_{NOE}, can be written as:

$$\frac{dS_{NOE}}{dt} = -(k_{22}[Ru - NOE - P] + k_{12}[Ru - COE - P])S_{NOE} - r_1 S_{NOE} \quad (4\text{-}11)$$

In equation (4-10) and equation (4-11), the r_1 is the spin-lattice relaxation of monomer for COE or NOE. They can be expanded to describe the individual monomer signals of C1 ~ C4 for both monomers.

4.4.5 Data Analysis

The raw NMR data were zero filled to 65536 complex data points, and an exponential window function with 3 Hz line broadening was applied before Fourier transform. Fourier transform was done using Topspin Software (Bruker Biospin). Peaks were integrated using Matlab (The Math Works, Natick, MA). The spin-lattice relaxation of hyperpolarized monomer, r_1, was determined from an experiment acquired using pure toluene instead of the catalyst solution. Single exponential equation with a decay rate constant characterizing the sum of λ describing a pulse effect ($\lambda = \frac{-\ln(\cos(\alpha))}{t_d}$) and r_1 is used for the calculation.[86] In this study λ=0.06 and the determined r_1 values are: 0.03 s^{-1}, 0.01 s^{-1}, 0.04 s^{-1}, and 0.04 s^{-1} for C1 to C4 of norbornene; 0.03 s^{-1}, 0.01 s^{-1}, 0.04 s^{-1}, and 0.04 s^{-1} for C1 to C4 of cyclooctene. The difference of the r_1 calculated from the monomer mixture with different monomer feed ratio (*f*) is within 0.01 s^{-1}.

For copolymerization, monomer signal of C1 to C4 from the data acquired using *f* = 20: 80, 50: 50, and 80: 20 were analyzed for calculating rate constants: k_{11}, k_{22}, k_{12}, and k_{21}. The calculation was done by numerically fitting norbornene C1 to C4 and cyclooctene C1 to C4 using equation (4-1) and equation (4-2). The time-dependent concentrations of each species are described in equation (4-4) to equation (4-7). The initial concentration of monomers is determined by separate experiments measured using ^{1}H non-hyperpolarized NMR without the addition of catalysts. Specifically, the ^{1}H NMR signals integrals from a standard sample with known concentration are compared with the signal integral of the monomers acquired after the injection. The determined values are: $[COE]_0$= 0.035 M and $[NOE]_0$= 0.140 M for *f* = 20: 80; $[COE]_0$= 0.088 M and $[NOE]_0$= 0.088 M for *f* = 50: 50;

$[COE]_0$= 0.140 M and $[NOE]_0$= 0.035 M for f = 80: 20. The concentration ratio of two monomers after the dilution is the same as the volume ratio prepared in the monomer feed for hyperpolarization. The initial concentration of Ru-COE-P and Ru-NOE-P are set to be the weight averaged of the catalyst concentration using equation (4-12) and equation (4-13). These Equations are based on the rate equation considering only the first monomer metathesis process with rate constants, k_{11} and k_{22}. This approximation is valid because G3 catalyst is a fast initiation catalyst that the active propagating sites are generated instantaneously.[110] The ratio of the concentration of Ru-COE-P and Ru-NOE-P is proportional to the ratios of the initial formation rates.

$$[Ru-COE-P]_0 = [C]_0 \frac{k_{11}[COE]_0}{k_{11}[COE]_0 + k_{22}[NOE]_0} \tag{4-12}$$

$$[Ru-NOE-P]_0 = [C]_0 \frac{k_{22}[NOE]_0}{k_{11}[COE]_0 + k_{22}[NOE]_0} \tag{4-13}$$

The fit parameters in this calculation are the self-propagation and cross-propagation rate constants and the initial monomer signal, $S_{COE}(0)$ and $S_{NOE}(0)$. The fitting procedure included a successive numerical solution of the differential equations followed by multiplication with cos(α) to account for the signal depletion due to each radio-frequency (rf) pulse.[66] The residual sum of squares was minimized using a multi-start algorithm in Matlab. The fitting results are in Figure 4-2 and Figure 4-3.

For homopolymerization, monomer signal of C1 to C4 from the data acquired using f = 100: 0 and f = 0: 100 were used to calculate the self-propagation rate constants by simultaneously fitting the data using equation (4-3). The residual sum of squares was minimized using Matlab. The results of data fitting are in Figure 4-4.

5. INTERMOLECULAR INTERACTIONS DETERMINED BY NOE BUILD-UP IN MACROMOLECULES FROM HYPERPOLARIZED SMALL MOLECULES[1]

5.1 Introduction

The nuclear Overhauser effect (NOE), with its steep r^{-6} dependence on distance, is widely used in NMR for determining molecular structure and interactions.[65] In the NOE experiment, the population distribution of one of the spins is disturbed away from equilibrium. Subsequent cross relaxation via the double quantum and zero quantum transitions then occurs, resulting in the NOE. Observable is a typically small fractional change in signal obtained after the perturbation. This change can either be quantified directly in one-dimensional spectra, or can give rise to cross peaks in multidimensional NMR.

For structure determination, for example of proteins, it is often sufficient to know whether or not an NOE between two specific spins has been observed. The NOE cross peak may further be classified into one of the categories of strong, intermediate or weak. Because structure calculations rely on the observation of a large number of NOE cross peaks, this information is sufficient. In other cases, the quantitative measurement of cross relaxation rates is desired. Cross relaxation rates, along with the auto relaxation rates of the same spins, can be determined from transient NOE buildup curves. The measurements,

[1] Reproduced in part from "Intermolecular Interactions Determined by NOE Build-up in Macromolecules from Hyperpolarized Small Molecules" by Chen, C.-H.; Wang, Y.; Hilty, C. *Methods* 2018. (In Press: doi.org/10.1016/j.ymeth.2018.02.015) Copyright [2018] by Elsevier.

which require the acquisition of spectra at multiple mixing times, are time-consuming due to the relative weakness of signal changes.

Traditional NOE experiments, both of one-dimensional or multi-dimensional type, rely either on saturation, or on inversion of nuclear spin populations. Therefore, the largest deviation from equilibrium, in the inversion experiment, is equal to twice the equilibrium population difference. Deviations that are orders of magnitude larger can be achieved through nuclear spin hyperpolarization. These enhancements directly transfer to an enhancement of the NOE. A challenge in realizing such enhancements is in finding hyperpolarization methods for liquid samples, compatible with macromolecular NMR. With the advent of dissolution dynamic nuclear polarization (D-DNP) over the past decade, a method has become available that is capable of generating high spin polarization levels that can be used in these experiments.[82] In D-DNP, polarization is first transferred from electrons spins to nuclear spins in a frozen aliquot, by a mechanism involving microwave saturation of a spin transition. The sample is then dissolved, and can subsequently be injected into a high-field NMR spectrometer for high sensitivity liquid state NMR spectroscopy. The D-DNP method can be used to polarize various NMR active nuclei, in particular those with spin-1/2. The signal enhancement depends on the efficiency of the polarization process in the solid state, which is a function of the sample and the polarization temperature. During the dissolution, polarization decay due to the spin relaxation is inevitable. Polarization loss can be minimized by rapid sample injector devices, which shorten the transfer time.[100,137] The hyperpolarized sample transferred to

the NMR spectrometer can mix with different substances for the characterization of reactions or intermolecular interactions.

For a D-DNP enhanced NOE experiment, a ligand or other molecule is mixed with a target, such as a protein or other macromolecule. Using hyperpolarized ligand, selective signal enhancement on the macromolecule provides information on ligand binding sites. The ^{1}H NMR spectrum shows a finger-print of enhanced protein signal from hyperpolarized ligand, which was shown to be close to the frequency profile of a saturation transfer difference (STD) NMR experiment.[138] Site specific polarization transfer can be identified with higher resolution in ^{1}H NMR spectrum using ^{13}C single quantum selection. In the interaction of folic acid with dihydrofolate reductase (DHFR), the resolved NOE peaks in the protein methyl group region were identified to match with the ligand binding site.[139] Two-step polarization transfer between competitively binding ligands, mediated by protein has been reported. Signal build up on the second ligand has been used to determine the ligand binding epitope.[140]

Polarization transfer to proteins can also be observed from hyperpolarized water. In this case, polarization transfer occurs predominantly due to the chemical exchange. In the DNP-water-LOGSY experiment, hyperpolarized water is used to characterize the ligand binding. Free and bound ligand can be differentiated based on signals with different sign.[141] Polarization transfer to amide proton in protein has also been observed using hyperpolarized water. Site-resolved spectroscopy can be realized using the ultrafast 2D NMR method.[142] Selective enhancement originating from hyperpolarized water to an

intrinsically disordered protein has further been used to give information about protein folding and unfolding.[143]

Using the D-DNP NMR method, signal build up curves due to polarization transfer from hyperpolarized molecules to macromolecules can be acquired and quantified in real-time. We have previously studied the interaction of hyperpolarized water and protein, where the signal build up is predominantly caused from the exchange.[144] We have also developed methods for the quantification of heteronuclear intermolecular NOE in small-molecule solutes.[145] In this paper, we demonstrate the application of D-DNP hyperpolarization to the determination of cross relaxation rates between small molecules and macromolecules. The interaction of third generation polyamidoamine (G3 PAMAM) dendrimer, with phenylbutrazone (PBZ) is used as a model. PAMAM contains repeated amide and tertiary amine groups within the branched structure, while the surface is decorated with primary amine groups.[146] When dissolved in aqueous solvent, the interior of the dendrimer is less polar than its outer shell. The difference in inner pocket and outer surface allows it to encapsulate hydrophobic compounds such as the small-molecule pharmaceutical PBZ via host-guest interaction.[147,148] The acquisition of time dependent NMR spectra shows polarization transfer from PBZ to dendrimer. From these spectra, we determine signal transfer rates, which indicate the sites of preferential location of the guests within the host molecule. We compare these results to conventional NMR spectroscopy, and discuss applications enabled by the increased sensitivity and the ability to complete signal acquisition within several seconds.

5.2 Results and Discussion

A ^{1}H NMR spectrum measured 0.61 s after mixing hyperpolarized PBZ with G3-PAMAM dendrimer is shown in Figure 5-1a. The spectrum acquired using the same sample without hyperpolarization is included for comparison. It can be seen that the ratio of signal intensity between PBZ and dendrimer is larger in the spectrum with hyperpolarized PBZ compared to the non-hyperpolarized spectrum. This difference arises because of the signal enhancement due to hyperpolarization, which is 2166, 655, 461, 600, and 1406 for the protons at positions (1/2), 3, 4, 5 and 6 on PBZ. The aforementioned signal enhancements were determined from the comparison of the two spectra in Figure 1a, and already include the relaxation losses that occurred during sample injection. The absolute signal intensities from the G3-PAMAM dendrimer are also larger in the spectrum with hyperpolarization, because of NOE transfer from the hyperpolarized PBZ.

Signal enhancements of the dendrimer due to NOE transfer can be evaluated from data, where the PBZ is hyperpolarized either to positive or to negative spin temperature. These two cases correspond to the appearance PBZ signals with positive or negative sign, respectively. Spectra from both of these experiments are shown in Figure 5-1b and Figure 5-1c. Since the region of the spectrum containing signals from the dendrimer is close to the signal of H_3 from PBZ, a baseline correction consisting of a subtraction of the Lorentzian shape determined from H_3 is included. The solid line in the figure indicates the signals acquired at the time points t = 0.61 to 2.61, at intervals of 0.4 s, after mixing with dendrimer. The dashed line shows the spectrum acquired from thermal polarization, after the D-DNP experiment using the same sample. Signal enhancement on the dendrimer are

primarily localized in the methylene in the inner layer, *i.e.* H_a, H_c, H_b, and H_d. H_A and H_C, locating in the outer layer, have no signal enlargement. The selective signal enhancement can also be found in the spectrum acquired using PBZ polarized at negative spin temperature (Figure 5-1c). In this experiment, negative NOE on the dendrimer signals, H_a, H_c, H_b, and H_d are observed. The experiments prove the increased signals in dendrimer are from the NOE.

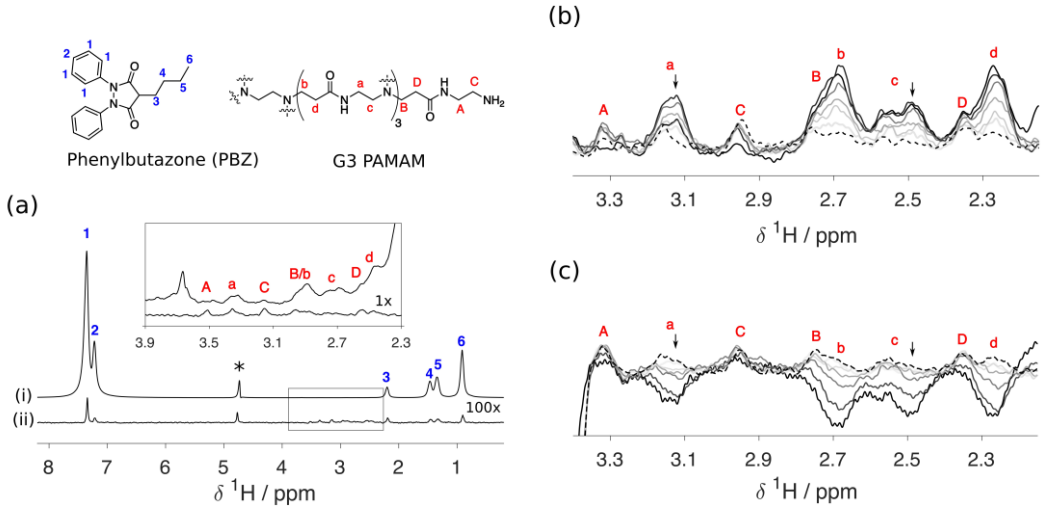

Figure 5-1. (a) Structure of phenylbutazone (PBZ), structure of G3 PAMAM dendrimer and ^{1}H spectrum acquired with (i) hyperpolarized PBZ mixed with G3 PAMAM dendrimer and (ii) non-hyperpolairzed PBZ with the G3 PAMAM. The inset shows the region of the spectrum containing dendrimer signals. These signals are assigned according to ref. 149, with H_A, H_B, H_C, H_D designating signals from the outer layer, and H_a, H_b, H_c, and H_d signals from the inner layer. * indicates water signal. (b) and (c) are ^{1}H spectra after baseline correction. The solid lines indicate the spectra acquired with (b) positively hyperpolarized PBZ or (c) negatively hyperpolarized PBZ mixed with preloaded G3 PAMAM dendrimer at t = 0.61 – 2.61 s with interval of 0.4 s. The dashed lines indicate the spectra of the same sample without hyperpolarization.

A closer look at the H_a and H_c signals shows that the signal enhancement in these peaks is not symmetrical. The shoulder of the H_a and H_c at lower chemical shift (black arrow in Figure 5-1b) shows a larger enhancement than the left shoulder. To examine the origin of the uneven transfer of polarization to the dendrimer, CPMG experiments using different echo duration were performed (Figure 5-2). These experiments indicate a larger T_2 relaxation rate at the lower chemical shift positions of the peaks for H_a and H_c, which is consistent with these positions stemming from the inner layer of the dendrimer, which are expected to be more rigid.

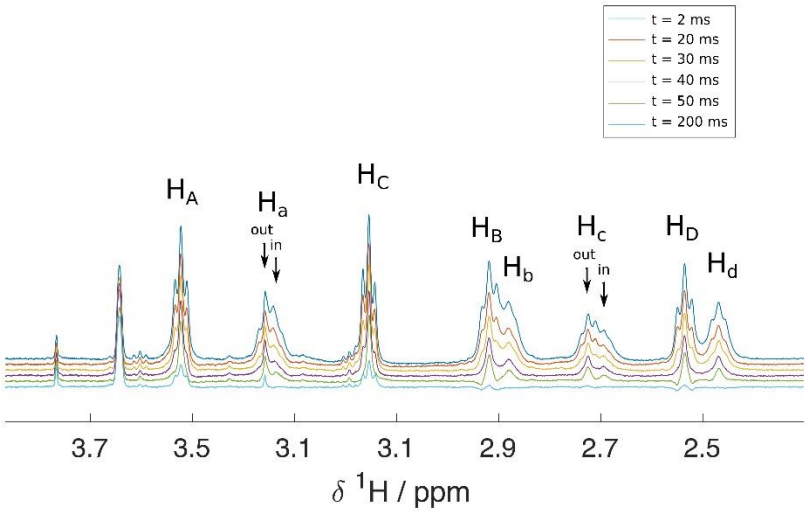

Figure 5-2. The ^{1}H spectra acquired using CPMG sequence with different echo duration, t.[150,151]

In the hyperpolarized spectra, a larger signal transfer from PBZ to the methylene in the inner layer of the dendrimer was identified in the spectrum at t = 0.61 s. Larger

cross-relaxation rates may be due to reduced internal motions, and additionally the local concentration of PBZ may differ in the inner and outer layers.

Figure 5-3 shows the time evolution of signal integrals from the spectra containing hyperpolarized PBZ mixed with G3 PAMAM dendrimer. As described above, primarily signals from the interior of the dendrimer are enhanced, corresponding to peaks designated by lowercase letters. For these peaks, the maximum transferred signal is between approximately $2 \cdot 10^{-4}$ and $3 \cdot 10^{-4}$ of the PBZ signal intensity. This corresponds to an enhancement of approximately 2 to 3-fold compared to signals from these spins at thermal polarization in NMR magnet. The magnitude of thermally polarized signals can be seen at the end of each time-resolved trace, where the hyperpolarization has decayed.

Signal build-up and decay rates can be obtained from fitting this data with the Solomon equation for a two spin system, as described in the Experimental section. This two-spin approximation neglects any effects caused by spin diffusion. Because the origin of transferred polarization is not known from the signals shown in Figure 5-3, the sum of all signals from hyperpolarized PBZ was treated as spin S. The individual dendrimer signals, which are resolved in the acquired spectra, were individually treated as the second spin I. An exception are the signals from positions B/b and D/d, where the interior and exterior signals were grouped based on their signal overlap.

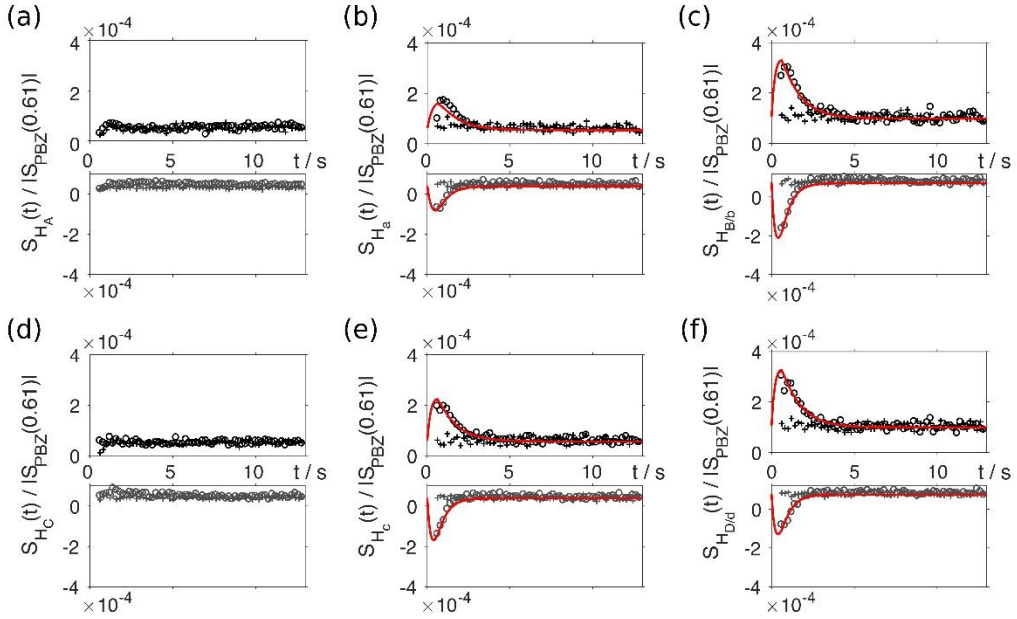

Figure 5-3. Time dependence of ^{1}H NMR signal integrals of PAMAM-G3 dendrimer after mixing with hyperpolarized PBZ, for (a) H_A, (b) H_a, (c) $H_{B/b}$, (d) H_C, (e) H_c, and (f) $H_{D/d}$. The integral values were normalized by the PBZ signal at t = 0.61 s, which is the time of the first acquired data point. Data points (○) indicate the signal integrals from hyperpolarized spectra. Data points (+) indicate the signal integrals from sample acquired after hyperpolarization. The top panel in each plot is obtained using PBZ hyperpolarized to positive spin temperature, and the bottom panel is obtained from hyperpolarization to negative spin temperature. Solid lines indicate the fitting result. For fitting, auto relaxation rate from inversion recovery experiments were used, $r_I(H_a)$ = 2.5 s^{-1}, $r_I(H_c)$ = 3.9 s^{-1}, $r_I(H_{B/b})$ = 4.0 s^{-1}, $r_I(H_{D/d})$ = 4.1 s^{-1}, for the sample of positively polarized PBZ and $r_I(H_a)$ = 2.8 s^{-1}, $r_I(H_c)$ = 4.5 s^{-1}, $r_I(H_{B/b})$ = 4.2 s^{-1}, $r_I(H_{D/d})$ = 4.3 s^{-1}, for the sample of negatively polarized PBZ.

The results from these fits are shown as a solid line in Figure 5-3. Auto relaxation for averaged hyperpolarized spin, r_S, were determined from the data fitting as r_S = 0.45±0.01 s^{-1} and 1.4±0.05 s^{-1} using positively hyperpolairzed PBZ and negatively hyperpolarized PBZ, respectively. The error range indicates the 95% confidence intervals from the fitting.

The fit indicates both a lower amplitude and more rapid decay for signals originating from PBZ with negative spin polarization. A difference in the signal evolution from positive and negative polarization is expected because relaxation returns spin polarization to a positive equilibrium. In the data from Figure 5-3, the maximum of the signals transferred from hyperpolarization is approximately three times larger than the equilibrium signal, hence the negative maximum is of lower magnitude. Additionally contributing to the observed differences is likely also the instability of the spin system at negative polarization. We have previously observed spontaneous emissions NMR signals from ^{1}H hyperpolarized to negative spin temperature, which could be modeled using equations similar to those describing the microwave amplification using stimulated emission (MASER) effect, and which among other effects reduced the signal amplitude after injection.[152]

Apparent cross relaxation rates stemming from the polarization transfer of positively hyperpolarized PBZ to individual dendrimer peaks were determined as $\sigma_{Ha} = (-3.2\pm0.8) \cdot 10^{-4}\ s^{-1}$, $\sigma_{Hc} = (-7.8\pm1.2) \cdot 10^{-4}\ s^{-1}$, $\sigma_{HB/b} = (-9.5\pm1.3) \cdot 10^{-4}\ s^{-1}$, and $\sigma_{HD/d} = (-9.5\pm1.3) \cdot 10^{-4}\ s^{-1}$. The apparent cross relaxation rates from the polarization transfer of negatively hyperpolarized PBZ were $\sigma_{Ha} = (-3.0\pm1.6) \cdot 10^{-4}\ s^{-1}$, $\sigma_{Hc} = (-6.8\pm2.6) \cdot 10^{-4}\ s^{-1}$, $\sigma_{HB/b} = (-8.9\pm2.4) \cdot 10^{-4}\ s^{-1}$, and $\sigma_{HD/d} = (-6.6\pm2.5) \cdot 10^{-3}\ s^{-1}$. The larger error margin when using negatively polarized PBZ is presumably due to the more rapid signal decay. However, it can be noted that the difference in the cross-relaxation rates determined from the data sets using the two types of polarization is not significant.

The cross-relaxation rates that are observed depend on the $\langle r^{-6} \rangle$ weighted average of distances between source and target spin, as well as on the correlation time for molecular motions. The latter is likely different within the different layers of the dendrimer. The calculated apparent cross relaxation rates therefore also indicate an average over different layers. Regardless, some comparisons are possible. For example, H_a and H_c are two nearby protons with the same spin concentration. Assuming that the correlation times of these two protons are similar within each layer, the larger σ_{Hc} indicates that PBZ is closer in space to H_c than to H_a.

The signal build-up observed in the hyperpolarized NOE experiments can further be compared with conventional 2D-NOESY. [^{1}H,^{1}H]-NOESY spectra were measured using the sample collected after a D-DNP experiment. Figure 5-4 shows the region of such a NOESY spectrum, which contains the cross-peaks between H_1 and H_a, H_c, $H_{B/b}$ and $H_{D/d}$. Although this spectrum was measured on a 500 MHz NMR spectrometer with cryoprobe, a measurement time of 54 h was required.

Due to the relatively long measurement time, the 2D-NOESY was acquired only for one mixing time of 100 ms. In the absence of a NOE build-up curve, the cross relaxation rate can be determined using the initial build up at short mixing time.[153] Although the mixing time of 100 ms may be sufficiently long to cause an error when using the short time approximation, its use increased the signal strength of cross-peaks to a detectable level. Comparable to the fraction of spin polarization transferred in the hyperpolarized experiments, the ratio of cross-peaks to diagonal peaks in the 2D-NOESY ranged from $1.5 \cdot 10^{-5}$ and to $6.5 \cdot 10^{-5}$. Using the short-time approximation, cross-relaxation

rates were determined from the slope of the volume ratio of cross peak integrals divided by the diagonal peak integrals. The resulting cross-relaxation rates for cross-peaks correlating the phenyl group of PBZ with the protons from the interior of the dendrimer were $\sigma_{Ha} = -1.5 \cdot 10^{-4}\ s^{-1}$, $\sigma_{Hc} = -4.5 \cdot 10^{-4}\ s^{-1}$, $\sigma_{HB/b} = -6.5 \cdot 10^{-4}\ s^{-1}$, and $\sigma_{HD/d} = -6.3 \cdot 10^{-4}\ s^{-1}$. The result shows a similar trend as the cross-relaxation rates determined using the D-DNP method. The σ_{Hc} is larger than σ_{Ha}, and $\sigma_{HB/b}$ is larger than $\sigma_{HD/d}$. Other cross-peaks were not observed.

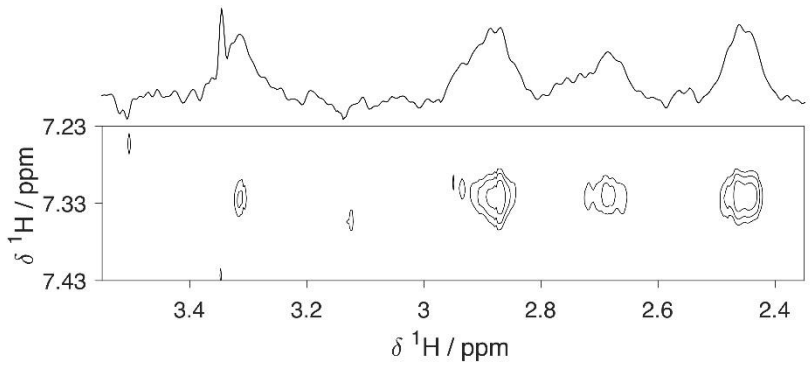

Figure 5-4. Enlarged area of ^{1}H-^{1}H NOESY spectrum of PBZ with G3-PAMAM dendrimer. 4096 x 512 complex points were collected with mixing time of 100 ms and 256 scans. The spectrum of the top is the 1D slice showing the highest signal intensity in this region. The signal at 3.48 ppm is from the residual methanol from the stock solution of PAMAM.

The signal-to-noise ratio, 4.1, is determined using the signal intensity of H_b at 2.89 ppm in the sliced 1D spectrum showing the highest cross peak intensity. Further decreasing the mixing time to more accurately determine cross relaxation rates in the initial build-up therefore seems prohibitive. The signal-to-noise ratio in the hyperpolarized

spectrum measured at t = 0.61 s shown in Figure 5-1b was determined as 15 using the signal intensity of H_b at 2.89 ppm. The NOE build up can be directly observed in a single experiment using D-DNP NMR spectroscopy. The hyperpolarized spectroscopy therefore offers a higher sensitivity despite the use of an experiment time of several days for the conventional NOESY spectrum, and of an NMR instrument equipped with cryoprobe at the higher magnetic field of 11.74 T.

Other than the convention NOESY, the hyperpolarized experiment on the other hand does not directly provide site resolution for the origin of polarization in the NOE transfer. Site resolution could potentially be introduced by using rapid two-dimensional NMR techniques, potentially at the expense of the inability to record time resolved build-up curves.[154,155] Alternatively, signal contributions from individual source spins can be estimated by performing experiments including selective inversion pulses (see Section 5.4.3 Hyperpolarized NMR Experiment Scheme 5-1). This option is shown in Figure 5-5. Selective inversion pulses were applied to the phenyl (H_1/H_2) or the methyl groups (H_3-H_6) of PBZ near the start of the NMR experiment. Potential problems of this comparison are the variations of the signal enhancement and sample concentration in different experiments. Therefore, the data from each experiment is normalized by the signal enhancement of the methyl or phenyl group that is not inverted. The variation of the sample concentration between two data sets was negligible as determined from the signals observed at later time after the polarization has decayed (see Figure 5-5 for $t > 10$ s). By comparing the signal acquired with inversion pulse from the signal acquired without the inversion pulses, large reductions in the polarization transfer were observed in the case

when the phenyl group is irradiated with the inversion pulse (Figure 5-5a to d). Whereas, the data acquired with methyl group inversion in Figure 5-5e to h shows a smaller, but non-negligible change.

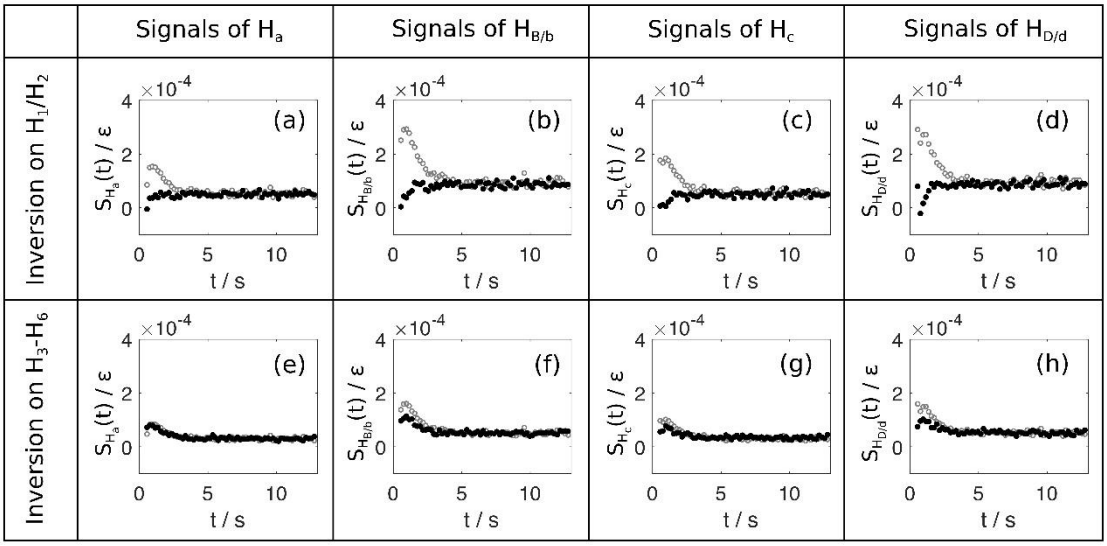

Figure 5-5. Comparison of signal contribution from phenyl group (H_1/H_2) or methyl group (H_3-H_6) of PBZ using selective inversion experiments. Data points with filled circles (●) indicate the signal integrals from hyperpolarized spectra with the inversion pulse applied on (a) to (d) phenyl group or (e) to (h) methyl group. Data points with open circles (○) indicate the signal integrals from hyperpolarized spectra with no inversion pulse (same data as in Figure 2). The signals in (a) to (d) are normalized by the signal enhancement, ε, determined from the methyl group of PBZ, which is not inverted in this experiment. The signals in (e) to (h) are normalized by the signal enhancement, ε, determined from the phenyl group of PBZ, which is not inverted in this experiment.

The larger polarization transfer from the phenyl group may be related to a larger number of spins, slower auto relaxation rates, and perhaps more efficient cross relaxation rates between the phenyl group and the dendrimer. It is worth to note the NOE from the methyl group of PBZ to dendrimer was only observed in the hyperpolarized spectrum, and

was not above the noise level in the 2D NOESY acquired on 54 hours on a 500 MHz NMR instrument with cryoprobe. This illustrates that the D-DNP NMR method increases sensitivity and can allow for the identification of NOE crosspeaks due to weak interactions that are not otherwise readily observable.

5.3 Conclusions

In summary, we observed site specific NOE build up in G3 PAMAM dendrimer from polarization transfer of positively and negatively polarized PBZ. The time evolution of signal allows for determining the cross relaxation rate that is specific to different sites on the dendrimer. NOE from hyperpolarized PBZ to the dendrimer, H_a, $H_{B/b}$, H_c, $H_{D/d}$, has been characterized. The D-DNP experiment provides increased signal-to-noise ratio to characterize intermolecular interactions in a short time compared to the conventional NOESY experiments. Such improvement is especially desirable for the detection of low concentration samples, high-cost molecules, or experiments with unstable samples not suitable for long term experiments. It may further be of interest for investigating the dynamics of macromolecules exhibiting conformational changes in real time.

5.4 Experimental Section

5.4.1 Materials

Phenylbutazone was purchased from Alfa Aesar. PAMAM dendrimer, ethylenediamine core, generation 3.0 solution (20 wt. % in methanol) was purchased from Sigma-Aldrich. D_2O, d_6-ethylene glycol and NaOD were purchased from Cambridge

Isotope Laboratories. The dendrimer solutions were prepared by air drying 4 µl of sample from stock solution, and redissolving into 50 µl of 100 mM sodium phosphate buffer at pH 7.

5.4.2 Dynamic Nuclear Polarization

Samples of 1.2 M of phenylbutazone (PBZ) were prepared in D_2O/d_6-ethylene glycol solution (3:7 v/v) containing 1.5 M NaOD and 15 mM 4-hydroxy-2,2,6,6-tetramethylpiperidin-1-oxyl (TEMPOL). 20 µl aliquot of this solution was hyperpolarized using a HyperSense DNP polarizer (Oxford Instruments, Abingdon, U.K.). Hyperpolarization to positive spin temperature occurred at 1.4 K under the irradiation of microwaves at 94.005 GHz, near $\nu_e - \nu_N$, and a power of 100 mW. ν_e and ν_N are the frequencies of electron and nuclear spins in the magnetic field of the DNP polarizer. For hyperpolarization to negative spin temperature, microwave radiation at 94.270 GHz, near $\nu_e + \nu_N$, was used. In both cases, microwave radiation was applied for a duration of 20 min. The hyperpolarized sample was then dissolved in 4 mL of D_2O buffer. This dissolution solvent contained 100 mM sodium phosphate buffer at pH 7, and was heated until a pressure 800 kPa was reached at a temperature of approximately 400 K. The injection was accomplished with N_2 gas at a forward pressure of 1790 kPa applied against a back pressure of 1030 kPa for t_{inj} = 380 ms to transfer the hyperpolarized sample to the NMR spectromer, followed by a stabilization time of t_{stab} = 100 ms.[100] The hyperpolarized sample was mixed with dendrimer solution in the NMR tube due to turbulence arising

during the injection. The final concentration of PBZ in the NMR tube was estimated as 10 mM, and dendrimer concentration was 0.3 mM. The final temperature was 303 K.

5.4.3 Hyperpolarized NMR Experiment

The NMR spectra from hyperpolarized samples were acquired using a Bruker 400 MHz NMR spectrometer equipped with a boradband observe probe containing three pulsed field gradients (Bruker Biospin, Billerica, MA). The NMR experiment consisted of a sequence of small flip angle excitation pulses (Scheme 5-1). This experiment was triggered after the hyperpolarized sample was delivered to the NMR tube. Solvent suppression included a saturation pulse of 400 ms duration and a strength of $\gamma B_1/(2\pi)$ = 22 kHz was applied at the frequency of ethylene glycol at 3.63 ppm, in order to suppress signals of hyperpolarized residual protons. Water suppression consisted of the application of a sequence of three EBURP2 shaped $\pi/2$ pulses of 20 ms duration followed by pulsed-field gradients G_x (39 G/cm, 1 ms), G_y (39 G/cm, 1 ms), and G_z (45 G/cm, 1 ms). The flip angle for the excitation pulse was $\alpha = \pi/6$. The time interval between acquisitions was 0.2 s. For the inversion experiment, the phenyl group or the methyl group on PBZ are irradiated by an additional IBURP2 pulse of 20 ms after the t_{stab} as indicated inside the parenthesis in Scheme 5-1. For all hyperpolarized NMR measurements, each data set with total acquisition time of 25.6 s included 64 transients separated by 200 ms. In each transient, 1916 data points were collected.

The spin-lattice relaxation rates of dendrimer, r_1, were measured from the same sample collected after D-DNP experiments using an inversion-recovery pulse sequence.

Spectra containing recovery times of 0.01, 0.05, 0.1, 0.15, 0.2, 0.25, 0.3, 0.4, 0.5, 0.8, 1, 1.5, 2, 2.5, 3, and 3.5 s were acquired. Each spectrum was measured using $\gamma B_1/(2\pi)$ = 22 kHz, acquisition time of 1 s and 4 scans.

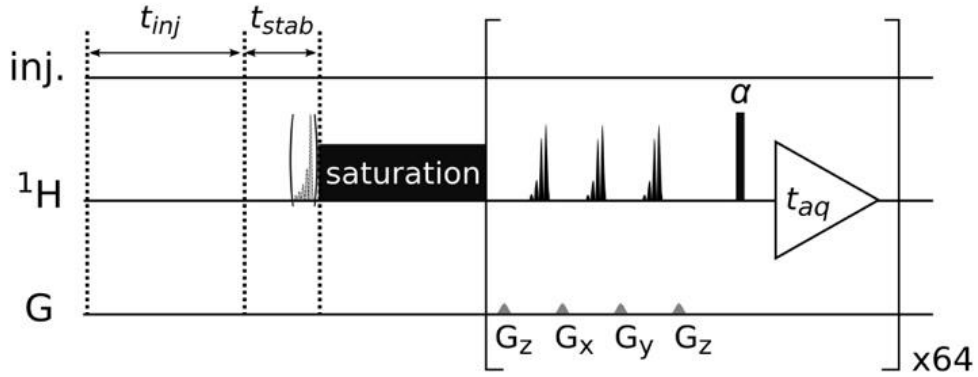

Scheme 5-1. Pulse scheme for the D-DNP experiments. Injection pressure (inj.) was applied during the injection time (t_{inj} = 380 ms). The sample was equilibrated for the stablization time (t_{stab} = 100 ms). The hyperpolarized small molecule (PBZ) and non-hyperpolarized macromolecule (dendrimer) mixed during these time intervals. A saturation pulse of 400 ms duration and a strength of $\gamma B_1/(2\pi)$ = 22 kHz was applied at the resonance frequency of hyperpolarized solvent (ethylene glycol at 3.63 ppm). The water resonance was selectively excited by EBURP2 shaped π/2 pulses of 20 ms duration and dephased by pulsed filed gradients G_x (39 G/cm, 1 ms), G_y (39 G/cm, 1 ms), and G_z (45 G/cm, 1 ms). The flip angle for the excitation pulse was $\alpha = \pi/6$. The time interval between acquisitions was 0.2 s. The shaded shaped pulse in the parenthesis represents a IBURP2 shaped π pulse of 20 ms, which was optionally used for selectively inverting the phenyl (H_1/H_2) or methyl group (H_3-H_6) of PBZ.

5.4.4 Reference NMR Experiment

A ^{1}H-^{1}H NOESY experiment and ^{1}H CPMG experiments in Figure 5-2 were measured on a 500 MHz NMR spectrometer with a TCI cryoprobe (Bruker Biospin, Billerica, MA). The sample used for this experiment was collected after a D-DNP NMR experiment to ensure comparable conditions. In the indirect and direct dimensions, 512 ×

2048 complex points were collected, with 256 scans per increment. The maximum acquisition times were $t_{1,max}$ = 39 ms and $t_{2,max}$ = 204 ms in the indirect and direct dimensions, respectively. The NOE mixing time was 100 ms, and the relaxation delay was 1 s. The temperature was 303 K. The data were processed with zero filling into 4096 × 2048 complex points and a sine-squared window function using Topspin 3.5. The total experiment time takes 54 h. The cross relaxation rates were estimated using the volume ratio of the cross peaks over the diagonal peaks.[153] Mixing time of 100 ms is applied here for acquiring spectrum with good signal-to-noise ratio in a reasonable experimental time.

In Figure 5-2, the CPMG pulse sequence was applied for 2, 20, 30, 40, 50, 200 ms after the $\pi/2$ pulse excitation with a strength of $\gamma B_1/(2\pi)$ = 18 kHz.[150,151]

5.4.5 Data Analysis

The raw NMR data were zero filled to 8192 complex data points, and an exponential window function with 5 Hz line broadening was applied before Fourier transform (Topspin software, Bruker Biospin). Chemical shifts were referenced to the signal of ethylene glycol. The chemical shift of ethylene glycol was calibrated against 4,4-dimethyl-4-silapentane-1-sulfonic acid (DSS) using a separate sample.[117]

Peaks from PBZ and dendrimer were integrated using Matlab (The Math Works, Natick, MA). Integration of dendrimer peaks included subtraction of the Lorentzian shape fitted on the nearest PBZ signal, H_3. The NOE polarization transfer was analyzed using the Solomon equations for a two spin system containing spins I and S.[156] The PBZ signals were grouped together by adding signal integrals and considered as spin S. Individual

dendrimer signals, H_a, H_c, $H_{B/b}$, and $H_{D/d}$, were considered as spin I. The signal shown in Figure 2 and Figure S2 are normalized by the signal of PBZ at t = 0.61 s, $S_{PBZ}(0.61)$. Equations (5-1)-(5-7) (see below and ref. 148) were used for fitting the time evolution of the signals. The fitted parameters were the average spin-lattice relaxation rate of the hyperpolarized spins, r_S, the total initial signal amplitude from hyperpolarized spin at t = 0, $S_{PBZ}(0)$, and the cross relaxation rate, σ_{Ha}, σ_{Hc}, $\sigma_{HB/b}$, and $\sigma_{HD/d}$ representing the polarization transfer to different sites of the dendrimer. The depletion of spin polarization by each radio frequency pulse was accounted for by performing the data fitting step-by-step for each data point. The polarization for each spin after a pulse was calculated by multiplying the polarization before the pulse with cos(α), where α is the flip angle.[145] The time point t = 0 was defined by the sum of half of the injection time t_{inj}, the stabilization time t_{stab}, the time for presaturation (0.4 s), the time for water suppression pulses. The fitting was performed using the nonlinear least square method in the Matlab program. The errors are determined from the 95 % confidence interval from the data fitting.

Here, Let I_z and S_z represent the ensemble average magnetizations of spins I and S. Solution of Solomon equations in two spin system is described as ref. 156:

$$\Delta S_z(t) = a_{SI}\Delta I_z(0) + a_{SS}\Delta S_z(0) \quad (5\text{-}1)$$

$$\Delta I_z(t) = a_{II}\Delta I_z(0) + a_{IS}\Delta S_z(0) \quad (5\text{-}2)$$

$$a_{II}(t) = \frac{1}{2}e^{-R_L t}\left[\left(1 - \frac{r_I - r_S}{R_C}\right) + \left(1 + \frac{r_I - r_S}{R_C}\right)e^{-R_C t}\right] \quad (5\text{-}3)$$

$$a_{SS}(t) = \frac{1}{2} e^{-R_L t} \left[\left(1 + \frac{r_{I-} r_S}{R_C} \right) + \left(1 - \frac{r_{I-} r_S}{R_C} \right) e^{-R_C t} \right] \quad (5\text{-}4)$$

$$a_{SI}(t) = a_{IS}(t) = \frac{-\sigma}{R_C} e^{-R_L t} (1 - e^{-R_C t}) \quad (5\text{-}5)$$

$$R_C = [(r_{I-} r_S)^2 + 4\sigma^2]^{0.5} \quad (5\text{-}6)$$

$$R_L = \frac{1}{2} [(r_{I-} r_S) - [(r_{I-} r_S)^2 + 4\sigma^2]^{0.5}] \quad (5\text{-}7)$$

where I_{eq} and S_{eq} are the magnetizations at thermal equilibrium; $\Delta S_z(t) = S_z(t) - S_{z,eq}$, and $\Delta I_z(t) = I_z(t) - I_{z,eq}$; $\Delta S_z(0)$ and $\Delta I_z(0)$ are the initial signal intensities at the beginning of the time period under consideration; r_I and r_S are the auto relaxation rate, and σ is the cross relaxation rate.

The data shown in Figure 5-5 are normalized by the signal enhancement determined from the ligand group that is not selectively inverted. Specifically, for the result comparing the inversion pulse on phenyl group, both data sets are normalized by the signal enhancement individually determined from the methyl group at t = 0.61 s. Similarly, for the result comparing the inversion pulse on methyl group, both data sets are normalized by the signal enhancement individually determined from the phenyl group at t = 0.61 s.

6. GENERAL CONCLUSIONS

In this dissertation, we have characterized reaction mechanisms, kinetics, and intermolecular interaction in polymers, using D-DNP NMR spectroscopy. This technique combines the advantages of observing low sensitivity NMR nuclei such as ^{13}C in a single scan with the capability to measure time evolutions.

We have identified signals pertaining to the microstructure of polymers generated *in situ* by mixing hyperpolarized monomers with catalysts in time-resolved spectra. The specific structures observed are isotactic, atactic polyolefins in metallocene-catalyzed polymerization, and polynorbornene with E/Z stereostructures in ring-opening metathesis polymerization. The hyperpolarized NMR signals are observable on the second time scale, in contrast, similar structural information requires signal averages for several hours in non-hyperpolarized NMR measurement.

The time-evolution of NMR signals acquired from polymerization reaction was used to describe different polymerization mechanisms. Notably, we have identified a living polymerization and polymerization subject to deactivation or slow initiation. These mechanisms can be readily distinguished using the time-evolution of monomer signals plotted on a logarithmic scale. A straight line in this graph indicates a living polymerization mechanism. A curve with a decreasing signal attenuation at later time is for the deactivation, in contrast, a curve with an accelerating signal attenuation is due to slow initiation. Rate constants of propagation, deactivation, or initiation were calculated based on data fitting using the corresponding model equations. Because of the fast time

scale of the measurement, the analysis using D-DNP NMR spectroscopy only considers side reactions occurred in the early time of a reaction. Secondary reactions at a later time can be ignored. This feature results in a simplification of the kinetic calculation.

The polymer species generally have more rapid signal decays in the hyperpolarized NMR spectra. The stopped-flow measurement enabled by a sample injector designed for D-DNP NMR was sufficiently rapid to detect the polymer signal build-up due to the reaction. Notably, the polymer signal build-up specific to different polymer stereostructures can be acquired by this method. D-DNP NMR therefore is a unique tool for obtaining information complementary to that observed by conventional NMR spectroscopy.

A similar analytical method was developed for the copolymerization reaction. As described in Chapter 3, we determined the rate constants related to the two monomers with different propagating catalytic sites. The feasibility of the real-time measurement shortens the time needed for acquiring the rate constants, which can then be used to determine the copolymer composition. This work demonstrates the potential of applying D-DNP NMR spectroscopy in analyzing a broad range of monomers as well as the final composition in the copolymerization.

Another application of D-DNP NMR in polymer science is the characterization of intermolecular interactions. These interactions are generally weak, and their observation by NMR requires signal averages, resulting in a long measurement time. We demonstrate that hyperpolarized NMR techniques significantly shorten the measurement of intermolecular interactions.

In conclusion, the hyperpolarized NMR provides substantial signal enhancement and increased sensitivity allowing the identification of polymer signals in a high resolution. Combining the stopped-flow techniques with hyperpolarization, we demonstrated a simultaneous characterization of polymer microstructures and chemical reactions. The obtainable information is inaccessible or difficult to be acquired using non-hyperpolarized NMR making D-DNP NMR spectroscopy a unique technique in advanced researches in the polymer chemistry.

REFERENCES

(1) *Protein NMR Spectroscopy: Principles and Practice*, 2nd ed.; Cavanagh, J., Ed.; Academic Press: Amsterdam ; Boston, 2007.

(2) Hatada, K.; Kitayama, T. *NMR Spectroscopy of Polymers*; Springer Berlin Heidelberg: Berlin, Heidelberg, 2004.

(3) *NMR Spectroscopy of Polymers*; Ibbett, R. N., Ed.; Springer Netherlands: Dordrecht, 1993.

(4) Ardenkjaer-Larsen, J.-H.; Boebinger, G. S.; Comment, A.; Duckett, S.; Edison, A. S.; Engelke, F.; Griesinger, C.; Griffin, R. G.; Hilty, C.; Maeda, H.; et al. Facing and Overcoming Sensitivity Challenges in Biomolecular NMR Spectroscopy. *Angew. Chem. Int. Ed.* **2015**, *54* (32), 9162–9185.

(5) Cherubini, A.; Bifone, A. Hyperpolarised Xenon in Biology. *Prog. Nucl. Magn. Reson. Spectrosc.* **2003**, *42* (1–2), 1–30.

(6) Green, R. A.; Adams, R. W.; Duckett, S. B.; Mewis, R. E.; Williamson, D. C.; Green, G. G. R. The Theory and Practice of Hyperpolarization in Magnetic Resonance Using Parahydrogen. *Prog. Nucl. Magn. Reson. Spectrosc.* **2012**, *67*, 1–48.

(7) Lilly Thankamony, A. S.; Wittmann, J. J.; Kaushik, M.; Corzilius, B. Dynamic Nuclear Polarization for Sensitivity Enhancement in Modern Solid-State NMR. *Prog. Nucl. Magn. Reson. Spectrosc.* **2017**, *102–103*, 120–195.

(8) Lee, J. H.; Okuno, Y.; Cavagnero, S. Sensitivity Enhancement in Solution NMR: Emerging Ideas and New Frontiers. *J. Magn. Reson.* **2014**, *241*, 18–31.

(9) Walker, T. G.; Happer, W. Spin-Exchange Optical Pumping of Noble-Gas Nuclei. *Rev. Mod. Phys.* **1997**, *69* (2), 629–642.

(10) Cocivera, M. Optically Induced Overhauser Effect in Solution. Nuclear Magnetic Resonance Emission. *J. Am. Chem. Soc.* **1968**, *90* (12), 3261–3263.

(11) Natterer, J.; Bargon, J. Parahydrogen Induced Polarization. *Prog. Nucl. Magn. Reson. Spectrosc.* **1997**, *31* (4), 293–315.

(12) Griffin, R. G.; Prisner, T. F. High Field Dynamic Nuclear Polarization—the Renaissance. *Phys. Chem. Chem. Phys.* **2010**, *12* (22), 5737.

(13) Reynolds, S.; Patel, H. Monitoring the Solid-State Polarization of 13C, 15N, 2H, 29Si and 31P. *Appl. Magn. Reson.* **2008**, *34* (3–4), 495–508.

(14) Lumata, L.; Jindal, A. K.; Merritt, M. E.; Malloy, C. R.; Sherry, A. D.; Kovacs, Z. DNP by Thermal Mixing under Optimized Conditions Yields >60 000-Fold Enhancement of ^{89} Y NMR Signal. *J. Am. Chem. Soc.* **2011**, *133* (22), 8673–8680.

(15) Lumata, L.; Merritt, M. E.; Hashami, Z.; Ratnakar, S. J.; Kovacs, Z. Production and NMR Characterization of Hyperpolarized 107,109Ag Complexes. *Angew. Chem. Int. Ed.* **2012**, *51* (2), 525–527.

(16) Ardenkjaer-Larsen, J. H.; Fridlund, B.; Gram, A.; Hansson, G.; Hansson, L.; Lerche, M. H.; Servin, R.; Thaning, M.; Golman, K. Increase in Signal-to-Noise Ratio of > 10,000 Times in Liquid-State NMR. *Proc. Natl. Acad. Sci.* **2003**, *100* (18), 10158–10163.

(17) Ardenkjaer-Larsen, J. H. On the Present and Future of Dissolution-DNP. *J. Magn. Reson.* **2016**, *264*, 3–12.

(18) Gallagher, F. A.; Kettunen, M. I.; Day, S. E.; Hu, D.-E.; Ardenkjær-Larsen, J. H.; Zandt, R. in 't; Jensen, P. R.; Karlsson, M.; Golman, K.; Lerche, M. H.; et al. Magnetic Resonance Imaging of PH in Vivo Using Hyperpolarized 13C-Labelled Bicarbonate. *Nature* **2008**, *453* (7197), 940–943.

(19) Lippert, A. R.; Keshari, K. R.; Kurhanewicz, J.; Chang, C. J. A Hydrogen Peroxide-Responsive Hyperpolarized ^{13}C MRI Contrast Agent. *J. Am. Chem. Soc.* **2011**, *133* (11), 3776–3779.

(20) Doura, T.; Hata, R.; Nonaka, H.; Ichikawa, K.; Sando, S. Design of a ^{13}C Magnetic Resonance Probe Using a Deuterated Methoxy Group as a Long-Lived Hyperpolarization Unit. *Angew. Chem. Int. Ed.* **2012**, *51* (40), 10114–10117.

(21) Keshari, K. R.; Kurhanewicz, J.; Bok, R.; Larson, P. E. Z.; Vigneron, D. B.; Wilson, D. M. Hyperpolarized 13C Dehydroascorbate as an Endogenous Redox Sensor for in Vivo Metabolic Imaging. *Proc. Natl. Acad. Sci.* **2011**, *108* (46), 18606–18611.

(22) Bohndiek, S. E.; Kettunen, M. I.; Hu, D.; Kennedy, B. W. C.; Boren, J.; Gallagher, F. A.; Brindle, K. M. Hyperpolarized [1-^{13}C]-Ascorbic and Dehydroascorbic Acid: Vitamin C as a Probe for Imaging Redox Status in Vivo. *J. Am. Chem. Soc.* **2011**, *133* (30), 11795–11801.

(23) Bowen, S.; Hilty, C. Time-Resolved Dynamic Nuclear Polarization Enhanced NMR Spectroscopy. *Angew. Chem. Int. Ed.* **2008**, *47* (28), 5235–5237.

(24) Lee, Y.; Heo, G. S.; Zeng, H.; Wooley, K. L.; Hilty, C. Detection of Living Anionic Species in Polymerization Reactions Using Hyperpolarized NMR. *J. Am. Chem. Soc.* **2013**, *135* (12), 4636–4639.

(25) Jeffries, C. D. Polarization of Nuclei by Resonance Saturation in Paramagnetic Crystals. *Phys. Rev.* **1957**, *106* (1), 164–165.

(26) Hwang, C. F.; Hill, D. A. New Effect in Dynamic Polarization. *Phys. Rev. Lett.* **1967**, *18* (4), 110–112.

(27) Wollan, D. S. Dynamic Nuclear Polarization with an Inhomogeneously Broadened ESR Line. I. Theory. *Phys. Rev. B* **1976**, *13* (9), 3671–3685.

(28) Borghini, M. Spin-Temperature Model of Nuclear Dynamic Polarization Using Free Radicals. *Phys. Rev. Lett.* **1968**, *20* (9), 419–421.

(29) A Abragam and M Goldman. Principles of Dynamic Nuclear Polarisation. *Rep. Prog. Phys.* **1978**, *41* (3), 395.

(30) Atsarkin, V. A.; Rodak, M. I. TEMPERATURE OF SPIN-SPIN INTERACTIONS IN ELECTRON SPIN RESONANCE. *Sov. Phys. Uspekhi* **1972**, *15* (3), 251–265.

(31) Lumata, L. L.; Merritt, M. E.; Malloy, C. R.; Sherry, A. D.; van Tol, J.; Song, L.; Kovacs, Z. Dissolution DNP-NMR Spectroscopy Using Galvinoxyl as a Polarizing Agent. *J. Magn. Reson.* **2013**, *227*, 14–19.

(32) Lumata, L.; Merritt, M.; Khemtong, C.; Ratnakar, S. J.; van Tol, J.; Yu, L.; Song, L.; Kovacs, Z. The Efficiency of DPPH as a Polarising Agent for DNP-NMR Spectroscopy. *RSC Adv.* **2012**, *2* (33), 12812.

(33) Lumata, L.; Ratnakar, S. J.; Jindal, A.; Merritt, M.; Comment, A.; Malloy, C.; Sherry, A. D.; Kovacs, Z. BDPA: An Efficient Polarizing Agent for Fast Dissolution Dynamic Nuclear Polarization NMR Spectroscopy. *Chem. - Eur. J.* **2011**, *17* (39), 10825–10827.

(34) Reddy, T. J.; Iwama, T.; Halpern, H. J.; Rawal, V. H. General Synthesis of Persistent Trityl Radicals for EPR Imaging of Biological Systems. *J. Org. Chem.* **2002**, *67* (14), 4635–4639.

(35) Jannin, S.; Comment, A.; Kurdzesau, F.; Konter, J. A.; Hautle, P.; van den Brandt, B.; van der Klink, J. J. A 140GHz Prepolarizer for Dissolution Dynamic Nuclear Polarization. *J. Chem. Phys.* **2008**, *128* (24), 241102.

(36) Lumata, L.; Kovacs, Z.; Malloy, C.; Sherry, A. D.; Merritt, M. The Effect of ^{13}C Enrichment in the Glassing Matrix on Dynamic Nuclear Polarization of [1-^{13}C]Pyruvate. *Phys. Med. Biol.* **2011**, *56* (5), N85–N92.

(37) Jannin, S.; Bornet, A.; Colombo, S.; Bodenhausen, G. Low-Temperature Cross Polarization in View of Enhancing Dissolution Dynamic Nuclear Polarization in NMR. *Chem. Phys. Lett.* **2011**, *517* (4–6), 234–236.

(38) Batel, M.; Däpp, A.; Hunkeler, A.; Meier, B. H.; Kozerke, S.; Ernst, M. Cross-Polarization for Dissolution Dynamic Nuclear Polarization. *Phys Chem Chem Phys* **2014**, *16* (39), 21407–21416.

(39) Bornet, A.; Melzi, R.; Perez Linde, A. J.; Hautle, P.; van den Brandt, B.; Jannin, S.; Bodenhausen, G. Boosting Dissolution Dynamic Nuclear Polarization by Cross Polarization. *J. Phys. Chem. Lett.* **2013**, *4* (1), 111–114.

(40) Bowen, S.; Hilty, C. Rapid Sample Injection for Hyperpolarized NMR Spectroscopy. *Phys. Chem. Chem. Phys.* **2010**, *12* (22), 5766.

(41) Chen, H.-Y.; Hilty, C. Implementation and Characterization of Flow Injection in Dissolution Dynamic Nuclear Polarization NMR Spectroscopy. *ChemPhysChem* **2015**, *16* (12), 2646–2652.

(42) Leggett, J.; Hunter, R.; Granwehr, J.; Panek, R.; Perez-Linde, A. J.; Horsewill, A. J.; McMaster, J.; Smith, G.; Köckenberger, W. A Dedicated Spectrometer for Dissolution DNP NMR Spectroscopy. *Phys. Chem. Chem. Phys.* **2010**, *12* (22), 5883.

(43) Ahola, S.; Zhivonitko, V. V.; Mankinen, O.; Zhang, G.; Kantola, A. M.; Chen, H.-Y.; Hilty, C.; Koptyug, I. V.; Telkki, V.-V. Ultrafast Multidimensional Laplace NMR for a Rapid and Sensitive Chemical Analysis. *Nat. Commun.* **2015**, *6* (1).

(44) Bowen, S.; Hilty, C. Time-Resolved Dynamic Nuclear Polarization Enhanced NMR Spectroscopy. *Angew. Chem. Int. Ed.* **2008**, *47* (28), 5235–5237.

(45) Miéville, P.; Ahuja, P.; Sarkar, R.; Jannin, S.; Vasos, P. R.; Gerber-Lemaire, S.; Mishkovsky, M.; Comment, A.; Gruetter, R.; Ouari, O.; et al. Scavenging Free Radicals To Preserve Enhancement and Extend Relaxation Times in NMR Using Dynamic Nuclear Polarization. *Angew. Chem. Int. Ed.* **2010**, *49* (35), 6182–6185.

(46) Vuichoud, B.; Bornet, A.; de Nanteuil, F.; Milani, J.; Canet, E.; Ji, X.; Miéville, P.; Weber, E.; Kurzbach, D.; Flamm, A.; et al. Filterable Agents for Hyperpolarization of Water, Metabolites, and Proteins. *Chem. - Eur. J.* **2016**, *22* (41), 14696–14700.

(47) Gajan, D.; Bornet, A.; Vuichoud, B.; Milani, J.; Melzi, R.; van Kalkeren, H. A.; Veyre, L.; Thieuleux, C.; Conley, M. P.; Gruning, W. R.; et al. Hybrid Polarizing Solids for Pure Hyperpolarized Liquids through Dissolution Dynamic Nuclear Polarization. *Proc. Natl. Acad. Sci.* **2014**, *111* (41), 14693–14697.

(48) Zeng, H.; Lee, Y.; Hilty, C. Quantitative Rate Determination by Dynamic Nuclear Polarization Enhanced NMR of a Diels−Alder Reaction. *Anal. Chem.* **2010**, *82* (21), 8897–8902.

(49) Bowen, S.; Hilty, C. Temporal Chemical Shift Correlations in Reactions Studied by Hyperpolarized Nuclear Magnetic Resonance. *Anal. Chem.* **2009**, *81* (11), 4543–4547.

(50) Bakhmutov, V. I. *Practical NMR Relaxation for Chemists*; Wiley: Chichester, West Sussex, England ; Hoboken, NJ, 2004.

(51) Nagashima, K. Optimum Pulse Flip Angles for Multi-Scan Acquisition of Hyperpolarized NMR and MRI. *J. Magn. Reson.* **2008**, *190* (2), 183–188.

(52) Zhao, L.; Mulkern, R.; Tseng, C.-H.; Williamson, D.; Patz, S.; Kraft, R.; Walsworth, R. L.; Jolesz, F. A.; Albert, M. S. Gradient-Echo Imaging Considerations for Hyperpolarized129Xe MR. *J. Magn. Reson. B* **1996**, *113* (2), 179–183.

(53) Bowen, S.; Zeng, H.; Hilty, C. Chemical Shift Correlations from Hyperpolarized NMR by Off-Resonance Decoupling. *Anal. Chem.* **2008**, *80* (15), 5794–5798.

(54) Zhang, G.; Schilling, F.; Glaser, S. J.; Hilty, C. Chemical Shift Correlations from Hyperpolarized NMR Using a Single SHOT. *Anal. Chem.* **2013**, *85* (5), 2875–2881.

(55) Zhang, G.; Schilling, F.; Glaser, S. J.; Hilty, C. Reaction Monitoring Using Hyperpolarized NMR with Scaling of Heteronuclear Couplings by Optimal Tracking. *J. Magn. Reson.* **2016**, *272*, 123–128.

(56) Bowen, S.; Hilty, C. Temporal Chemical Shift Correlations in Reactions Studied by Hyperpolarized Nuclear Magnetic Resonance. *Anal. Chem.* **2009**, *81* (11), 4543–4547.

(57) Kim, Y.; Chen, C.-H.; Hilty, C. Direct Observation of Ru-Alkylidene Forming into Ethylene in Ring-Closing Metathesis from Hyperpolarized ^{1}H NMR. *Chem. Commun.* **2018**, *54* (34), 4333–4336.

(58) Frydman, L.; Blazina, D. Ultrafast Two-Dimensional Nuclear Magnetic Resonance Spectroscopy of Hyperpolarized Solutions. *Nat. Phys.* **2007**, *3* (6), 415–419.

(59) Giraudeau, P.; Frydman, L. Ultrafast 2D NMR: An Emerging Tool in Analytical Spectroscopy. *Annu. Rev. Anal. Chem.* **2014**, *7* (1), 129–161.

(60) Mishkovsky, M.; Frydman, L. Progress in Hyperpolarized Ultrafast 2D NMR Spectroscopy. *ChemPhysChem* **2008**, *9* (16), 2340–2348.

(61) Frydman, L.; Scherf, T.; Lupulescu, A. The Acquisition of Multidimensional NMR Spectra within a Single Scan. *Proc. Natl. Acad. Sci.* **2002**, *99* (25), 15858–15862.

(62) Schanda, P.; Brutscher, B. Very Fast Two-Dimensional NMR Spectroscopy for Real-Time Investigation of Dynamic Events in Proteins on the Time Scale of Seconds. *J. Am. Chem. Soc.* **2005**, *127* (22), 8014–8015.

(63) Schanda, P.; Kupče, Ē.; Brutscher, B. SOFAST-HMQC Experiments for Recording Two-Dimensional Deteronuclear Correlation Spectra of Proteins within a Few Seconds. *J. Biomol. NMR* **2005**, *33* (4), 199–211.

(64) Szekely, O.; Olsen, G. L.; Felli, I. C.; Frydman, L. High-Resolution 2D NMR of Disordered Proteins Enhanced by Hyperpolarized Water. *Anal. Chem.* **2018**, *90* (10), 6169–6177.

(65) Overhauser, A. W. Polarization of Nuclei in Metals. *Phys. Rev.* **1953**, *92* (2), 411–415.

(66) Kim, J.; Liu, M.; Chen, H.-Y.; Hilty, C. Determination of Intermolecular Interactions Using Polarization Compensated Heteronuclear Overhauser Effect of Hyperpolarized Spins. *Anal. Chem.* **2015**, *87* (21), 10982–10987.

(67) Min, H.; Sekar, G.; Hilty, C. Polarization Transfer from Ligands Hyperpolarized by Dissolution Dynamic Nuclear Polarization for Screening in Drug Discovery. *ChemMedChem* **2015**, *10* (9), 1559–1563.

(68) Wang, Y.; Ragavan, M.; Hilty, C. Site Specific Polarization Transfer from a Hyperpolarized Ligand of Dihydrofolate Reductase. *J. Biomol. NMR* **2016**, *65* (1), 41–48.

(69) Coates, G. W. Precise Control of Polyolefin Stereochemistry Using Single-Site Metal Catalysts. *Chem. Rev.* **2000**, *100* (4), 1223–1252.

(70) Resconi, L.; Cavallo, L.; Fait, A.; Piemontesi, F. Selectivity in Propene Polymerization with Metallocene Catalysts. *Chem. Rev.* **2000**, *100* (4), 1253–1346.

(71) Brintzinger, H. H.; Fischer, D.; Mülhaupt, R.; Rieger, B.; Waymouth, R. M. Stereospecific Olefin Polymerization with Chiral Metallocene Catalysts. *Angew. Chem. Int. Ed. Engl.* **1995**, *34* (11), 1143–1170.

(72) Bochmann, M. Kinetic and Mechanistic Aspects of Metallocene Polymerisation Catalysts. *J. Organomet. Chem.* **2004**, *689* (24), 3982–3998.

(73) Liu, Z.; Somsook, E.; White, C. B.; Rosaaen, K. A.; Landis, C. R. Kinetics of Initiation, Propagation, and Termination for the [*Rac* -(C_2H_4(1-Indenyl)$_2$)ZrMe][$MeB(C_6F_5)_3$]-Catalyzed Polymerization of 1-Hexene. *J. Am. Chem. Soc.* **2001**, *123* (45), 11193–11207.

(74) Novstrup, K. A.; Travia, N. E.; Medvedev, G. A.; Stanciu, C.; Switzer, J. M.; Thomson, K. T.; Delgass, W. N.; Abu-Omar, M. M.; Caruthers, J. M. Mechanistic Detail Revealed via Comprehensive Kinetic Modeling of [*Rac* -C_2H_4(1-Indenyl)$_2$$ZrMe_2$]-Catalyzed 1-Hexene Polymerization. *J. Am. Chem. Soc.* **2010**, *132* (2), 558–566.

(75) Song, F.; Cannon, R. D.; Bochmann, M. Zirconocene-Catalyzed Propene Polymerization: A Quenched-Flow Kinetic Study. *J. Am. Chem. Soc.* **2003**, *125* (25), 7641–7653.

(76) Landis, C. R.; Christianson, M. D. Metallocene-Catalyzed Alkene Polymerization and the Observation of Zr-Allyls. *Proc. Natl. Acad. Sci.* **2006**, *103* (42), 15349–15354.

(77) Al-Humydi, A.; Garrison, J. C.; Mohammed, M.; Youngs, W. J.; Collins, S. Propene Polymerization Using Ansa-Metallocenium Ions: Catalyst Deactivation

Processes during Monomer Consumption and Molecular Structures of the Products Formed. *Polyhedron* **2005**, *24* (11), 1234–1249.

(78) Margl, P. M.; Woo, T. K.; Ziegler, T. Potential Catalyst Deactivation Reaction in Homogeneous Ziegler−Natta Polymerization of Olefins: Formation of an Allyl Intermediate. *Organometallics* **1998**, *17* (23), 4997–5002.

(79) Vatamanu, M.; Stojcevic, G.; Baird, M. C. Detection of an η^1-Alkene Intermediate of the Type $[Cp_2Zr(Me)(\eta^1\text{-Alkene})]^+$: The Role of Such Species in Metallocene Catalyst Deactivation to Allylic Species. *J. Am. Chem. Soc.* **2008**, *130* (2), 454–456.

(80) Vatamanu, M. Synthesis, Structures, and Dynamic Features of d^0 Zirconocene–Allyl Complexes. *Organometallics* **2014**, *33* (14), 3683–3694.

(81) Sauriol, F.; Wong, E.; Leung, A. M. H.; Donaghue, I. E.; Baird, M. C.; Wondimagegn, T.; Ziegler, T. Structures and Properties of Nonchelated, d^0 Alkyl Alkene Complexes of the Type $[Cp_2ZrMe(Alkene)]^+$: Elusive Intermediates during Ziegler-Natta Polymerizations of Alkenes. *Angew. Chem. Int. Ed.* **2009**, *48* (18), 3342–3345.

(82) Ardenkjaer-Larsen, J. H.; Fridlund, B.; Gram, A.; Hansson, G.; Hansson, L.; Lerche, M. H.; Servin, R.; Thaning, M.; Golman, K. Increase in Signal-to-Noise Ratio of > 10,000 Times in Liquid-State NMR. *Proc. Natl. Acad. Sci.* **2003**, *100* (18), 10158–10163.

(83) Keshari, K. R.; Wilson, D. M. Chemistry and Biochemistry of ^{13}C Hyperpolarized Magnetic Resonance Using Dynamic Nuclear Polarization. *Chem Soc Rev* **2014**, *43* (5), 1627–1659.

(84) Lee, Y.; Heo, G. S.; Zeng, H.; Wooley, K. L.; Hilty, C. Detection of Living Anionic Species in Polymerization Reactions Using Hyperpolarized NMR. *J. Am. Chem. Soc.* **2013**, *135* (12), 4636–4639.

(85) Bowen, S.; Hilty, C. Time-Resolved Dynamic Nuclear Polarization Enhanced NMR Spectroscopy. *Angew. Chem. Int. Ed.* **2008**, *47* (28), 5235–5237.

(86) Zeng, H.; Lee, Y.; Hilty, C. Quantitative Rate Determination by Dynamic Nuclear Polarization Enhanced NMR of a Diels−Alder Reaction. *Anal. Chem.* **2010**, *82* (21), 8897–8902.

(87) Asakura, T.; Demura, M.; Nishiyama, Y. Carbon-13 NMR Spectral Assignment of Five Polyolefins Determined from the Chemical Shift Calculation and the Polymerization Mechanism. *Macromolecules* **1991**, *24* (9), 2334–2340.

(88) Alan E. Tonelli. *NMR Spectroscopy and Polymer Microstructure: The Conformational Connection*; Wiley-VCH: New York, 1989.

(89) Subramanyam, U.; Rajamohanan, P. .; Sivaram, S. A Study of the Structure of Poly(Hexene-1) Prepared by Nickel(α-Diimine)/MAO Catalyst Using High Resolution NMR Spectroscopy. *Polymer* **2004**, *45* (12), 4063–4076.

(90) Segal, S.; Goldberg, I.; Kol, M. Zirconium and Titanium Diamine Bis(Phenolate) Catalysts for α-Olefin Polymerization: From Atactic Oligo(1-Hexene) to Ultrahigh-

Molecular-Weight Isotactic Poly(1-Hexene). *Organometallics* **2005**, *24* (2), 200–202.

(91) Bowen, S.; Hilty, C. Temporal Chemical Shift Correlations in Reactions Studied by Hyperpolarized Nuclear Magnetic Resonance. *Anal. Chem.* **2009**, *81* (11), 4543–4547.

(92) Harvey, B. G.; Meylemans, H. A. 1-Hexene: A Renewable C6 Platform for Full-Performance Jet and Diesel Fuels. *Green Chem* **2014**, *16* (2), 770–776.

(93) Babu, G. N.; Newmark, R. A.; Chien, J. C. W. Microstructure of Poly(1-Hexene) Produced by Ansa-Zirconocenium Catalysis. *Macromolecules* **1994**, *27* (12), 3383–3388.

(94) Landis, C. R.; Rosaaen, K. A.; Sillars, D. R. Direct Observation of Insertion Events at *r Ac* -(C_2H_4(1-Indenyl)$_2$)Zr(MeB(C_6F_5)$_3$)−Polymeryl Intermediates: Distinction between Continuous and Intermittent Propagation Modes. *J. Am. Chem. Soc.* **2003**, *125* (7), 1710–1711.

(95) Wu, F.; Dash, A. K.; Jordan, R. F. Structures and Reactivity of Zr(IV) Chlorobenzene Complexes. *J. Am. Chem. Soc.* **2004**, *126* (47), 15360–15361.

(96) Christianson, M. D.; Tan, E. H. P.; Landis, C. R. Stopped-Flow NMR: Determining the Kinetics of [*Rac* -(C_2H_4(1-Indenyl)$_2$)ZrMe][MeB(C_6F_5)$_3$]-Catalyzed Polymerization of 1-Hexene by Direct Observation. *J. Am. Chem. Soc.* **2010**, *132* (33), 11461–11463.

(97) Kaminsky, W.; Engehausen, R.; Zoumis, K.; Spaleck, W.; Rohrmann, J. Standardized Polymerizations of Ethylene and Propene with Bridged and

Unbridged Metallocene Derivatives: A Comparison. *Macromol. Chem. Phys.* **1992**, *193* (7), 1643.

(98) Soga, K.; Lee, D. H.; Morikawa, Y. Difference in Propagation Profiles between Isotactic and Atactic Polymerizations with Ziegler-Natta Catalysts. *Polymer* **1992**, *33* (11), 2408–2411.

(99) Camara, J. M.; Petros, R. A.; Norton, J. R. Zirconium-Catalyzed Carboalumination of α-Olefins and Chain Growth of Aluminum Alkyls: Kinetics and Mechanism. *J. Am. Chem. Soc.* **2011**, *133* (14), 5263–5273.

(100) Bowen, S.; Hilty, C. Rapid Sample Injection for Hyperpolarized NMR Spectroscopy. *Phys. Chem. Chem. Phys.* **2010**, *12* (22), 5766.

(101) Hilf, S.; Kilbinger, A. F. M. Functional End Groups for Polymers Prepared Using Ring-Opening Metathesis Polymerization. *Nat. Chem.* **2009**, *1* (7), 537–546.

(102) Sutthasupa, S.; Shiotsuki, M.; Sanda, F. Recent Advances in Ring-Opening Metathesis Polymerization, and Application to Synthesis of Functional Materials. *Polym. J.* **2010**, *42* (12), 905–915.

(103) Buchmeiser, M. R. Homogeneous Metathesis Polymerization by Well-Defined Group VI and Group VIII Transition-Metal Alkylidenes: Fundamentals and Applications in the Preparation of Advanced Materials. *Chem. Rev.* **2000**, *100* (4), 1565–1604.

(104) Bielawski, C. W.; Grubbs, R. H. Living Ring-Opening Metathesis Polymerization. *Prog. Polym. Sci.* **2007**, *32* (1), 1–29.

(105) Leitgeb, A.; Wappel, J.; Slugovc, C. The ROMP Toolbox Upgraded. *Polymer* **2010**, *51* (14), 2927–2946.

(106) Samojłowicz, C.; Bieniek, M.; Grela, K. Ruthenium-Based Olefin Metathesis Catalysts Bearing *N* -Heterocyclic Carbene Ligands. *Chem. Rev.* **2009**, *109* (8), 3708–3742.

(107) Vougioukalakis, G. C.; Grubbs, R. H. Ruthenium-Based Heterocyclic Carbene-Coordinated Olefin Metathesis Catalysts †. *Chem. Rev.* **2010**, *110* (3), 1746–1787.

(108) Ivin, K. J.; Mol, J. C. *Olefin Metathesis and Metathesis Polymerization*; Academic Press: San Diego, CA, 1997.

(109) Bielawski, C.; Grubbs, R. Highly Efficient Ring-Opening Metathesis Polymerization (ROMP) Using New Ruthenium Catalysts Containing N-Heterocyclic Carbene Ligands. *Angew. Chem.* **2000**, *39* (16), 2903–2906.

(110) Choi, T.-L.; Grubbs, R. H. Controlled Living Ring-Opening-Metathesis Polymerization by a Fast-Initiating Ruthenium Catalyst. *Angew. Chem. Int. Ed.* **2003**, *42* (15), 1743–1746.

(111) Sanford, M. S.; Ulman, M.; Grubbs, R. H. New Insights into the Mechanism of Ruthenium-Catalyzed Olefin Metathesis Reactions. *J. Am. Chem. Soc.* **2001**, *123* (4), 749–750.

(112) Sanford, M. S.; Love, J. A.; Grubbs, R. H. Mechanism and Activity of Ruthenium Olefin Metathesis Catalysts. *J. Am. Chem. Soc.* **2001**, *123* (27), 6543–6554.

(113) Romero, P. E.; Piers, W. E. Direct Observation of a 14-Electron Ruthenacyclobutane Relevant to Olefin Metathesis. *J. Am. Chem. Soc.* **2005**, *127* (14), 5032–5033.

(114) Walsh, D. J.; Lau, S. H.; Hyatt, M. G.; Guironnet, D. Kinetic Study of Living Ring-Opening Metathesis Polymerization with Third-Generation Grubbs Catalysts. *J. Am. Chem. Soc.* **2017**, *139* (39), 13644–13647.

(115) Düz, B.; Elbistan, C. K.; Ece, A.; Sevin, F. Application of Carbon Arc-Generated Mo- and W-Based Catalyst Systems to the ROMP of Norbornene. *Appl. Organomet. Chem.* **2009**, *23* (9), 359–364.

(116) Chen, C.-H.; Shih, W.-C.; Hilty, C. *In Situ* Determination of Tacticity, Deactivation, and Kinetics in [*Rac* -(C_2H_4(1-Indenyl)$_2$)ZrMe][$B(C_6F_5)_4$] and [Cp_2ZrMe][$B(C_6F_5)_4$]-Catalyzed Polymerization of 1-Hexene Using ^{13}C Hyperpolarized NMR. *J. Am. Chem. Soc.* **2015**, *137* (21), 6965–6971.

(117) Harris, R. K.; Becker, E. D.; Cabral de Menezes, S. M.; Goodfellow, R.; Granger, P. NMR Nomenclature: Nuclear Spin Properties and Conventions for Chemical Shifts. IUPAC Recommendations 2001. International Union of Pure and Applied Chemistry. Physical Chemistry Division. Commission on Molecular Structure and Spectroscopy. *Magn. Reson. Chem.* **2002**, *40* (7), 489–505.

(118) Nelson, D. J.; Manzini, S.; Urbina-Blanco, C. A.; Nolan, S. P. Key Processes in Ruthenium-Catalysed Olefin Metathesis. *Chem. Commun.* **2014**, *50* (72), 10355.

(119) Ivin, K. J.; Laverty, D. T.; Rooney, J. J. The 13C NMR Spectra of Poly(1-pentenylene) and Poly(1,3-cyclopentylenevinylene). *Macromol. Chem. Phys.* **1977**, *178* (5), 1545–1560.

(120) Ivin, K. J.; Laverty, D. T.; O'Donnell, J. H.; Rooney, J. J.; Stewart, C. D. Cis-trans Double Bond Distribution in Poly(1,3-cyclopentylenevinylene); Dependence on Metathesis Catalyst, Cocatalyst, and Additives. *Macromol. Chem. Phys.* **1979**, *180* (8), 1989–2000.

(121) Greene, R. M. E.; Hamilton, J. G.; Ivin, K. J.; Rooney, J. J. Cis/Trans Reactivity Ratios in the Ring-opening Polymerization of Bicyclo[2.2.1]Hept-2-ene; the Nature of the Propagating Species in Olefin Metathesis. *Macromol. Chem. Phys.* **1986**, *187* (3), 619–632.

(122) Parthiban, A. *Synthesis and Applications of Copolymers*; Wiley: Somerset, UNITED STATES, 2014.

(123) Hawker, C. J.; Wooley, K. L. The Convergence of Synthetic Organic and Polymer Chemistries. *Science* **2005**, *309* (5738), 1200–1205.

(124) Chu, T.-Y.; Lu, J.; Beaupré, S.; Zhang, Y.; Pouliot, J.-R.; Wakim, S.; Zhou, J.; Leclerc, M.; Li, Z.; Ding, J.; et al. Bulk Heterojunction Solar Cells Using Thieno[3,4- *c*]Pyrrole-4,6-Dione and Dithieno[3,2- *b* :2′,3′- *d*]Silole Copolymer with a Power Conversion Efficiency of 7.3%. *J. Am. Chem. Soc.* **2011**, *133* (12), 4250–4253.

(125) Nakatani, K.; Terashima, T.; Sawamoto, M. Concurrent Tandem Living Radical Polymerization: Gradient Copolymers via In Situ Monomer Transformation with Alcohols. *J. Am. Chem. Soc.* **2009**, *131* (38), 13600–13601.

(126) Patten, T. E.; Matyjaszewski, K. Atom Transfer Radical Polymerization and the Synthesis of Polymeric Materials. *Adv. Mater.* **1998**, *10* (12), 901–915.

(127) Bockstaller, M. R.; Mickiewicz, R. A.; Thomas, E. L. Block Copolymer Nanocomposites: Perspectives for Tailored Functional Materials. *Adv. Mater.* **2005**, *17* (11), 1331–1349.

(128) Mayo, F. R.; Lewis, F. M. Copolymerization. I. A Basis for Comparing the Behavior of Monomers in Copolymerization; The Copolymerization of Styrene and Methyl Methacrylate. *J. Am. Chem. Soc.* **1944**, *66* (9), 1594–1601.

(129) Mayo, F. R.; Walling, C. Copolymerization. *Chem. Rev.* **1950**, *46* (2), 191–287.

(130) Hagiopol, C. Estimation of Reactivity Ratios. In *Copolymerization*; Springer US: Boston, MA, 1999; pp 19–100.

(131) Song, F.; Cannon, R. D.; Bochmann, M. Zirconocene-Catalyzed Propene Polymerization: A Quenched-Flow Kinetic Study. *J. Am. Chem. Soc.* **2003**, *125* (25), 7641–7653.

(132) Aguilar, M. R.; Gallardo, A.; Fernández, M. del M.; Román, J. S. In Situ Quantitative ^{1}H NMR Monitoring of Monomer Consumption: A Simple and Fast Way of Estimating Reactivity Ratios. *Macromolecules* **2002**, *35* (6), 2036–2041.

(133) Ito, H.; Dalby, C.; Pomerantz, A.; Sherwood, M.; Sato, R.; Sooriyakumaran, R.; Guy, K.; Breyta, G. Monomer Reactivities and Kinetics in Radical

Copolymerization of Hydroxystyrene Derivatives and *Tert* -Butyl (Meth)Acrylate. *Macromolecules* **2000**, *33* (14), 5080–5089.

(134) Keshari, K. R.; Wilson, D. M. Chemistry and Biochemistry of 13C Hyperpolarized Magnetic Resonance Using Dynamic Nuclear Polarization. *Chem. Soc. Rev.* **2014**, *43* (5), 1627.

(135) Chen, C.-H.; Kim, Y.; Zhang, G.; Hilty, C. Unpublished Result.

(136) Ivin, K. J.; Lapienis, G.; Rooney, J. J. Ring-opening Copolymerization of Cycloalkenes Investigated by 13C NMR Spectroscopy. *Makromol. Chem.* **1982**, *183* (1), 9–28.

(137) Chen, H.-Y.; Hilty, C. Implementation and Characterization of Flow Injection in Dissolution Dynamic Nuclear Polarization NMR Spectroscopy. *ChemPhysChem* **2015**, *16* (12), 2646–2652.

(138) Min, H.; Sekar, G.; Hilty, C. Polarization Transfer from Ligands Hyperpolarized by Dissolution Dynamic Nuclear Polarization for Screening in Drug Discovery. *ChemMedChem* **2015**, *10* (9), 1559–1563.

(139) Wang, Y.; Li, H. Beale–Kato–Madja Type Criteria of Smooth Solutions to 3D Hall-MHD Flows. *Appl. Math. Comput.* **2016**, *286*, 41–48.

(140) Lee, Y.; Zeng, H.; Mazur, A.; Wegstroth, M.; Carlomagno, T.; Reese, M.; Lee, D.; Becker, S.; Griesinger, C.; Hilty, C. Hyperpolarized Binding Pocket Nuclear Overhauser Effect for Determination of Competitive Ligand Binding. *Angew. Chem. Int. Ed.* **2012**, *51* (21), 5179–5182.

(141) Chappuis, Q.; Milani, J.; Vuichoud, B.; Bornet, A.; Gossert, A. D.; Bodenhausen, G.; Jannin, S. Hyperpolarized Water to Study Protein–Ligand Interactions. *J. Phys. Chem. Lett.* **2015**, *6* (9), 1674–1678.

(142) Olsen, G.; Markhasin, E.; Szekely, O.; Bretschneider, C.; Frydman, L. Optimizing Water Hyperpolarization and Dissolution for Sensitivity-Enhanced 2D Biomolecular NMR. *J. Magn. Reson.* **2016**, *264*, 49–58.

(143) Kurzbach, D.; Canet, E.; Flamm, A. G.; Jhajharia, A.; Weber, E. M. M.; Konrat, R.; Bodenhausen, G. Investigation of Intrinsically Disordered Proteins through Exchange with Hyperpolarized Water. *Angew. Chem. Int. Ed.* **2017**, *56* (1), 389–392.

(144) Kim, J.; Liu, M.; Hilty, C. Modeling of Polarization Transfer Kinetics in Protein Hydration Using Hyperpolarized Water. *J. Phys. Chem. B* **2017**, *121* (27), 6492–6498.

(145) Kim, J.; Liu, M.; Chen, H.-Y.; Hilty, C. Determination of Intermolecular Interactions Using Polarization Compensated Heteronuclear Overhauser Effect of Hyperpolarized Spins. *Anal. Chem.* **2015**, *87* (21), 10982–10987.

(146) Tomalia, D. A.; Baker, H.; Dewald, J.; Hall, M.; Kallos, G.; Martin, S.; Roeck, J.; Ryder, J.; Smith, P. A New Class of Polymers: Starburst-Dendritic Macromolecules. *Polym. J.* **1985**, *17* (1), 117–132.

(147) Gillies, E.; Frechet, J. Dendrimers and Dendritic Polymers in Drug Delivery. *Drug Discov. Today* **2005**, *10* (1), 35–43.

(148) Kesharwani, P.; Jain, K.; Jain, N. K. Dendrimer as Nanocarrier for Drug Delivery. *Prog. Polym. Sci.* **2014**, *39* (2), 268–307.

(149) Zhao, L.; Cheng, Y.; Hu, J.; Wu, Q.; Xu, T. Host−Guest Chemistry of Dendrimer−Drug Complexes. 3. Competitive Binding of Multiple Drugs by a Single Dendrimer for Combination Therapy. *J. Phys. Chem. B* **2009**, *113* (43), 14172–14179.

(150) Carr, H. Y.; Purcell, E. M. Effects of Diffusion on Free Precession in Nuclear Magnetic Resonance Experiments. *Phys. Rev.* **1954**, *94* (3), 630–638.

(151) Meiboom, S.; Gill, D. Modified Spin-Echo Method for Measuring Nuclear Relaxation Times. *Rev. Sci. Instrum.* **1958**, *29* (8), 688–691.

(152) Chen, H.-Y.; Lee, Y.; Bowen, S.; Hilty, C. Spontaneous Emission of NMR Signals in Hyperpolarized Proton Spin Systems. *J. Magn. Reson.* **2011**, *208* (2), 204–209.

(153) Macur, S.; Farmer, B. .; Brown, L. . An Improved Method for the Determination of Cross-Relaxation Rates from NOE Data. *J. Magn. Reson. 1969* **1986**, *70* (3), 493–499.

(154) Frydman, L.; Scherf, T.; Lupulescu, A. The Acquisition of Multidimensional NMR Spectra within a Single Scan. *Proc. Natl. Acad. Sci.* **2002**, *99* (25), 15858–15862.

(155) Frydman, L.; Blazina, D. Ultrafast Two-Dimensional Nuclear Magnetic Resonance Spectroscopy of Hyperpolarized Solutions. *Nat. Phys.* **2007**, *3* (6), 415–419.

(156) *Protein NMR Spectroscopy: Principles and Practice*, 2. ed.; Cavanagh, J., Ed.; Elsevier, Acad. Press: Amsterdam, 2007.